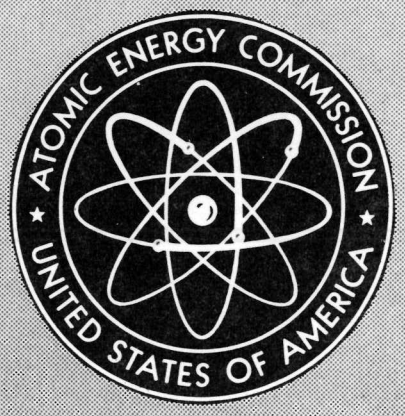

GEAP-3899

BURNOUT CONDITIONS FOR SINGLE ROD IN ANNULAR GEOMETRY, WATER AT 600 TO 1400 PSIA

By
E. Janssen
J. A. Kervinen

February 1963

Atomic Power Equipment Department
General Electric Company
San Jose, California

UNITED STATES ATOMIC ENERGY COMMISSION • DIVISION OF TECHNICAL INFORMATION

LEGAL NOTICE

SAEC O on Te hn a nfo ma on E en on Oak R dge Tenne ee

GEAP-3899
REACTOR TECHNOLOGY

BURNOUT CONDITIONS FOR SINGLE ROD IN ANNULAR GEOMETRY, WATER AT 600 TO 1400 PSIA

by

E. Janssen
J. A. Kervinen

February 1963

U. S. ATOMIC ENERGY COMMISSION
CONTRACT AT(04-3)-189
PROJECT AGREEMENT 11

ATOMIC POWER EQUIPMENT DEPARTMENT
GENERAL ELECTRIC
SAN JOSE, CALIFORNIA

ACKNOWLEDGMENTS

The work reported here was done as part of Task B of the Fuel Cycle Program, sponsored by the U. S. Atomic Energy Commission.

Many people at APED contributed to the single-rod burnout program and to this report of it. The following in particular deserve mention: Mr. E. E. Polomik who did the pioneering work in single-rod burnout at APED; Dr. S. Levy who gave encouragement and suggestions on the many problems which arose during the course of the program; Dr. F. E. Tippets whose ideas have been helpful in the writing of this report; Mr. B. Duncan and the other people in Building G working under his direction, who set up and conducted the tests and recorded the data; and Mrs. Annalee Wright, our cheerful and efficient secretary, who took care of the many little details that are the province of secretaries, and who did the typing chores on this report.

FOREWORD

The report which follows describes an extensive program for the experimental determination of burnout conditions for a single rod in an annular geometry. Two other reports on the subject of burnout under Task B of the Fuel Cycle Program have been published prior to the publication of this one: These are:

Tippets, F. E., "Critical Heat Flux and Flow Pattern Characteristics of High Pressure Boiling Water in Forced Convection," GEAP-3766, April 1962.

Levy, S., "Prediction of the Critical Heat Flux in Forced Convection Flow," GEAP-3961, June 20, 1962.

These already-published reports describe analytical models and procedures for the correlation and prediction of the burnout heat flux for rectangular and circular geometries, as well as for annular. Some of the data from the report which follows, as well as from other sources, were used in the verification of these analytical models.

The report which follows is the first complete reporting of the single-rod results.

TABLE OF CONTENTS

LIST OF TABLES

SUMMARY

Tests were run at General Electric Company, Atomic Power Equipment Department, to determine burnout conditions for a rod in an annular geometry. An electrically heated rod was placed in a circular tube to form the annular flow path for the water coolant. Only the rod was heated, the outer surface (tube) being essentially adiabatic. Orientation was vertical, with flow up. The tests covered the following range of conditions (corresponding to conditions which might exist in a reactor core):

Rod O.D.	:	0.375 to 0 540 inch
Tube I.D.	:	0.555 to 1.250 inch
Hydraulic diameter	:	0.180 to 0.875 inch
Heated length	:	29 to 108 inches
Pressure	:	600 to 1450 psia
Flow rate	:	0.14×10^6 to 6.2×10^6 lb/hr-ft^2
Steam quality	:	Slightly subcooled to 61.5 per cent

For each condition the electrical power was increased until burnout was reached, thus establishing a burnout condition for the particular rod and tube geometry.

The basic test geometry was a straight concentric annulus. The burnout results for this geometry showed that:

1. When burnout heat flux is plotted versus quality (other variables held constant), the points (except for experimental scatter of the order of $\pm$ 10 per cent maximum) lie on a straight line. The line slopes downward in the direction of increasing quality.
2. An increase in flow (other variables constant) results in a decrease in burnout heat flux, for flows up to about 2×10^6 lb/hr-ft^2.
3. An increase in the hydraulic diameter (other variables constant) from 0.18 inch to 0.25 inch results in an increase in the burnout heat flux.

For an increase from about 0.25 inch to 0.5 inch, the burnout heat flux goes through a maximum. An increase from 0.5 inch to 0.875 inch results in a decrease in the burnout heat flux.

4. An increase in pressure (other variables constant) results in a decrease in burnout heat flux, for pressures in the range 600 to 1450 psia.

Of the basic test geometry data which fall within the following range of conditions,

Hydraulic diameter	:	0.25 to 0.875 inch
Pressure	:	600 to 1450 psia
Flow	:	0.14×10^6 to 6.2×10^6 lb/hr-ft^2
Quality	:	-0.12 to 0.45
Heat Flux	:	$\phi_{bo} > 0.35 \times 10^6$ Btu/hr-ft^2

ninety-five per cent are correlated to $\pm$ 20 per cent by

$$\frac{\phi_{bo(c)}}{10^6} = \frac{\left[1 + 0.16\left(\frac{1000-P}{400}\right) - 0.04\left(\frac{1000-P}{400}\right)^2\right]}{1 - 0.008\, B \left(\frac{G}{10^6}\right)^{0.8}} \left[0.0172 B \left(\frac{G}{10^6}\right)^{0.8} - \left\{0.3175 \left(\frac{G}{10^6}\right)^{-2}\right.\right.$$

$$\left. - 1.8534 \left(\frac{G}{10^6}\right)^{-1}\right\} - \left\{2.4 + 3.2\, D_h + 0.83\, D_h \left(\frac{G}{10^6}\right)\right\} \left\{ X \right.$$

$$\left.\left. - 0.0629 \left(\frac{G}{10^6}\right)^{-2} + 0.3429 \left(\frac{G}{10^6}\right)^{-1} - 3.2494 + 0.0020 \left(\frac{G}{10^6}\right)^2 \right\}\right]$$

The above range of conditions marks the limits of validity for this correlation.

Certain modifications of the basic test geometry were also tested. These are:

1. Eccentric rod
2. Simulated spacer
3. Sandblasted rod

} Special Geometries

4. Rough liner (.875" I.D. tube fitted with 0.70" I.D. x 0.080" rings on 1" centers)

The burnout results for these geometries show that:

1. When the rod is moved to 0.033 inch from the wall, the burnout heat flux may be reduced by from 22 per cent to 50 per cent.
2. The burnout heat flux remains unchanged when the flow is forced to separate from the heated surface (simulating flow just ahead of a plate-type spacer).
3. When the rod surface is roughened to 300 microinches as by sandblasting, the burnout heat flux may be reduced by from 35 per cent to 50 per cent.
4. Burnout heat flux for the rough liner is greater than for the smooth liner (i.e., basic test geometry), by about 40 per cent at a flow of 0.56×10^6 lb/hr-ft^2, 20 per cent at 1.12×10^6 lb/hr-ft^2. The slope of the burnout heat flux vs. quality curve through the data points is less for the rough liner at 1.12×10^6 lb/hr-ft^2 than for the smooth. The rough liner results show little or no flow effect.

The basic test geometry data are compared with other internally heated annular data, from Columbia University[11], Italy[12], and Great Britain[13]. Direct comparison cannot be made with the Italian results. Agreement with the Columbia results is good, with the British results, poor. Poor agreement with the British is attributed to the difference in conditions at the APED test section inlet (subcooled liquid) as compared with conditions at the British test section inlet (two-phase).

The basic test geometry data are compared with multirod data now available from Columbia[19], Hanford[20], and General Electric, APED[21]. The slope of the heat flux vs. quality curve for the multirod data is generally less than the corresponding curve for the single rod data (although the Columbia multirod data do not show this). There is little or no flow effect for the multirod. The differences between single and multirod results is attributed to flow disturbances in the multirod test sections. These flow disturbances

are caused by the provision for maintaining spacing between adjacent rods, made necessary by the strong electromagnetic forces acting between parallel conductors. The cleanest multirod flow channel (Columbia 7-rod, non-wrapped) gave results which are in good agreement with the single rod results.

INTRODUCTION

Boiling under either natural or forced circulation is being increasingly recognized as one of the most effective mechanisms for the transfer of heat. Developments in the nuclear reactor, missile, and process industries attest to this fact. Heat fluxes of well over a million Btu/hr-ft^2 have been observed, with the surface temperature only a few degrees above saturation.

Our concern here is with boiling water reactors. In this type of reactor, light water is used at high pressure to cool the fuel rods, with the resulting generation of net steam at the core exit. Boiling takes place at the fuel-water interface. As the heat flux is raised, the outside surface temperature of the fuel remains slightly above saturation, until a critical value of heat flux is attained. Past this point the surface temperature starts to rise rapidly, attended by oscillations. A plot of surface temperature versus heat flux which characterizes this behavior is shown in Figure 1.

The change in fuel surface temperature can be broken down into four principal regions:

1. In the forced convection region with the surface temperature below saturation, the temperature increases about linearly with heat flux.
2. As boiling starts, the heat transfer coefficient becomes very large, and a further increase in heat flux is accompanied by only a very small rise in surface temperature. This is known as the nucleate boiling regime. In this region the surface temperature never rises more than a few degrees above saturation.
3. As the critical heat flux point is passed,* the surface temperature starts to rise quite rapidly. The rise is attended by oscillations which increase,

---

* Description of events past the critical point are taken from Reference (1).

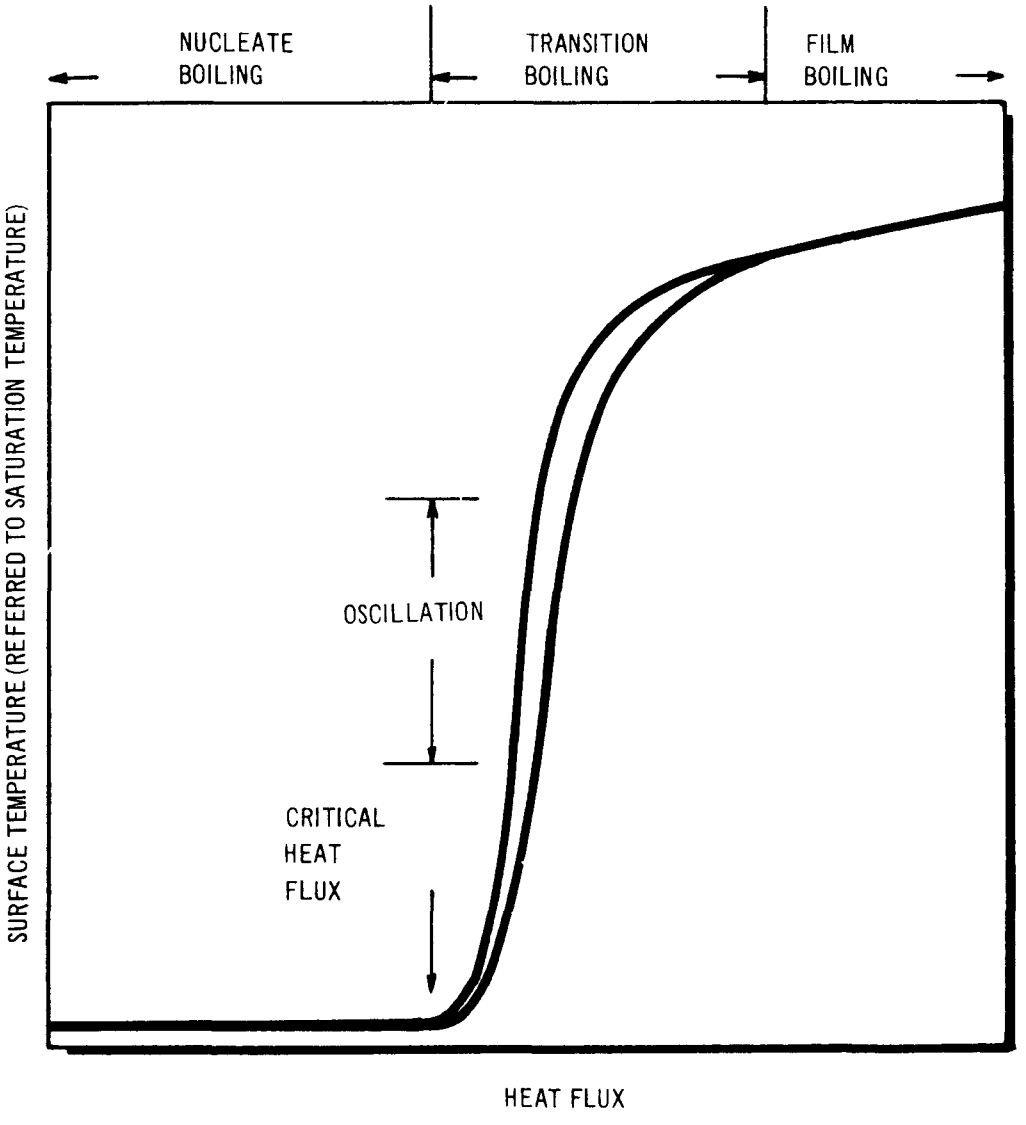

FIGURE 1 SURFACE TEMPERATURE vs HEAT FLUX NEAR THE CRITICAL POINT, FOR FORCED CIRCULATION BOILING.

pass through a maximum, and then decrease as the heat flux continues to be raised. These oscillations are presumed to be associated with the alternate forming and disappearing of localized steam blankets on the heater surface. This region is the transition region between nucleate and film boiling. The rate of temperature rise and the amplitude of oscillations are dependent upon conditions in the coolant channel. For instance, at low steam qualities the temperature rise may be quite abrupt and the oscillations very large.

4. As the heat flux is further increased, the oscillations tend to die out, and the temperature to reach a comparatively steady value. The difference between this new surface temperature and the saturation temperature is large, and may be several orders of magnitude greater than the corresponding difference for boiling in the nucleate regime. This is the film boiling regime, in which a relatively continuous steam blanket is presumed to form over the heater surface.

Steady state operation under film boiling conditions is possible. However, at low steam qualities the most commonly used materials would fail due to excessive surface temperature. This has led to the use of the word "burnout" in referring to the phenomena associated with heat fluxes past the critical.

"Burnout" as commonly used applies to the critical point* past which the surface temperature starts to rise rapidly as the heat flux is further increased. It will be so used in this report, even though this is a misleading usage under conditions where material failure does not occur at heat fluxes past the critical.(1)

The currently accepted practice in boiling water reactor design is to limit the design heat flux to a fraction of the burnout heat flux. The designer of

---

* This critical point is also referred to as the "departure from nucleate boiling" (DNB), and as the boiling "crisis."

a BWR (as of any water cooled and moderated reactor) must have accurate knowledge of the conditions at burnout. In recognition of this need, a considerable amount of work has already been reported. Much of this work was performed at a number of institutions in this country, including Purdue,[2] UCLA,[3], MIT,[4][5] NACA,[6] Battelle[7][8], ANL,[9], Westinghouse[10], and Columbia.[11] Some of the most recently reported work was performed in Italy[12], England[13], and Russia[14]. The geometries (except for some of the recent Columbia, Italian, and British data) were tubular or rectangular channels. Most of the published work, except for the recent work at Columbia, and the Italian, British, and Russian work, has been well summarized in Reference (10). All of the work was basically experimental, but with some effort being made to establish useful correlations.

About five years ago the Atomic Power Equipment Department (APED) of General Electric Company started a program of determining the conditions for burnout in an annular type geometry. The geometry consisted of a heated inner surface ("rod") and an unheated outer surface ("tube" or "liner"). The internally heated annulus was selected for the experimental determination of burnout because it simulates best the corner rod in a rod-type fuel bundle (Figures 2 and 3) where the heat flux is maximum due to flux peaking. Moreover, compared with the three possible fuel cell geometries shown in Figure 3, it has the highest, in fact the limiting, ratio of unheated to heated surface area. As such, it should give the minimum critical heat flux value for any of the three possible fuel cells, since the burnout point has been found to be minimum in the presence of an unheated surface.[12]

The work done at APED and reported here had as its objective the determination of burnout conditions for rod type fuel geometries. The following items were to be covered by this investigation:

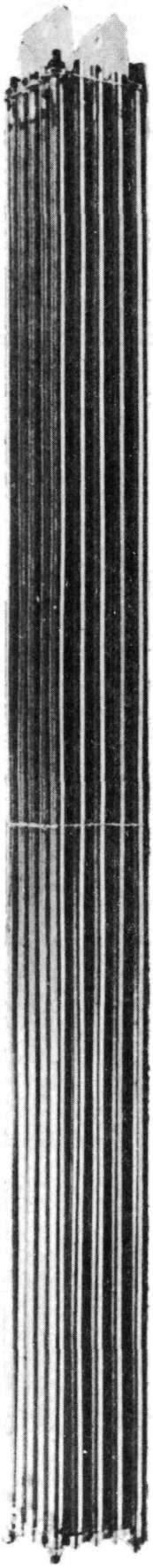

FIGURE 2 ROD TYPE FUEL BUNDLE TYPICAL OF CURRENT DESIGN

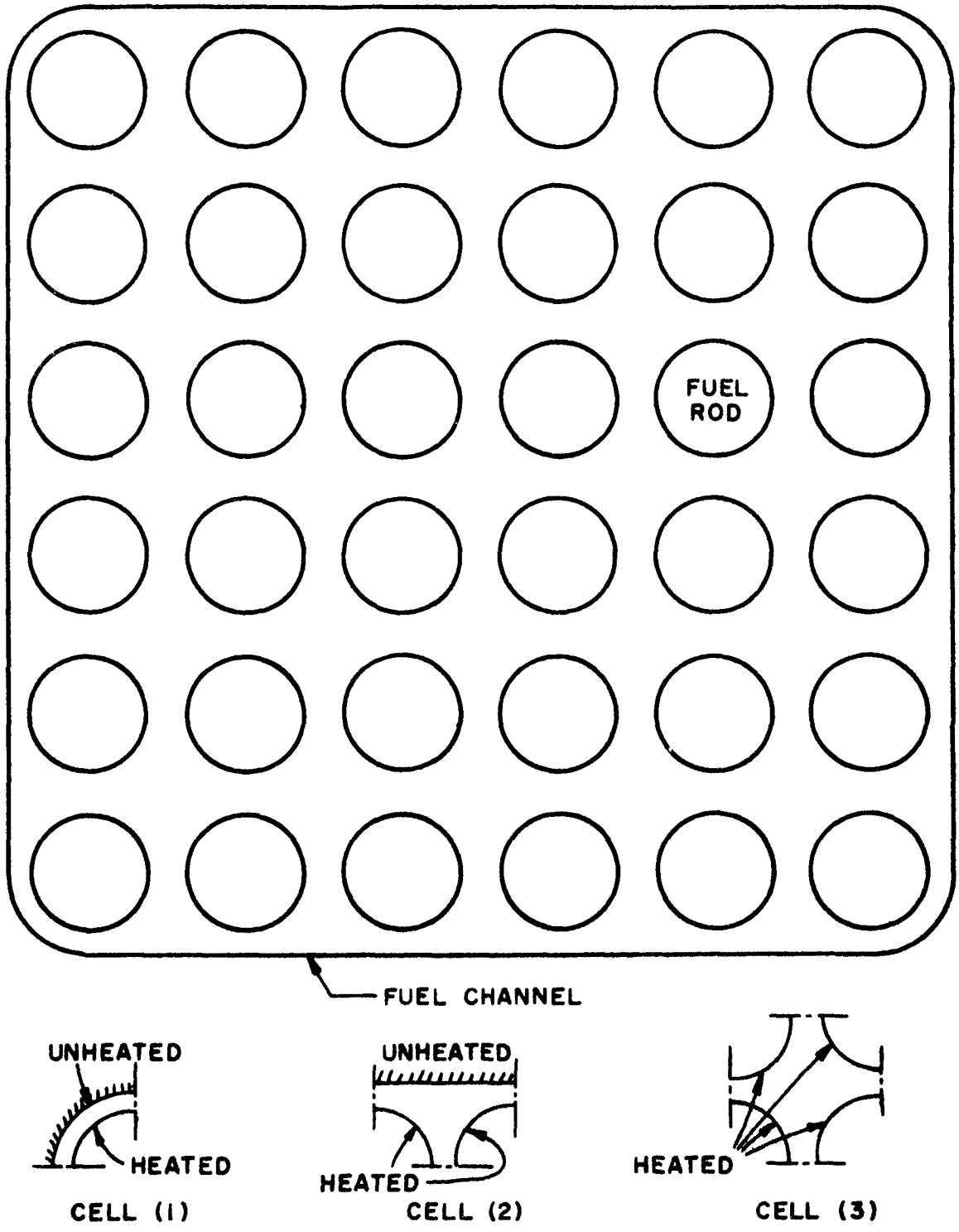

POSSIBLE FUEL CELL GEOMETRIES

FIGURE 3 — MULTIROD FUEL ASSEMBLY

1. The effect of quality (i.e., enthalpy) on burnout.
2. The effect of flow on burnout.
3. The effect of rod diameter and hydraulic diameter on burnout. (It was intended that the ratio of length to diameter L/D be kept large enough that there would be no L/D effect. L/D was always of the same order as that existing in actual reactors.)
4. The effect of pressure on burnout.
5. The effect on burnout of displacing one of the corner rods (see Figure 3) toward the channel corner.
6. The effect of plate-type spacers on burnout.
7. The effect of rod surface finish on burnout.
8. The effect of flow disturbing devices on burnout. (This was undertaken with the deliberate intent of raising the heat flux at the burnout point.)
9. A correlation of the data in terms of the parameters mentioned in items 1, 2, 3, and 4; the correlation to serve as a basis for predicting burnout under non-test conditions.

The report of the work follows.

EQUIPMENT

For each test the fuel rod was simulated by an electrically heated rod, placed in a circular tube test section to form an annular flow path for the water. The tube surface, i.e., the outer surface of the annulus, was unheated. The rod was tested under a series of conditions of pressure, flow, and inlet enthalpy simulating those which might occur in a reactor core. For each condition, the electrical power was increased until burnout was reached, thus establishing a burnout condition for the particular rod and tube geometry.

The equipment used to accomplish this simulation is described here.

Electrically Heated Rod

The heated portion of the electrically heated rod consisted of a section of seamless stainless steel tube. Copper extensions (electrodes) with the same O.D. were silver soldered to the ends. Thermocouples were passed through one of the electrodes and attached, by a spot welding technique, to the inside surface of the stainless steel tube, in the region of anticipated burnout. A typical assembled rod is shown in Figure 4; the location of the thermocouples is also shown.

All of the burnout runs were with rods which produced, to a good approximation, a uniform heat flux over the heated length. Three sizes of such rods were tested: 0.375 inch O.D., 0.500 inch O.D., and 0.540 inch O.D. The 0.375 and 0.540 inch rods were tested in lengths from 70 to 108 inches; the 0.500 inch rod lengths were 29 and 36 inches. For these uniform rods, the wall thickness of the stainless steel tube was very nearly uniform. Table 1 lists variations in wall thickness and electrical resistance measured on a sample from each of the three sizes. These variations are considered to be typical. The greatest variation in wall thickness is $\pm$ 3 per cent; the greatest

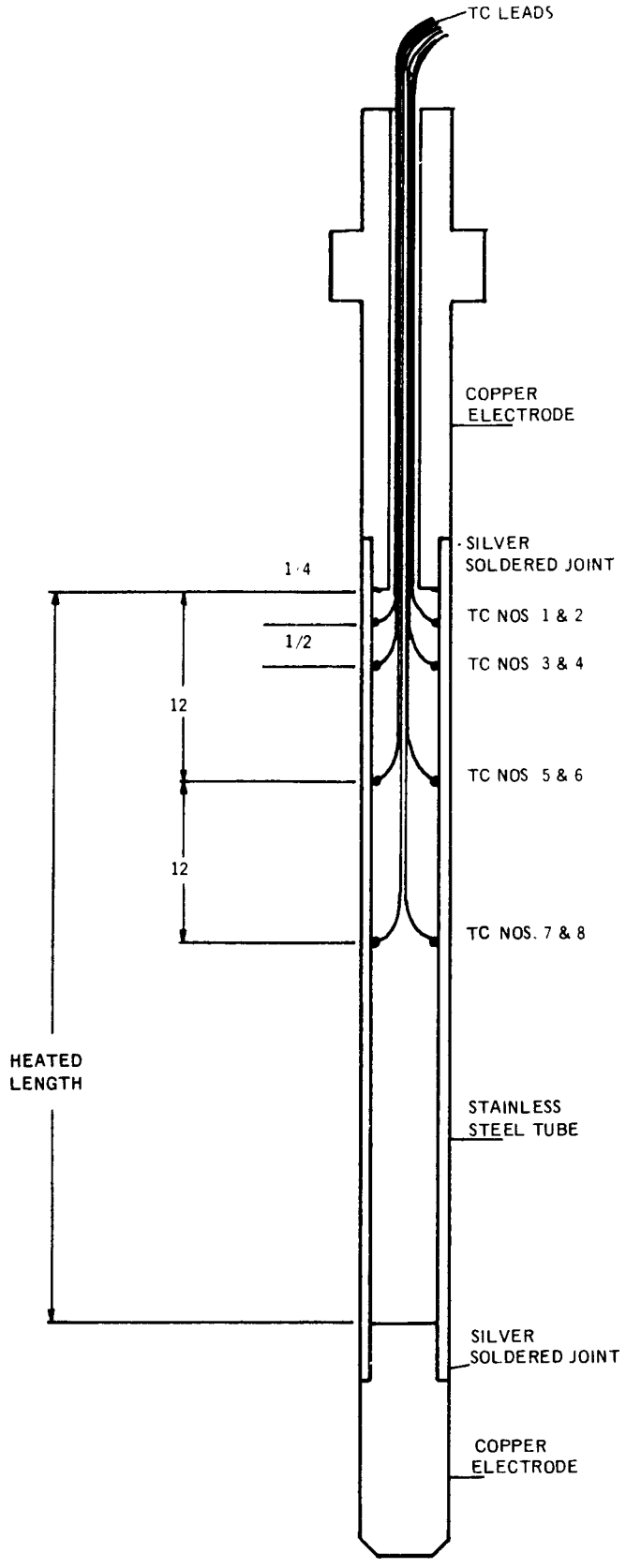

FIGURE 4 SIMULATED FUEL ROD

TABLE 1

VARIATION IN WALL THICKNESS AND RESISTANCE OF THREE HEATER RODS

Outside Diameter (inch)	Wall Thickness (inch)				Resistance (Ohms/inch)*		
	Nom.	Avg.	Min.	Max.	Avg.	Min.	Max.
.375	.058	.0571	.0566	.0575	.000998	.000991	.001005
			(-0.9%)	(+0.7%)		(-0.7%)	(+0.7%)
.500	.049	.0527	.0517	.0538	.000770	.000761	.000785
			(-1.9%)	(+2.1%)		(-1.1%)	(+1.9%)
.540	.049	.0501	.0486	.0516	.000755	.000745	.000772
			(-3.0%)	(+3.0%)		(-1.3%)	(+2.2%)

*Based measured resistance of 6-inch segments, at room temperature.

variation in resistance gradient is + 2.2, - 1.3 per cent. The corresponding variation in heat flux would be 3 per cent or less. Variations in heat flux due to variation in temperature, and hence in specific resistivity of the stainless steel, would amount to no more than an additional 1 per cent. The estimated maximum variation in heat flux for any of the uniform rods was ± 4 per cent.

Test Section

The rod was installed in a special tubular test section to form an annular flow path for the coolant. The flow cross section was constant over the entire length of the heated rod plus an unheated inlet length of 3 or more inches. The test section was mounted vertically, with flow up, for all the tests.

Two test sections were built; both were rated for 1500 psig system pressure. The first was in existence at the start of the program described in this report and is referred to hereinafter as the old test section. The second test section was built after the start of this program, and is referred to hereinafter as the new test section.

The old test section is shown in Figure 5. It has a fixed tube I.D. of 0.875 inch. The rod is held concentric in the tube by sapphire spacer pins. The spacer pins are arranged in groups of three (see detail, Figure 5). The three pins in each group are spaced at 120 degrees around the circumference and one inch apart along the axis. The groups, in turn, are spaced 24 inches apart along the axis. In addition, there are single sapphire pins located half way between adjacent groups. These single pins are all in a line, on one side of the test section.

The electrodes at the ends of the rod are attached to heavier electrodes

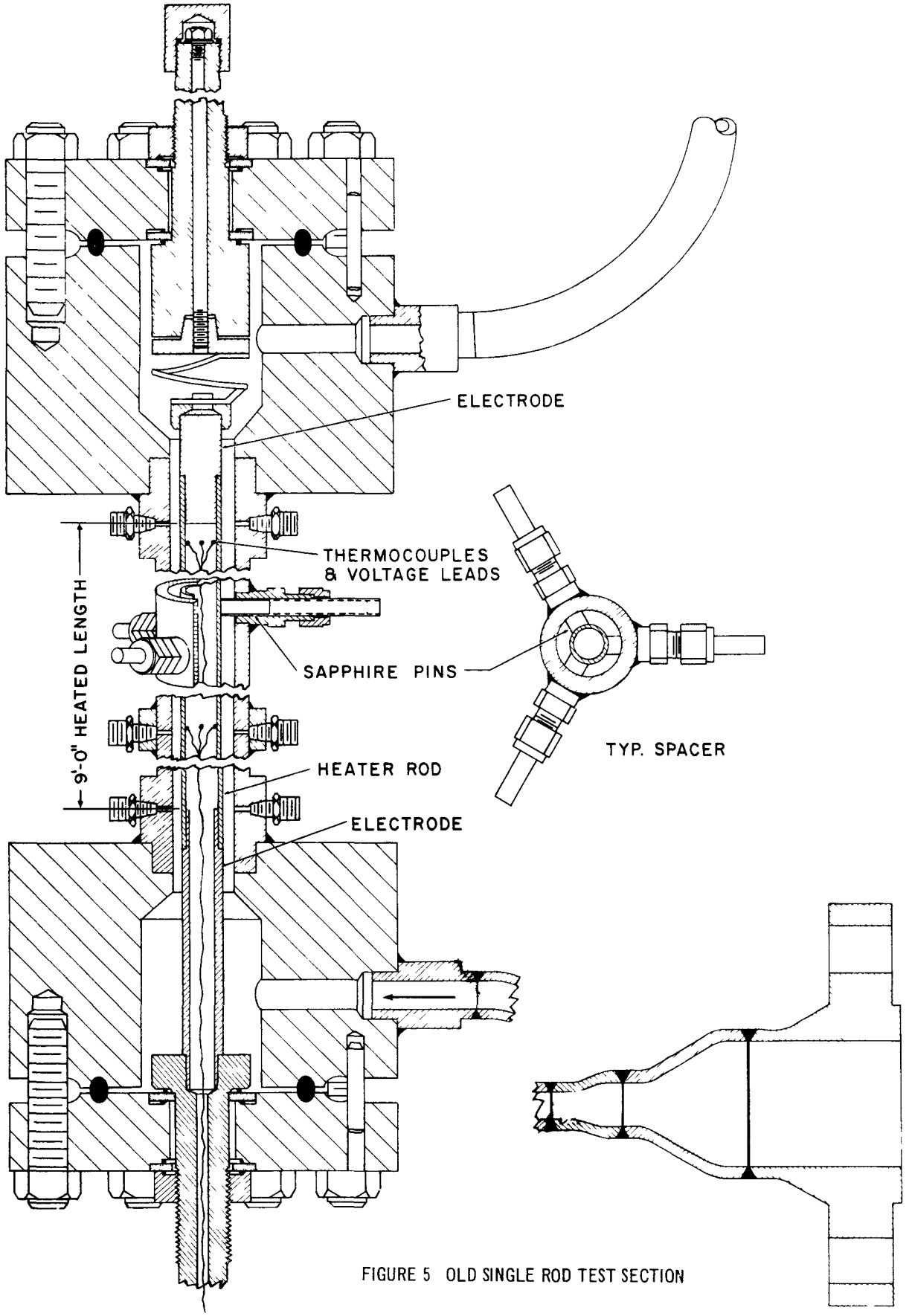

FIGURE 5 OLD SINGLE ROD TEST SECTION

which pass through flanges at the top and bottom. Ceramic washers insulate the electrodes from ground; the seal against 1500 psi system pressure is accomplished with aluminum covered asbestos rings. The attachment to the top electrode is through a flexible laminated copper helix which accommodates differential expansions of the rod due to heating. The attachment to the bottom electrode is rigid and leak-tight. The bottom electrode is drilled for the thermocouple leads from the rod.

There are plenum chambers at both the bottom (inlet) and at the top (exit) ends of the test section. Static pressure taps are spaced 18 inches apart along the axis of the test section to permit measurement of the static pressure profile. One of these taps is also used for measurement of system pressure. There is provision for inserting a sheathed thermocouple into the flow at the bottom end, for measurement of inlet temperature. This, plus system pressure, defines the inlet conditions.

The new test section is shown in Figures 6A and 6B. It offers two important new features in comparison to the old section: (1) a removable liner; and (2) light weight. The first feature makes it possible to vary one more geometrical parameter. Liners used have had the following I.D.'s: 0.555, 0.710, 0.75, 0.875, 1.00, and 1.25 inches. The second feature greatly facilitates servicing and changing rods and liners.

The new test section has other minor differences relative to the old. The spacer pins are of Rulon sheathed in stainless steel, with an unsheathed segment for insulating purposes. These hold the rod in as precise alignment as the sapphire pins, and they eliminate the problem of cracked sapphires. The new spacer pins are arranged in groups of three as before (see detail, Figure 6B), but the groups are spaced on 18-inch instead of

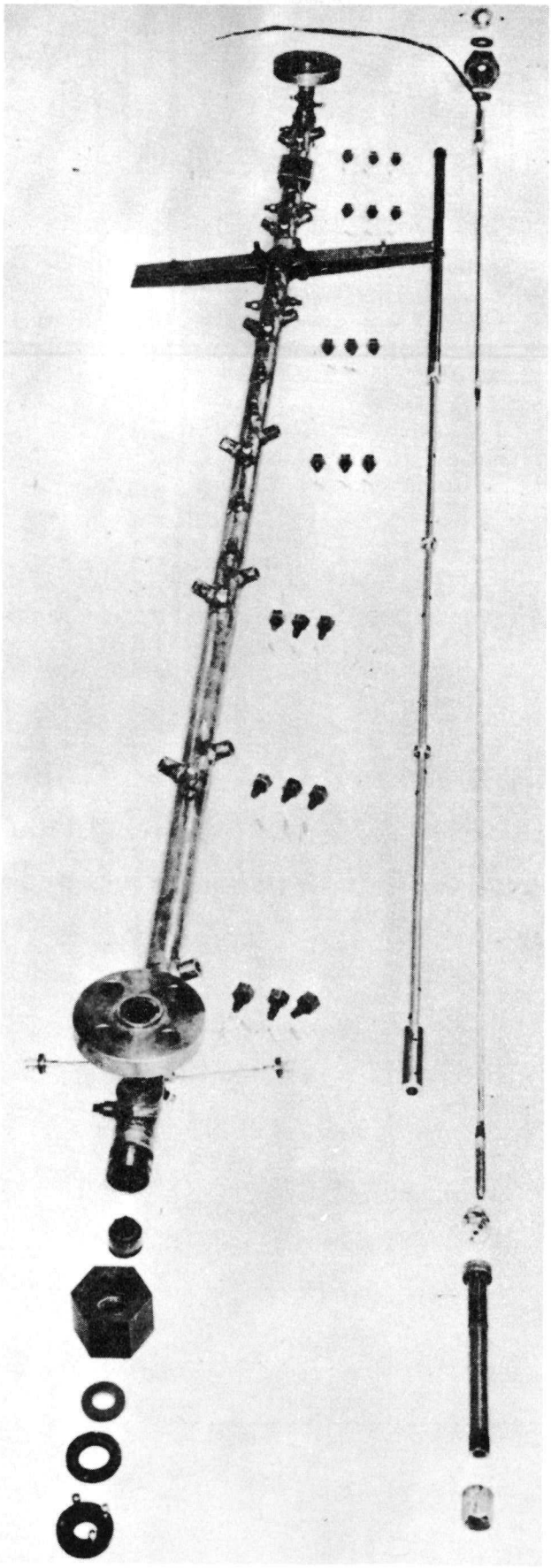

FIGURE 6A NEW SINGLE ROD TEST SECTION, EXPLODED VIEW. LINER AND ROD ARE SHOWN TO THE RIGHT OF THE TEST HOUSING.

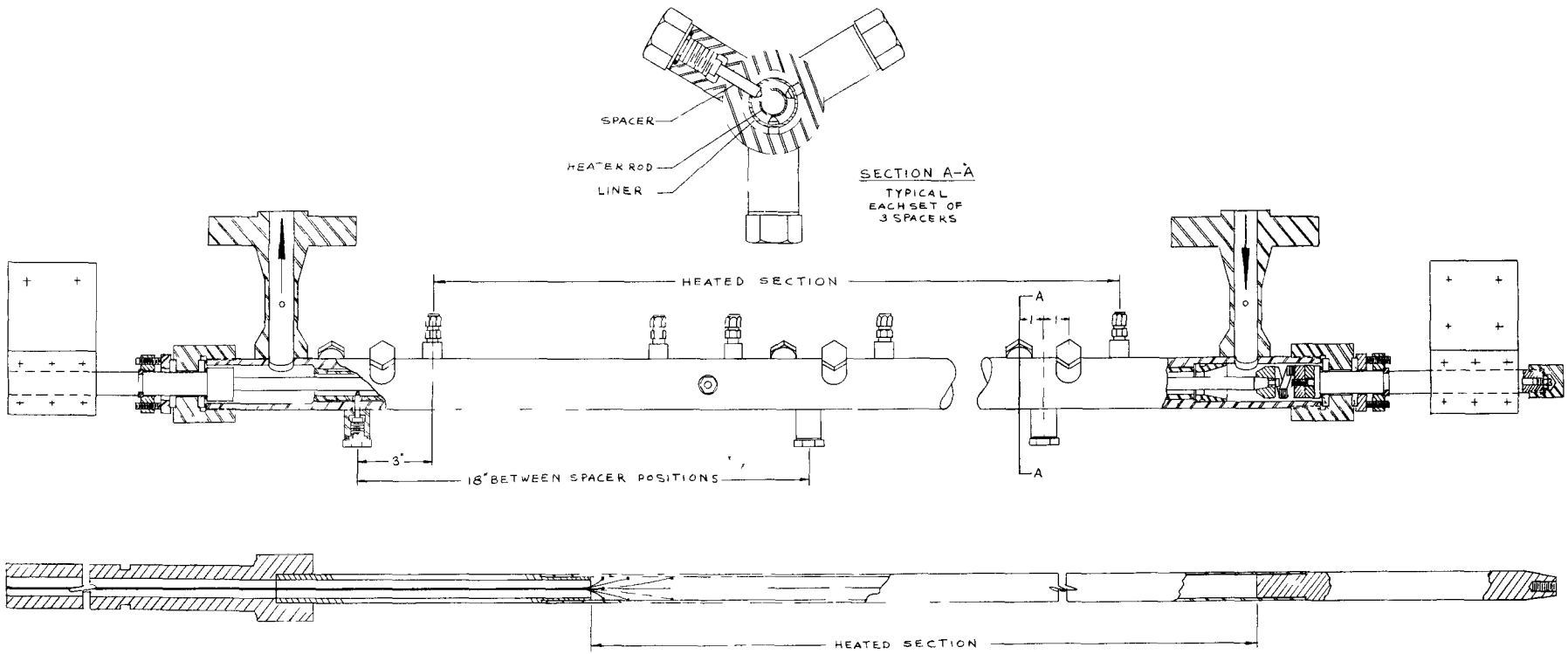

FIGURE 6B NEW SINGLE ROD TEST SECTION

24-inch centers, and there are no single intermediate pins. The heavy electrodes at top and bottom pass through nuts instead of flanges, and Rulon and Durabla washers are used for insulation and sealing. The flexible copper helix to accommodate differential expansion of the rod is normally at the bottom, and the thermocouple leads pass through the electrode at the top. There is provision for two thermocouples at the bottom (inlet) end. In other respects, the two test sections are essentially the same.

Flow Distribution in Test Section Annulus

Single-phase distribution measurements were made in the new test section with the 0.875 inch I.D. liner and a 0.540 inch diameter rod. Polar charts of the relative flow distribution around the annulus near the inlet and near the exit ends appear in Figure 7. Although the variation about the mean shown in Figure 7 (plus 6.1, minus 8.2 per cent) is not considered excessive, a special flow restricting device was built and inserted in the inlet end of the test section channel in an attempt to reduce the variation. This inlet restriction is shown in Figure 8. Polar charts of the relative flow distribution with restriction in place appear also in Figure 7. Variation about the mean at exit end with restriction is plus 4.7, minus 8.1 per cent. This is only a marginal improvement over the distribution with no restriction. Nevertheless, all the new test section runs were made with the restriction in place, except as noted in Table 3 (see PROCEDURE).

Heat Transfer Facility Loop

The test section was installed in the APED Heat Transfer Facility loop, with the flow vertical and upward. This loop has been described in an earlier report[15]. The general arrangement is shown in Figure 9. Figure 10 is

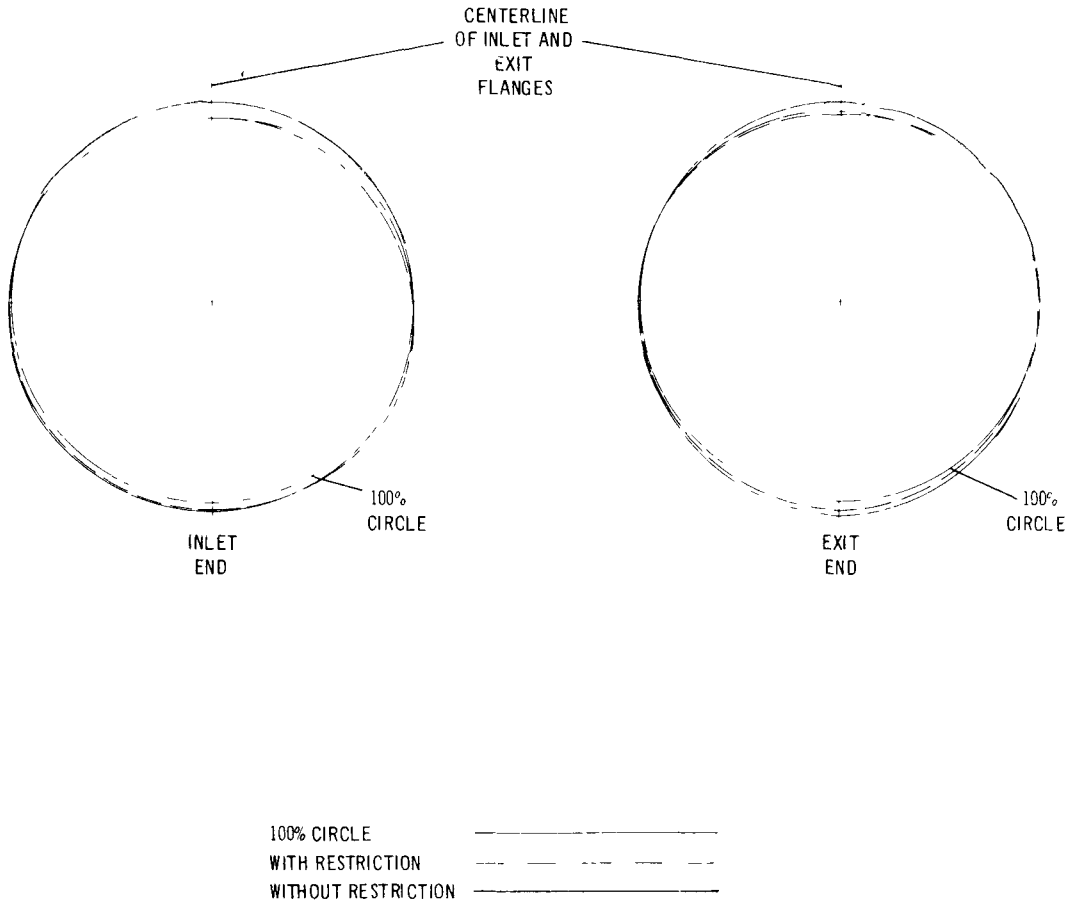

FIGURE 7 CIRCUMFERENTIAL DISTRIBUTION OF AXIAL VELOCITY FOR SINGLE PHASE FLOW IN NEW TEST SECTION, 0.540 INCH DIA. ROD, 0.875 INCH I.D. LINER

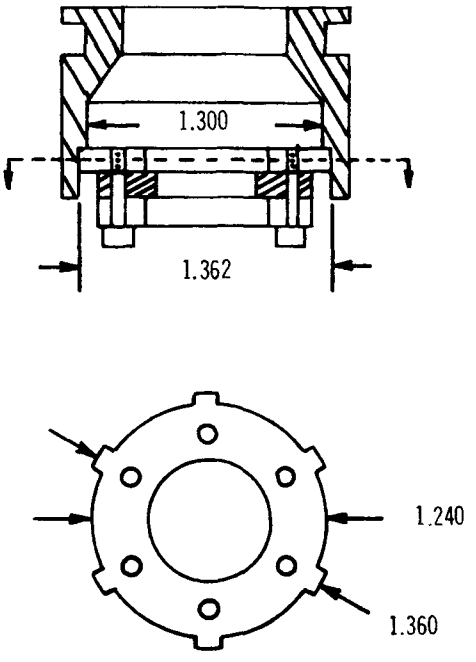

FIGURE 8 INLET RESTRICTION

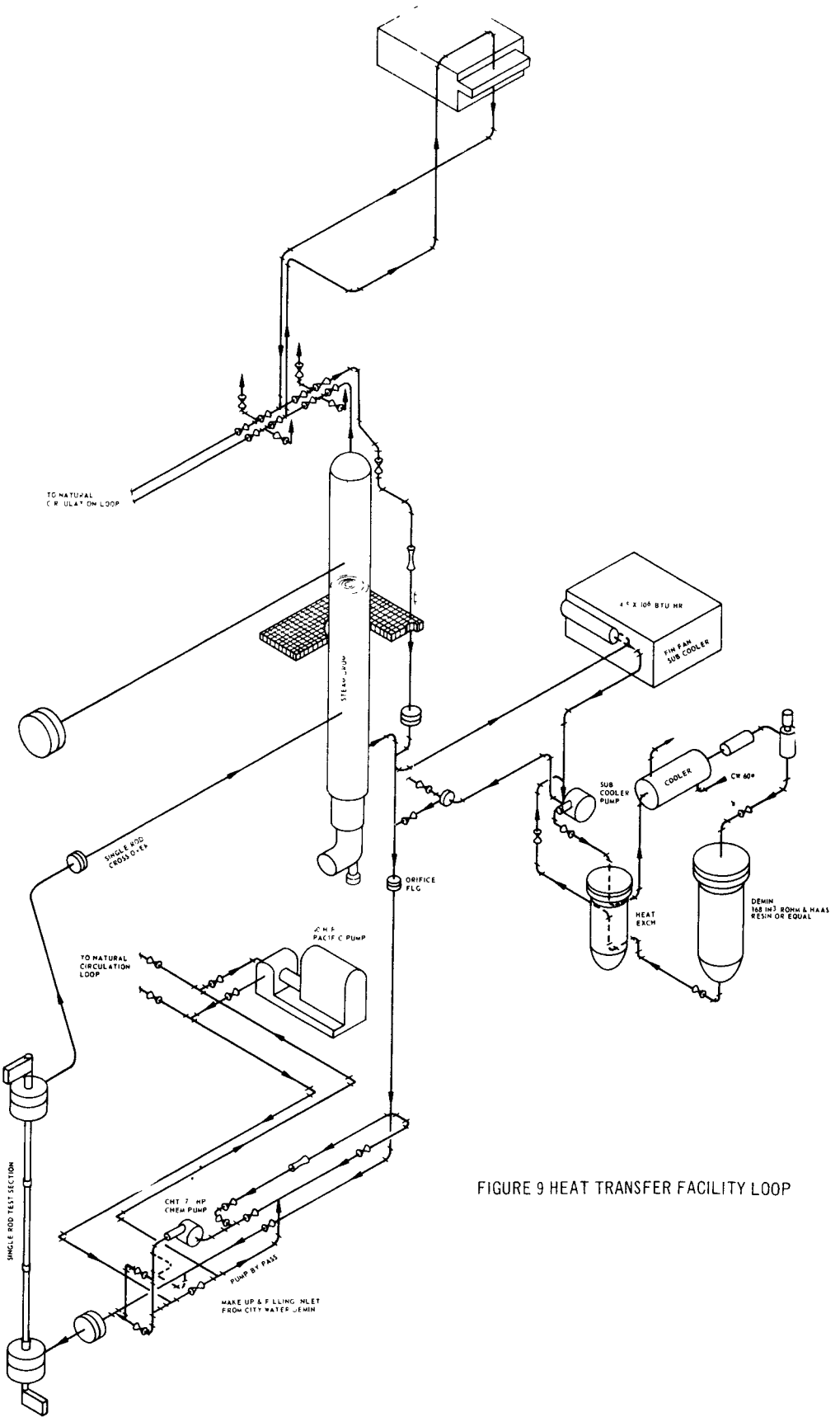

FIGURE 9 HEAT TRANSFER FACILITY LOOP

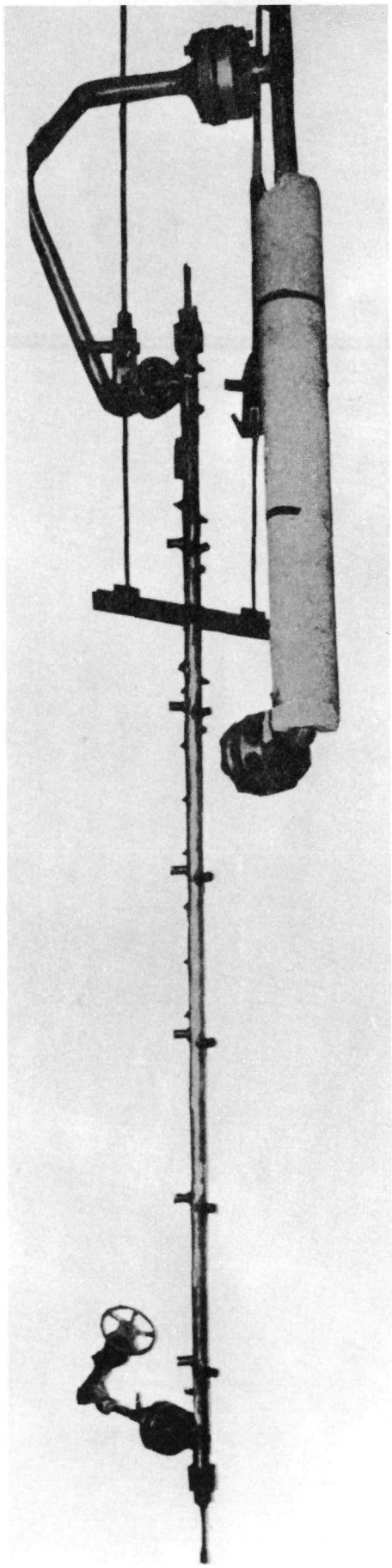

FIGURE 10 NEW SINGLE ROD TEST SECTION INSTALLED IN HEAT TRANSFER FACILITY LOOP

a photograph of the new test section in place. The loop is equipped with a pump for forced circulation, a valve for controlling the flow, a subcooler for controlling the test section inlet temperature, a riser above the test section, a steam drum, a finned condenser which functions as a heat sink (the test section is the heat source), and a louver arrangement for controlling the rate of condensation (by controlling the rate of cooling air over the outside of the condenser). The louvers are controlled by a pressure responsive servo which functions to hold system pressure constant to within $\pm$ 10 psia.

Demineralized water is used exclusively in the loop. Conductivity is used as the measure of quality of the water, and is maintained at better than 0.2 microlm·cm. The water comes directly from the demineralizer without degassing. Analysis of the water after operating the loop for a short period shows 0.1 to 0.4 ppm of dissolved oxygen. This can be taken as a measure of any air which may be in solution. On the basis of findings reported in Reference 10 on the neglibible effect of much larger amounts of dissolved hydrogen on burnout, the effect of any air in solution during the present tests is considered negligible.

An arrangement was provided, when the new test section was installed in the loop, for inserting a 25-foot section of 1/4-inch schedule 80 pipe. This arrangement is shown in Figure 11. When the 1/4-inch pipe is in the loop, it lengthens the flow path and increases the effective inertia of the water. It is exactly analogous to an inductance (except for non-linear resistance) in an electrical circuit. Insertion of the 1/4-inch pipe provided a way of altering the loop geometry external to the test section, to determine whether or not burnout was being affected by loop characteristics.

Two sizes of risers were used, .875-inch I.D. tube and 2-inch schedule 80 (1.93-inch I.D.) pipe. The risers are shown in Figures 12A and 12B. Interchanging the

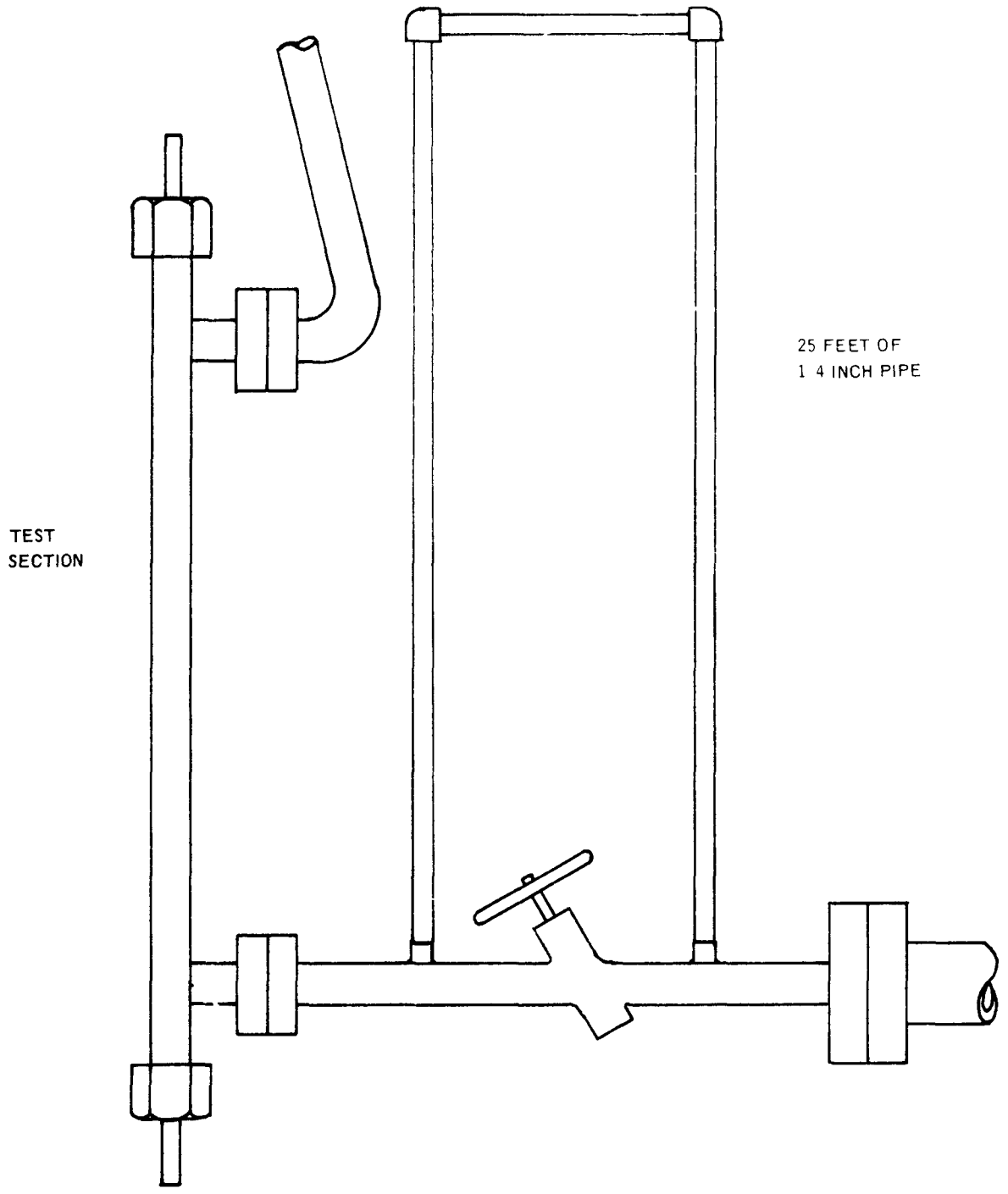

FIGURE 11 25 FEET OF 1/4 INCH PIPE AHEAD OF TEST SECTION

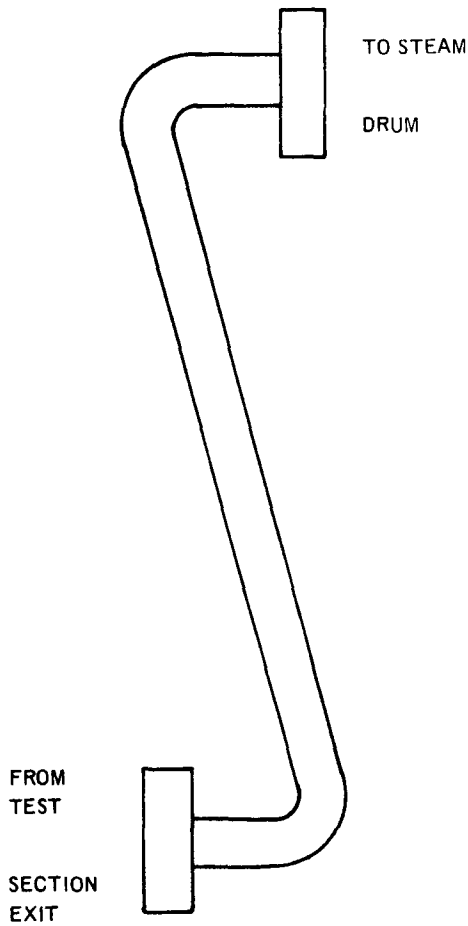

FIGURE 12A 0.875" ID RISER

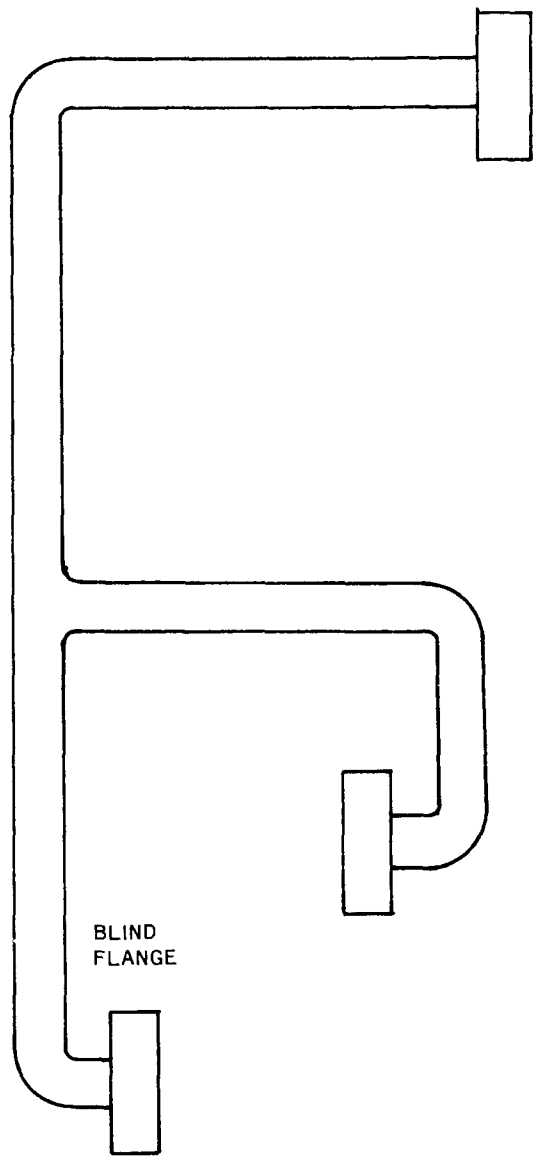

FIGURE 12B 1.93" ID RISER

two risers provided a second way of altering the loop characteristics external to the test section.

Afterheater

In order to maintain and control system pressure in the Heat Transfer Facility loop, net steam must be produced at the test section exit. The use of an "afterheater" in the top end of the test section makes it possible to obtain burnout data under subcooled conditions.

An afterheater can be added to the top end of the rod when the heated length is 6 feet or less. The principle restriction on the afterheater is that its flux must be low enough that the burnout will still occur on the test rod. The rod appearing in Figure 6A is equipped with an afterheater. An afterheater was used with all the runs made in the new test section except for the cases where the heated length was 102 to 108 inches.

Instruments

The loop is suitably instrumented to measure system pressure, flow rate, electrical power to the heated rod, and temperature at the test section inlet, as well as other less critical quantities. The more critical quantities are listed in Table 2 below, with type of measuring instrument and with estimated limits of error.

TABLE 2

Quantity	Instrument	Limits of Error
System Pressure	Heise gage, bourdon type, calibrated against dead weights and piston.	± 5 psi
Mass Rate	Orifice and 60-inch manometer. Temperature measured at orifice and manometer	± 2% (less at high flows)
Electrical Power	Recording kilowatt meter	± 3%
Test Section Inlet Temperature	Calibrated thermocouple, "cold" junction at 150 F ± 1 F, millivolts recorded with Brown Multipoint, occasional check with slide wire potentiometer.	± 3F.

Burnout Detection

In approaching the burnout point, the power is increased in small but finite steps of from one to two per cent of the total power. Detection of burnout depends upon having gone past the burnout point by a small amount (the order of one per cent or less), where upon the temperature of the affected portion of the rod starts to rise (in accordance with Figure 1). There is a corresponding rise in the local resistivity, and an attendant rise in the average resistance because of the positive thermal coefficient of resistivity for the rod material.

The burnout detection device detects small changes in resistance in that portion of the rod where burnout is anticipated. There are three voltage taps along the heater rod, typically placed with the first at the top of the rod (heated portion), the second 12 inches below the top, and the third, 24 inches below the top. The two segments of the rod thus set off by the voltage taps are made two legs of a resistance bridge. A rise in average resistance in the top segment produces an unbalance in the bridge. The resulting signal trips out the electrical power and indicates a burnout. A schematic circuit of the burnout detection device is shown in Figure 13.

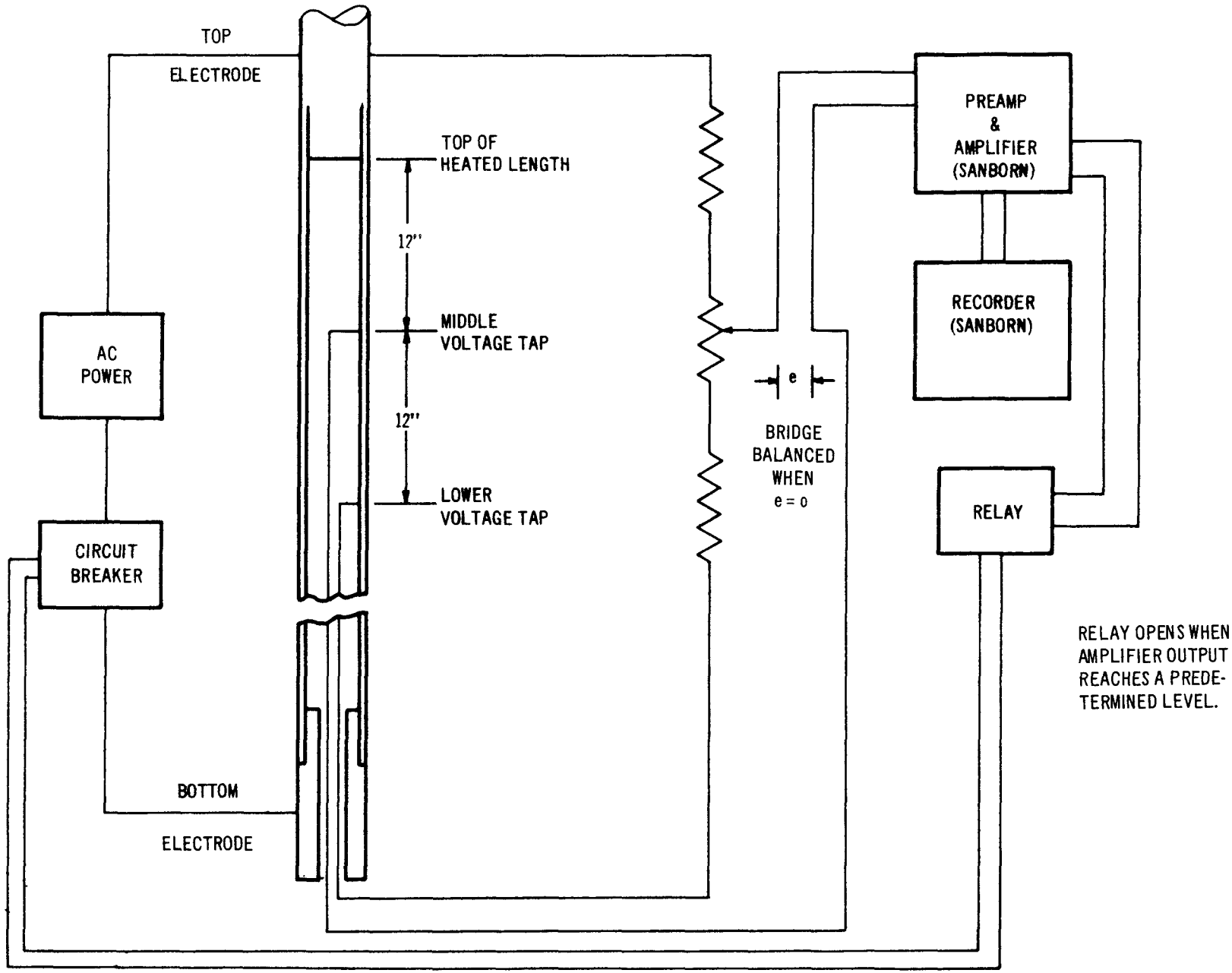

FIGURE 13 SCHEMATIC CIRCUIT OF BURNOUT DETECTION DEVICE

Once a power trip has been initiated, there is a delay of about 0.1 second before the electrical power is actually interrupted. The temperature will generally continue to climb during this period.

The detection device described above is backed up with thermocouples located in the region where burnout is anticipated. No burnout point is generally considered a valid one unless the temperature traces indicate a corresponding temperature rise at one or more thermocouple locations. A typical set of traces, in this example (run No. 602) for thermocouple Nos. 1, 2, 3, 4, and 5, is shown in Figure 14A (refer to Figure 4 for thermocouple locations).* The sixth trace appearing in Figure 14A is of the burnout detection signal Note the simultaneous rise in temperature indicated by thermocouple No. 1 and 2 and the loss of balance of the detection bridge indicated by the detection signal trace.

Special Geometries

Some variations on the simple annular geometry were also tested and are described in this subsection.

Eccentric rod tests were run,[16] in which the rod was displaced slightly from its central position in the annulus, as shown in Figure 15A. This was intended to simulate the displacement of a corner rod in a fuel bundle (see Figure 3B) toward the channel corner, due to bowing or buildup of manufacturing tolerances. These tests were completed prior to the inception of the program reported here, but are included for completeness.

---

* It will be noted that even prior to burnout the temperatures were about 200 F above saturation. This is because the thermocouples are located on the inside surface of the heater element. Heat transfer takes place because of the temperature difference between the inside and outside surfaces. When the power is tripped, the temperature drops rapidly to the test section inlet temperature.

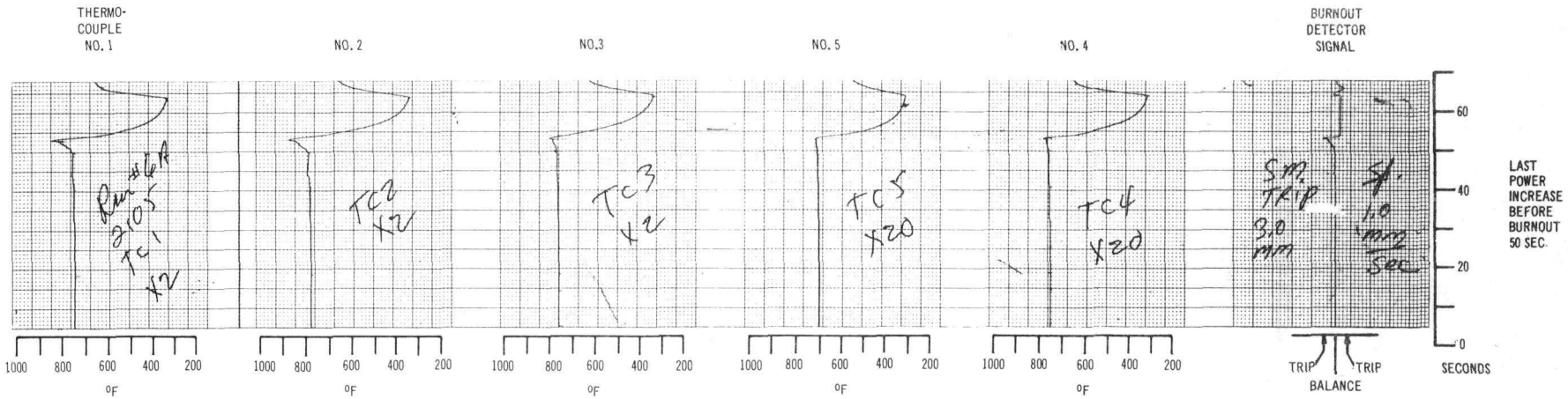

FIGURE 14A TEMPERATURE AND DETECTOR TRACES AT BURNOUT (RUN NO. 602)

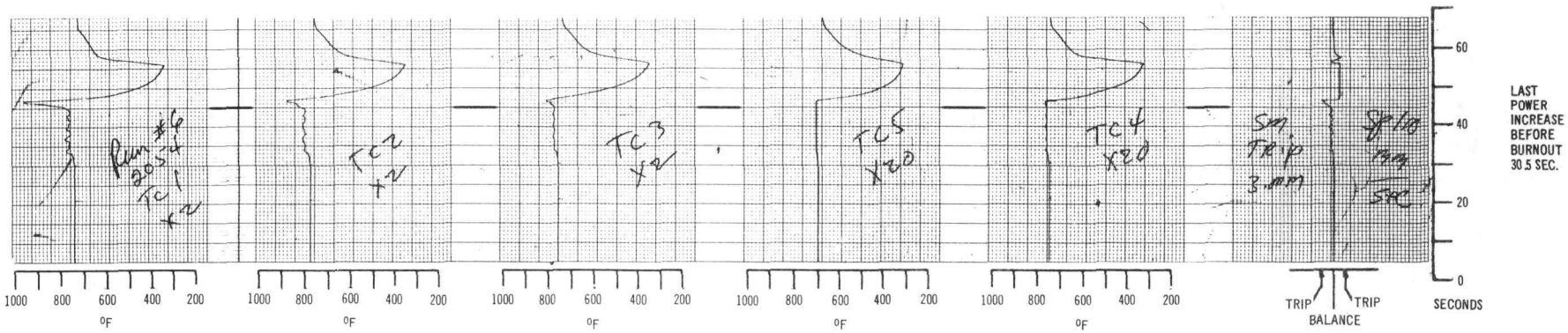

FIGURE 14B TEMPERATURE AND DETECTOR TRACES WITH OSCILLATIONS PRECEDING BURNOUT (RUN NO. 601)

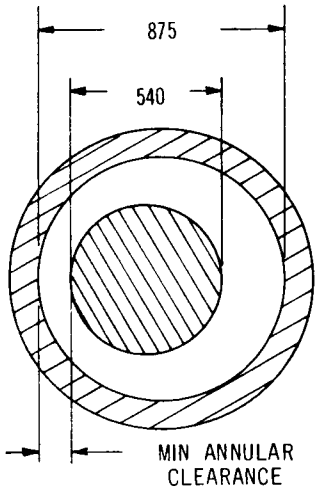

FIGURE 15A
ECCENTRIC ROD

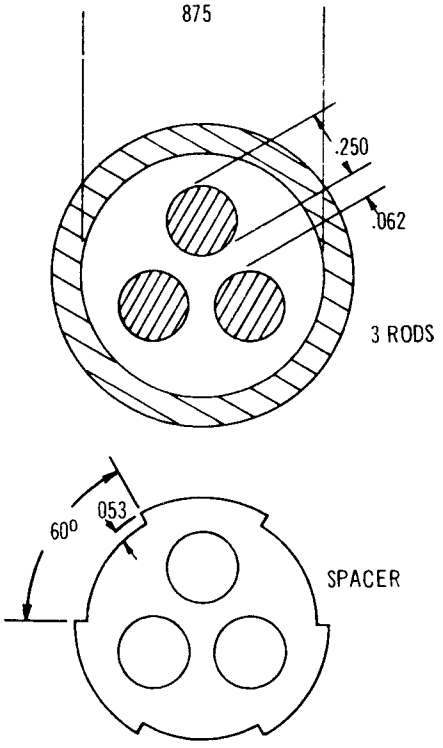

FIGURE 15B
CLUSTER OF THREE RODS

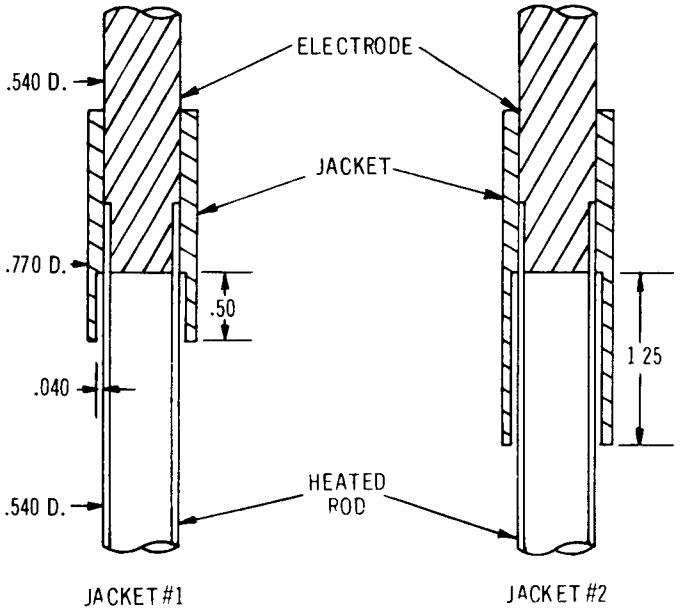

FIGURE 15C
SIMULATED SPACER

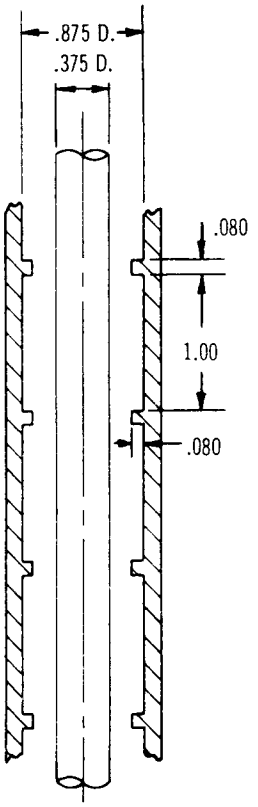

FIGURE 15D
ROUGH LINER

Tests were run with a jacket around the rod at the exit end, i.e., the burnout end,[17] as shown in Figure 15C. The jacket forced the flow to leave the heated surface at, or very near, the point of burnout. This was intended to simulate the flow conditions caused by a plate-type spacer. Two different jacket lengths were used, Jacket No. 1 covering 0.50 inch of the heated surface, and Jacket No. 2 covering 1.25 inches of the heated surface. A few runs were made with Jacket No. 1 slightly (0.015 inch) eccentric with respect to the rod. The jacket tests were also completed prior to the inception of the program reported here.

Tests were run using a rod roughened by sandblasting with coarse grit sand. One of the regular 0.540 inch rods was used for this purpose. The resulting surface did not have a high degree of uniformity, but an average roughness reading was about 300 microinches.

The last of the special annular geometry tests were run in a test section equipped with a special "rough" liner, as shown in Figure 15D. The rings produced periodic interruptions to flow along the unheated liner surface. Thus, a liquid film which might otherwise tend to form on the unheated surface was presumably forced over toward the heated surface. This particular design for the liner roughness was deliberately chosen with the intent of raising the heat flux at burnout.

In addition to the annular geometries with single rods described above, a few tests were run in the same test section using a cluster of three rods, each 1/4 inch O.D., and two simulated spacers[18], as shown in Figure 15B. This geometry was intended to simulate conditions on a reactor with plate-type spacers. These tests were also completed prior to the inception of the program reported here. The multirod results with these geometries are too few to provide a basis for any general conclusions, but are considered of sufficient interest to justify their inclusion in this report.

EQUATIONS FOR REDUCING THE DATA

The immediate goal in reducing the data is to present the burnout heat flux in terms of the parameters which govern it. As the results subsequently show, the most important parameters in addition to the geometrical dimensions, are the quality X (i.e., the enthalpy), the flow rate per unit area G, and the pressure P, at the burnout point. We need to calculate G, ϕ_{bo}, and X from the recorded data. The form of the recorded data before reduction is as follows:

Pressure, psig.

Orifice temperature, milivolts, chromel-alumel thermocouple.

Test section inlet temperature, milivolts, chromel-alumel thermocouple.

Flow, inches manometer deflection.

Room temperature, degrees F.

Power, kilowatts.

The pressure is converted to absolute pressure, P, by simply adding 15 psi to the Heise gage reading.

The orifice and test section inlet thermocouple readings are converted to degrees Fahrenheit by reference to a chart. The orifice and test section inlet temperatures are T_{13} and T_1, respectively.

The mass rate of flow is determined from the following relationships:

$$\frac{\dot{w}}{K} = w a_o \sqrt{2g\Delta h} \quad , \quad lb/sec \tag{1}$$

w = density of water at temperature T_{13}, lb/ft^3

(The steam table value for saturated liquid is used.)

$$a_o = a_{o\text{-}75}\left[1 + 2\alpha\left(T_{13} - 75\right)\right] \quad , \quad ft^2 \tag{2}$$

$a_{o\text{-}75}$ = Orifice area at 75^oF, ft^2

α = linear coefficient of expansion for 304 stainless steel (Both the orifice plate and flanges are of this material.)

g = 32.17 ft/sec^2

$$\Delta h = \frac{w_r}{w}\left[\left(\frac{w_{man}}{w_r} - 1\right)\frac{\Delta h'}{12} - \Delta z\left(1 - \frac{w}{w_r}\right)\right], \quad ft \tag{3}$$

w_r = density of water at room temperature T_r, lb/ft^3

w_{man} = density of manometer fluid at room temperature T_r, lb/ft^3

Δz = elevation of upstream orifice tap minus elevation of downstream orifice tap, ft.

K = Orifice discharge coefficient, which can be specified in terms of $\frac{N_R}{K}$

$$\frac{N_R}{K} = \frac{\dot{W}}{K}\frac{D_o}{a_o}\frac{1}{\mu} \tag{4}$$

D_o = orifice diameter, ft.

μ = viscosity of water at temperature T_{13}, lb/sec-ft

The total flow rate is obtained from

$$W = K\left(\frac{\dot{W}}{K}\right), \quad lb/sec \tag{5}$$

and the flow rate per unit area is equal to

$$G = \frac{\dot{W}}{a} \times 3600, \quad lb/hr\text{-}ft^2 \tag{6}$$

where a is the cross sectional area of flow.

The electrical power is converted to equivalent thermal units:

$$q = 0.948 \times (kilowatts), \quad Btu/sec \tag{7}$$

The heat flux ϕ is the thermal energy rate divided by the heat transfer area.

$$\phi = \frac{q}{A} \times 3600, \quad Btu/hr\text{-}ft^2 \tag{8}$$

The subcooling in enthalpy units is given by

$$\Delta h_s = h_f - h_1 \quad , \quad \text{Btu/lb} \tag{9}$$

where h_f is the enthalpy of saturated water at pressure P, and h_1 is the enthalpy of water at temperature T_1. (The steam table value for saturated water at temperature T_1 is used.)

The quality at test section exit is given by

$$X_e = \left[\frac{q}{w} - \Delta h_s\right] \frac{1}{h_{fg}} \tag{10}$$ *

Because, as discussed later, burnout occurs consistently at the exit end, the exit quality is also taken as the quality at burnout.

The foregoing relationships provide the means for calculation of G, ϕ_{bo}, and X directly from the test data.

---

* Note that the exit quality X_e is negative when the bulk state of the fluid at exit is subcooled. In this case

$$X_e = -(\text{Bulk subcooling at exit, Btu/lb}) \frac{1}{h_{fg}}$$

PROCEDURE

All of the combinations of geometrical plus pressure and flow parameters which were tested for burnout are listed in Table 3. The testing procedure for any given combination was as follows:

1. Supply electrical power to the test section until a quasi-steady condition is reached, whereby the steam drum contains both steam and water, in thermodynamic equilibrium.
2. Adjust the louver servo to regulate system pressure at the desired value.
3. Set the flow at some predetermined value and manually regulate the flow to hold this value constant.
4. Adjust the subcooler to give approximately the desired value of inlet subcooling.
5. Bring up slowly the electrical power until a burnout is indicated. The pressure, flow, power, and inlet subcooling which exist at the time of burnout indication constitute the data for a burnout point.
6. Either the subcooling or the flow is changed to a new value and step 5 is repeated.
7. Steps 5 and 6 are repeated several times until the burnout characteristics for the given rod, pressure, and the flow are adequately defined.

If, in step 6, for each succeeding run the inlet subcooling was changed and the flow held constant, the procedure outlined above is referred to hereinafter as the constant flow procedure.

If, on the other hand, the subcooling control was held at one position and the flow changed to a different value for each succeeding run, the procedure is referred to hereinafter as the variable flow procedure. This procedure was used exclusively at first but was for the most part discontinued early in the program, starting with combination number 12 of Table 3.

Even though, under the variable flow procedure, the subcooling control was held at one position, the subcooling decreased slightly as the flow was increased. However, it varied over only a limited range for a given setting of the control. The runs made under the variable flow procedure have been arbitrarily classified according to the level of inlet subcooling as follows:

Low subcooling runs:	$\Delta h_s \leq 125$ Btu/lb
Medium subcooling runs:	125 Btu/lb $< \Delta h_s \leq 175$ Btu/lb
High subcooling runs:	$\Delta h_s > 175$ Btu/lb

TABLE 3

SINGLE* ROD PARAMETER COMBINATIONS

ANNULAR CHANNEL, CONCENTRIC EXCEPT AS NOTED.

D_1 = Rod Dia. D_h = Hydraulic dia.

D_2 = Tube (liner) Dia. L = Heated length

Comb. No.	D_1 (in.)	D_2 (in.)	D_h (in.)	L (in.)	P (psia)	$G/10^6$ (lb/hr ft^2)	Special Features: (O=Old Test Sect. N=New Test Section)
1.	0.540	0.875	0.335	102	1000	0.26 - 1.19	O; rod concentric
2.						0.42 - 1.19	O; rod eccentric, 0.096 inch minimum annulus.
3.						0.44 - 1.29	O; rod eccentric, 0.061 inch minimum annulus.
4.						0.25 - 1.23	O; rod eccentric, 0.033 inch minimum annulus.
5.	three 0.250	0.875	0.355	54	1000	0.33 - 0.74	O; cluster of three rods, two sim. spacers.
6.	0.540	0.875	0.335	102	1000	0.65 - 1.27	O; Jacket No. 1 (sim. spacer)
7.						0.79 - 1.45	O; Jacket No. 1 - 0.015 in. eccentric
8.						0.58 - 1.38	O; Jacket No. 2
9.	0.540	0.875	0.335	102	1000	0.42 - 1.35	O.
10.					600	0.40 - 1.53	O.
11.					1000	0.39 - 1.48	O; rod sandblasted, 300 micro-inch rms.
12.						1.12	O.
13.						0.56	O.
14.						1.54	O.
15.						0.84	O.
16.					1450	1.12	O.
17.					600	1.12	O.
18.	0.540	0.875	0.335	108	1000	1.12	N; 0.875 inch I.D. riser ** (loop configuration No.1)
19.						0.56	N; 0.875 inch I.D. riser, 25 ft. of 1/4 inch pipe ahead of test section (configuration No. 2)
20.						1.12	N; 1.93 inch I.D. riser, restriction in test section inlet (configuration No. 3) ***
21.						0.56	N.
22.						1.68	N.
23.						0.29 - 1.68	N.
24.	0.540	0.875	0.335	72	1000	1.12	N.
25.						0.56	N.
26.						1.68	N.
27.						0.30 - 1.42	N.

* Except for the three rods of combination No. 5.

** All the preceding runs with the old test section were also with 0.875 inch I.D. riser.

*** The restriction was in place for all subsequent combinations except as noted. The two riser sizes were used interchangeably on all subsequent combinations, no effect due to riser size being discernable.

TABLE 3 (CONT.)

Comb. No.	(in.)	(in.)	(in.)	(in.)	(psia)	(lb/hr ft^2)	Special Features: (O = Old Test Sect. N = New Test Sect)
28.	0.375	0.875	0.500	108	1000	1.12	N.
29.						1.68	N.
30.						0.56	N.
31.						0.84	N.
32.	0.375	0.875	0.500	70	1000	1.12	N.
33.						1.68	N.
34.						0.56	N.
35.					600	1.12	N.
36.						1.68	N.
37.						0.56	N.
38.					800	1.12	N.
39.					1200	1.12	N.
40.					1400	1.12	N.
41.						1.68	N.
42.	0.375	1.250	0.875	70	1000	0.56	N.
43.						0.28	N.
44.						0.14	N.
45.						1.12	N.
46.	0.375	0.710	0.335	70	1000	2.24	N.
47.						1.68	N.
48.						1.12	N.
49.						0.56	N.
50.	0.375	0.555	0.180	70	1000	2.24	N.
51.						1.68	N.
52.	0.500	1.00	0.50	29,36	1000	4.0	N. *
53.				29,36		2.0	N. *
54.				36		1.68	N. *
55.				36		6.0	N. *
56.					1400	4.0	N. *
57.	0.500	0.75	0.25	36	1000	4.0	N. *
58.						2.0	N. *
59.					1400	4.0	N. *
60.					1000	6.0	N. *
61.	0.500	1.00	0.50	29	1000	0.4	N. *
62.						0.2	N. *
63.						0.6	N. *
64.	0.375	0.875	0.500	70	1000	0.56	N; rough liner.
65.						1.12	N; rough liner.
66.						1.68	N; rough liner.

* Restriction removed from test section inlet for this combination.

RESULTS AND DISCUSSION

General

The appearance of a rod prior to testing was characteristically that of stainless steel tubing as received from a tubing vendor. It had a bright metallic sheen, and the mill markings were still on the tube when installed in the test section. The rod was ordinarily not removed from the test section until it had actually failed, usually attributable to too slow a response on the part of the burnout detector. Occasionally, the rod was removed for other reasons, such as that the tests might be complete for that particular rod. The rod after testing still had a metallic appearance but was dulled and colored by what was apparently a very thin oxide film. The coloration suggested iron oxide. The color darkened abruptly in the region of burnout, usually to black, even though the rod might not actually have failed.

For every burnout run there is a set of Sanborn recorder traces indicating a temperature rise in the burnout region (i.e., the last one inch of the heated portion of the rod). A typical set of such traces appears in Figure 14A. The traces of Figure 14A are typical in that they display certain essential characteristics, viz, one or more thermocouples indicate a sharp rise of temperature in the burnout region, and the burnout detection signal trace indicates a bridge unbalance. For many of the other burnout runs the traces show characteristics in addition to those of Figure 14A, or are different in certain other respects, but are still considered valid evidence of burnout. For example, several of the runs ended by one of the technicians observing a sharp rise in one of the thermocouple traces, and shutting off the electrical power manually. There may have been little or no indication of bridge unbalance for such runs, but they are considered valid, nevertheless.

For a few of the runs the trace for one of the thermocouples located a foot ahead of the exit end also showed a temperature rise. It can only be concluded that conditions for burnout occurred relatively simultaneously over several inches of the heated rod. For such runs, the burnout condition has nevertheless been taken to be that at the exit end.

For perhaps 40 per cent of the runs there is evidence of impending burnout several seconds before the clear indication of burnout occurred. This evidence is in the form of oscillations in either one or more of the thermocouple traces, or in the burnout detection signal trace, or both. An example of a set of traces showing this behavior appears in Figure 14B. No study has been attempted of this before-burnout behavior.

Power at Burnout

At (or just past) the burnout point there is a change in the rod resistance, an essential condition for the burnout detection scheme to function. But this change is quite local and has a negligible effect on the total rod resistance and hence on the total power. There was never any evidence of power transients just prior to burnout. (The small transients associated with the gradual increase in power as the burnout point is approached, are, of course, excepted.)

Pressure at Burnout

The system pressure oscillated slightly ($\pm$ 10 psi maximum) about a mean, the period varying but being of the order of three minutes. There was no other change detected in the system pressure just prior to burnout.

Reproducibility of Data

An important measure of the quality of data is their reproducibility. Conditions may be duplicated within the limits of the techniques being employed, and tests

repeated. Variation in results is scatter. The quality of data bears an inverse relationship to that part of the scatter which is due to measurement error.

It must be borne in mind that absence of scatter does not insure that the data are error free. Constant errors may be present in both the original and repeated results. Conversely, the presence of scatter does not mean that the data points are necessarily in error. This may truly be a characteristic of the phenomenon under investigation, and will be referred to here as inherent scatter.

The evidence is that burnout data when obtained under carefully controlled conditions has very little inherent scatter (see for example the data of Figure 16A, for L = 70"). Moreover, because all of the instruments are calibrated, it is believed that any constant error is negligibly small. Therefore, the observed scatter is indicative of the total error, which is the cumulative effect of small errors associated with:

1. Imperfect duplication of geometry due to slight bending or eccentricity of the rod, slightly different inlet conditions (compare old and new test section data).
2. Error in reading instruments used in measuring conditions at burnout.

The scatter was as high as $\pm$ 15 per cent, but was generally less than this, indicating good reproducibility. The most rigorous check of reproducibility is shown in Figure 17B. The repeat runs were made four months after the original. For any given flow, the data fall within a $\pm$ 10 per cent limit, and are generally much better than $\pm$ 10 per cent.

Effect of Loop Characteristics on Flow and Burnout

In any experimental work one attempts to minimize the effect of, or at least hold constant, all of the variables which can possibly influence the results except those under investigation. Thus, in burnout work one undertakes to exercise some control over the purity of the water, the quality of finish of the heat transfer surface, the uniformity of heat flux, etc. One of the variables which it is important to minimize is the degree of dynamic coupling between the test section and the rest of the loop. If such a coupling exists, flow instability is a possibility, and can affect adversely the burnout performance under certain operating conditions.

A check was made to determine if such a coupling existed in the case of the single rod test section. Burnout data were obtained with the loop external to the test section in a normal configuration (Configuration No. 1, no restriction at inlet, .875 inch ID riser) using both the old and the new test sections. The flow was set at a certain value for each burnout run, and maintained at that value manually as the burnout point was approached by bringing up the power. There was no indication at any time of flow transients just prior to burnout. A sensitive pressure differential transducer across the orifice taps for a few of the runs confirmed the absence of any transients.

The configuration was then modified to:

Configuration No. 2 - (Twenty-five feet of 1/4-inch schedule 80 pipe inserted in the loop ahead of the new test section (Figure 11); this is analogous to adding an inductance to an electrical circuit) and

Configuration No. 3 - (Riser I.D. changed from 0.875 inch to 1.93 inches and a restriction (Figure 8) installed in the inlet end of the new test section annulus).

Burnout data were obtained with Configuration Nos. 2 and 3 and compared with the "normal" configuration No. 1, in Figures 30B and 30A, respectively. The changes included in Configurations 2 and 3 should tend to suppress coupling if it in fact existed, and hence raise the burnout heat flux.[14] But Figures 30A and 30B show that no change in heat flux resulted from the change to either configuration 2 or 3. It was concluded that any dynamic coupling which might exist between the test section and the rest of the loop was negligible for all three configurations.

For the remainder of all of the runs with the new test section, the inlet restriction of configuration No. 2 was in place (except as noted in Tables 3 and 4). This was primarily for the marginal improvement in annular flow distribution noted earlier (see section titled Equipment) for cold single-phase flow. The .875 and 1.93 inch I.D. risers were used interchangeable for the remainder of all of the runs with the new test section. It was not considered necessary to identify the riser for any particular run.

Inspection of burnout results reported by the Russians[14] supports the conclusion that the burnout results reported here are unaffected by loop characteristics. The data reported by the Russians obtained under hydraulically stable conditions varied about linearly with quality. The data reported here also varies about linearly with quality. On the other hand, when the Russians modified their loop to induce instabilities, the data varied in a non-linear manner with quality, and fell below the straight line through the stable data, particularly at low qualities. Data obtained elsewhere (see for example, Reference 13) which falls below the data reported here show the same kind of behavior at low qualities.

Burnout Results

The results of all the burnout runs are listed in Table 4. These results have been ordered in certain ways and so plotted on graphs to show the effect of certain parameters on burnout. A description follows of the effects of these parameters and of the graphs which display these effects.

Effect of Quality on Burnout

The data were obtained under procedures which caused the quality to change while all other parameters except flow or inlet subcooling were held constant. The results are presented in Figures 16A through 30B, and 33 through 35, as plots of heat flux at burnout ϕ_{bo} versus quality X, for each combination of the other parameters. Consistently and without exception, these plots show a decrease in ϕ_{bo} with increase in X. This is in general agreement with results by other workers in the field for qualities up to about 50 per cent (see, for example, References 10 through 14). The exceptions observed by some at low qualities are believed to be due to flow instabilities present in their test loops.

Effect of Flow on Burnout

Most of the data were obtained under the constant flow-variable subcooling procedure. Each set of such data is characterized by a single value for the flow. Comparison of two sets, each at a different flow, shows the effect of flow on burnout.

Figure 16A is a plot of three sets of data, each at a different flow. The geometry (except for heated length) and the pressure are constant; 0.375 O.D. rod, 0.875 I.D. tube, 1000 psia. Figures 16B through 20 are similar to Figure 16A, each figure corresponding to a particular geometry and pressure, and each displaying three or more sets of data; each set at a particular value of flow. The geometry and pressure conditions for these figures are summarized below.

Fig. No.	D_1 (in.)	D_2 (in.)	L (in.)	P (psia)	
16A	.375	.875	70,108	1000	
16B			70	600	
16C			70	1400	
17A	.375	1.250	70	1000	
17B		.710	70	1000	
17C		.555	70	1000	
18A	.540	.875	70,102,108	1000	
18B			102	1000	
19A	.500	1.00	29,36	1000	
19B		.75	36	1000	
20	.375	.875	70	1000	"Rough Liner"

The same general description applies to all the figures from 16A through 19B. Consider one particular figure from this group. Inspection of this figure shows the following:

1. Within the range of test conditions, for any given flow, except for some experimental scatter (of the order of plus or minus 10 per cent maximum), the points lie on a straight line. The straight line slopes downward in the direction of increasing quality.
2. The straight line thus defined for each flow is nearly parallel to the straight lines for each of the other flows; although there is a tendency, particularly apparent in 16A, 18A, and 18B, for the lines to converge in the direction of decreasing quality.
3. At any given quality at which there are data for two flows, the line for the higher flow lies below the other line, i.e., the burnout heat flux is lower for the higher flows. This is the flow effect which is shown consistently by all the single rod data at flows of 2×10^6 lb/hr-ft^2 or less, except for the rough liner (Figure 20). Figures 16B and 16C show that it holds even at 600 and at 1400 psia.

The effect of flow on the burnout heat flux may better be illustrated by the curves of Figure 36, which are smoothed cross plots from the data of Figure 19A.

Other things being the same, a higher flow results in a lower burnout, up to flows of about 2 x 10^6 lb/hr-ft^2.* This is confirmed by all the data (except rough liner).

Figure 20 is in contrast to the other figures described above. For any given flow, the points may be fitted closely by a straight line, but the line for one flow is not parallel to the lines for either of the other two flows, the slope being small at the lowest flow and increasing as the flow increases. Moreover, at any given quality at which there are data for two flows, the value of burnout is very nearly the same for both flows. In other words, burnout for the rough liner is nearly independent of the flow.

Effect of Heated Length on Burnout

The length of rods tested varied from 29 inches to 9 feet, to correspond to actual lengths of fuel rods encountered in current reactor design. It was not anticipated that there would be a length effect (i.e., L/D effect). Some of the conditions for the 8-1/2 and 9-foot rods were repeated with the 6-foot rods to check this.

The plot of data for the middle flow condition ($G/10^6$ = 1.12) of Figure 18A may be considered a plot of two sets of data, both with the same rod and tube diameters (0.540 inch O.D. and 0.875 I.D., respectively), and at the same pressure (1000 psia), but with different heated lengths. The heated length for one set is 8-1/2 and 9 feet, and for the other set, it is 6 feet. In the range of qualities where these two sets may be compared, the points corresponding to L = 6 feet tend to be low. The tendency is strongest at the highest qualities and disappears at the lowest qualities. Even at the highest qualities, the points are still within the $\pm$ 10 per cent scatter. The same observations hold

---

* There is some indication that this trend may be reversed for flows past about 4 x 10^6 lb/hr-ft^2 (see Figure 36).

for $G/10^6 = 1.68$. For $G/10^6 = 0.56$, there is no discernible difference between the L = $8\frac{1}{2}$ - 9 ft., and the L = 6 ft. sets.

Figure 16A is similar to Figure 18A, each displaying for each flow two sets of data corresponding to two different heated lengths. The heated lengths are again 9 feet for one set and 6 feet for the other. In the case of Figure 16A, however, the points corresponding to L = 6 feet tend to be high, the tendency being strongest at the highest qualities and disappearing at the lowest qualities. Even at the highest qualities, the points are still within $\pm$ 15 per cent scatter.

It is obvious in comparing data for L = 6 feet and L = 9 feet in Figures 16A and 18A that (a) there is no consistent trend with heated length and, (b) any differences in burnout associated with differences in heated length are still within acceptable experimental scatter.

Comparisons can be made between results taken at $G/10^6 = 1.68$ with L = 29 inches (Figure 19A) and with L = 9 feet (Figure 16A). In addition to the differences in heated length, the rod diameters are different (D_1 = 0.50" and D_1 = 0.375", respectively). The results are in agreement within experimental scatter.

It is concluded in a later subsection, independent of the considerations for this subsection, that rod diameter is not a significant parameter. It can be concluded here that the heated length is also not a significant parameter in the range of lengths from 29 inches to 9 feet.

Effect of Hydraulic Diameter on Burnout

The hydraulic diameters tested varied from 0.180 inch to 0.875 inch, which brackets current reactor design practice. It was not practical to test at the

same flow conditions for the largest hydraulic diameter as were employed for the smallest. However, with three intermediate diameters there was substantial overlapping of conditions.

Comparison of two or more sets of data, each for a different hydraulic diameter but in every other respect the same, shows the effect of hydraulic diameter on burnout. Figure 21A is a plot of two sets of data at two different hydraulic diameters $D_h = 0.180$ and $D_h = 0.335$. The rod diameter, flow, and pressure are constant; 0.375 inch, 2.24×10^6 lb/hr-ft^2, and 1000 psia. Figures 21B through 22D are similar to 21A, each figure corresponding to a particular rod diameter, flow and pressure and each displaying two or more sets of data, each set for a particular hydraulic diameter. The flow, rod diameters, and pressure condition for these figures are summarized below:

Fig. No.	D_1 (in)	$\frac{G}{10^6}$	P psia	Fig. No.	D_1 (in)	$\frac{G}{10^6}$	P psia
21A	0.375	2.24	1000	22A	0.500	2.0	1000
21B	0.375	1.68	1000	22B	0.500	4.0	1000
21C	0.375	1.12	1000	22C	0.500	6.0	1000
21D	0.375	0.56	1000	22D	0.500	4.0	1400

The effect of hydraulic diameter on burnout is not as pronounced as, say, the effect of flow. But it is apparent from inspection of Figures 21A through 22D that hydraulic diameters which are less than 0.25 in. and hydraulic diameters which are greater than about 0.5 in. both result in a reduction in the burnout heat flux.

To show this effect more clearly, cross plots have been prepared from the data of Figures 21B through 22D, at the two qualities $X = 0.03$ and $X = 0.12$. The resulting points are plotted in Figure 37. The curves through the points of Figure 37 show the relative effect of hydraulic diameter on the heat flux at burnout.

The hydraulic diameter appears to have little, if any, effect in the range $0.25 \text{ in.} \leq D_h \leq 0.50 \text{ in.}$ But when D_h is decreased to 0.18 in., there is a definite reduction in the burnout heat flux. When it is increased to 0.875 in., there is again a definite reduction in the burnout heat flux.

It appears that the optimum value for the hydraulic diameter lies in the neighborhood of 0.25 in. to 0.50 in., at least for a system pressure of 1000 psia and flows up to about 2×10^6 lb/hr-ft^2. There are too few data at pressures other than 1000 psia, or at flows greater than 2×10^6 lb/hr-ft^2, to show whether and how the hydraulic diameter effect is influenced by high or low pressures or high flows.

Effect of Rod Diameter on Burnout

The rod diameters tested varied from 0.375 in.* to 0.540 in. Comparison of two or more sets of data, each for a different rod diameter but in every other respect the same, should show the effect of rod diameter on burnout. Figure 23A is a plot of six sets of data corresponding to two different rod diameters and three flows. The hydraulic diameter and pressures are constant. Figure 23B is similar to 23A except that it is for just one flow. The hydraulic diameter, flows and pressure for these two figures are:

Fig. No.	D_1 (in)	$\frac{G}{10^6}$	P psia
23A	0.375	0.56	1000
		1.12	
		1.68	
	0.540	0.56	
		1.12	
		1.68	
23B	0.375	1.68	1000
	0.500		

For all three flow conditions of Figure 23A there appears to be a slight tendency for the $D_1 = 0.540$ in. points to lie above the $D_1 = 0.375$ in. points at lower qualities. The tendency is well within the $\pm$ 15 per cent experimental scatter.

* A few runs were made with an array of three 1/4" rods, as already noted; however, these could not be used in a direct comparison of results on the basis of rod diameter, so are not included here.

For Figure 23B the D_1 = 0.500 points lie slightly below the D_1 = 0.375 points. This is within $\pm$ 10 per cent experimental scatter.

As with heated length, it may be stated that (a) there is no consistent trend with rod diameter, and (b) any differences in burnout associated with differences in rod diameter are still within experimental scatter. It is concluded that the rod diameter is not a significant parameter.

Effect of Pressure on Burnout

The pressures at which the burnout tests were run varied from 600 to 1400 psia, with a few runs being made at 1450 psia. Comparison of two or more sets of data, each for a different pressure but in every other respect the same, shows the effect of pressure on burnout. Figure 24A is a plot of five such sets of data, at five different pressures: 600, 800, 1000, 1200, and 1400 psia. In every other respect the conditions are the same. Figures 24B through 25C are similar to 24A, each figure corresponding to a particular rod diameter, hydraulic diameter, heated length and flow. The geometry and flow conditions for these figures are summarized below:

Fig. No.	D_1 (in)	D_2 (in)	L (in)	$\frac{G}{10^6}$ (lb/in-ft^2)	Pressure Range From (psia)	To (psia)
24A	.375	.875	70	1.12	600	1400
24B				1.68	600	1400
25A	.540	.875	102	1.12	600	1450
25B	.50	1.00	36	4.0	1000	1400
25C	.50	.75	36	4.0	1000	1400

The same general description applies to all the figures from 24A through 25C. Consider one particular figure from this group. Then

1. For any given pressure except for some experimental scatter (of the order of $\pm$ 10 per cent maximum) the points lie on a straight line. (This has already been observed in the case of the 1000 psia points.)

2. The straight line thus defined for each pressure is approximately parallel to the straight line for every other pressure.

3. At any given quality at which there are data for two (or more) pressures, the line for the higher pressure lies below the other line. In other words, the burnout heat flux is lower for higher pressures, or conversely, is higher for lower pressures (Figure 24A shows, however, that there is little to be gained by dropping the pressure from 800 psia down to 600 psia. Further reduction in pressure would eventually bring about a reversal in the trend, i.e., a decrease in burnout heat flux with decrease in pressure.)

The effect of pressure may better be shown by the curves of Figure 38, which are smoothed cross plots from the data of Figure 24A. These curves are not straight lines. At some pressure below 600 psia, each passes through a maximum. Going in the other direction, as the pressure is increased toward the critical, the curves decrease and converge (but do not approach zero as a limit because of forced convection.)

The pressure effect is probably to some degree dependent on flow, but the data are too few to be conclusive.

It is concluded that in general, in the range of pressures tested, the higher the pressure, the lower the burnout. This is the pressure effect which is shown consistently by all the single rod data.

Effect of Special Geometries

Certain special geometries were tested to determine their effect upon burnout. These geometries* have already been described, and are referred to as:

---

* In addition to these three, a special "rough" liner and a cluster of three rods were also tested. The rough liner results are described in the subsection titled Effect of Rough Liner. The three rod results are included in the subsection titled Comparison with Multirod Burnout.

1. Eccentric rod
2. Simulated spacer
3. Sandblasted rod

The variable flow procedure was used for testing all three of the special geometries listed above.

Tests were also run with a "standard" geometry (single concentric 0.540 inch diameter rod, $8\frac{1}{2}$ ft. heated length, no simulated spacers or sandblasted surfaces) using the variable flow procedure to serve as a basis for comparison. The results of these standard geometry runs are plotted in Figure 26. Best-fit curves have been fitted to the low subcooling ($\Delta hs < 125$ Btu/lb) and to the high subcooling ($\Delta hs > 175$ But/lb) points.

Eccentric Rod

For the rod and liner diameters used (0.540 inch and 0.875 inch, respectively) the annular clearance with rod concentric is 0.1675 inch. With the rod eccentric (see Figure 15A), the minimum clearance is always less than this.

Three different values of minimum clearance were tested, 0.096 inch, 0.061 inch, and 0.033 inch. The eccentric rod burnout points are plotted in Figure 27, with the best-fit curves for the concentric rod superposed for comparison.

Figure 27 shows that when the minimum clearance is 0.096 inch or 0.061 inch the burnout heat flux is essentially the same as for the concentric rod, both at low and at high inlet subcooling. When the minimum clearance is reduced to 0.033 inch, the burnout heat flux at low inlet subcooling is still essentially unchanged. On the other hand, the burnout heat flux at high inlet subcooling is significantly (above 30%) lower than for the concentric rod.

It is evident from Figure 27 that if one of the outside rods in a reactor fuel bundle is moved closer than 0.06 inch from the channel wall, its burnout heat

flux is thereby lowered. Furthermore, if the rod is 0.033 inch from the channel wall, its burnout heat flux may be as much as 30 per cent lower.

Simulated Spacer

The jackets with which the 0.540 inch rod was equipped for these tests (see Figure 15C) forced the flow to separate from the heated surface, thus simulating a plate type spacer. There was no flow between jacket and rod. A few burnouts (six total) occurred in this dead flow zone, as evidenced by thermocouple traces, but were not included in the data reported here. No dead zone of this type exists in a reactor, hence is not properly a part of this simulation.

The burnout points reported here (see Table 4) all occurred in the flow separation zone according to the thermocouple data. These points are plotted in Figure 28, with best-fit curves for the 0.540 inch rod without jacket superposed.

Except for one point, all the points belong in the low subcooling category. In this category all the points except three are within plus or minus 10 per cent of the best-fit curve for the rod without jacket. The three exceptions are from 20 to 25 per cent high.

It appears from Figure 28 that flow separation brought about by a plate type spacer has no adverse effect upon the burnout heat flux.

Sandblasted Rod

The effect of sandblasting (to produce a surface roughness of 300 microinches) on burnout is shown in Figure 29. The burnout heat flux is lowered by from 10 to 15 per cent for both low and high inlet subcooling. Sandblasting the surface has an adverse effect on burnout.

Comparison of Special Geometry with Constant Flow Results

Inlet subcooling is not as suitable a parameter as flow for correlation purposes because it describes only a condition at the test section inlet. In contrast, the flow describes a condition at the position of burnout. To obtain a comparison on the basis of flow as the parameter, all of the data of Figures 26, 27, 28, and 29 for which the flow is bracketed by 0.42 to 0.70 x 10^6 lb/hr-ft^2 and 0.98 to 1.26 x 10^6 lb/hr-ft^2 have been replotted in Figure 39. Best-fit* curves through the data of Figure 18A at the two flows 0.56 x 10^6 and 1.12 x 10^6 lb/hr-ft^2 have been superposed.

Consider first the standard geometry data of Figure 26. If one point is neglected the data are within $\pm$ 20 per cent at the low flow condition and - 30 per cent at the high flow condition. If five points are neglected, the data fall within $\pm$ 15 per cent for both flows, and are thus in good agreement with the data of Figure 18A.

Concerning the eccentric rod, Figure 39 shows that for a minimum clearance of 0.096 inch the burnout heat flux is essentially the same as for the concentric rod. When the minimum clearance is reduced to 0.033 inch, the burnout heat flux at the low flow is still essentially unchanged. But at the higher flow, the burnout heat flux is from 22 per cent to 50 per cent lower than the best-fit curve of Figure 18A. These observations, made with flow as the parameter, are in essential agreement with those based on Figure 27. If one of the rods in a reactor fuel bundle is moved to within 0.033 inch from the channel wall, its burnout heat flux may be reduced by as much as 50 percent.

---

* Neglecting one high point, the data of Figure 18A fit these "best-fit" curves to -18, $\pm$ 20 per cent at $G/10^6$ = 0.56 and -18, $\pm$ 15 per cent at $G/10^6$ = 1.12. Neglecting five low and two high points, the fit is $\pm$ 15 per cent for both flows.

Concerning the simulated spacer, Figure 39 shows that for Jacket No. 1 and Jacket No. 1 eccentric, both flow conditions, and for Jacket No. 2 at the low flow condition, the burnout heat flux is essentially the same as for the rod without jacket. For Jacket No. 2 at the higher flow condition, there are just two points, both low (by 23 per cent and 32 per cent, respectively). It is probable that, at least for these two points, burnout was initiated in the dead flow zone at a circumferential position removed from any thermocouple and that the effected area then extended downward far enough to be felt by thermocouples in the flow separation zone.

Jacket No. 1 with its relatively small dead flow zone does not show any reduction in burnout. It may be concluded on the basis of comparison at constant flow that flow separation brought about by a plate type spacer has no effect upon the burnout heat flux.

Concerning the sandblasted rod, Figure 39 shows reductions in burnout heat flux of as much as 35 per cent below the best-fit curve of Figure 18A at the low flow condition, and as much as 50 per cent at the high flow condition. This comparison with flow as the parameter confirms the conclusion that sandblasting has an adverse effect on burnout.

It may be noted that where differences in burnout heat flux exist between the special geometries and the standard geometry, comparison with the constant flow curves of Figure 18A gives values for these differences which do not in general agree with the values obtained by comparing with the "constant" subcooling curves of Figure 26. The difference in burnout heat flux with respect to the appropriate curve of Figure 18A is more significant than is the difference with respect to the appropriate curve of Figure 26. With flow as the parameter, both the flow and the quality are the same for the special geometry as for the standard geometry. With inlet subcooling as the parameter, only the quality is the same.

Effect of Rough Liner

The constant flow procedure was used for testing the "rough" liner configuration shown in Figure 15D. Rod diameter was 0.375 inch, liner diameter 0.875 inch (except at the ring positions). The burnout points for the rough liner at three different flows, $G/10^6$ = 0.56*, 1.12* and 1.68* are plotted versus quality in Figures 33, 34, and 35, respectively. The burnout points for a smooth liner at the same flows are also plotted for comparison.

It is apparent from these figures that a substantial improvement in the burnout heat flux is possible by such roughing. The burnout is increased as much as 40 per cent at $G/10^6$ = 0.56, 20 per cent at $G/10^6$ = 1.12, and 30 per cent at $G/10^6$ = 1.68. In addition to a general raising of the burnout points, the character of the data is altered in other respects. First, comparing the rough liner points at two different flows but the same quality (see Figure 20), there is little or no flow effect, in contrast to what has been noted for the smooth liners. Second, the (negative) slope of the ϕ_{bo} vs. X curve for the rough liner increases noticeably with increasing flow (being smaller than for the smooth liner at $G/10^6$ = 1.12 and larger at $G/10^6$ = 1.68), whereas the slope for the smooth liner is only slightly affected by the flow, other things being the same.

Pressure Drop

No single rod pressure drop data were obtained on the Fuel Cycle Program. Pressure drop measurements had been made on the old test section, however, and reported in Reference 14. These pressure drop results are reproduced here for completeness. They apply to a single geometry consisting of a 0.540 inch diameter rod in a 0.875 inch diameter tube. This is exactly the old test section geometry as shown in Figure 5, including the spacers.

---

* The corresponding velocity at each of the ring positions was, of course, considerably higher because of the reduced flow area.

Single phase pressure drop is listed in Table 5A and plotted vs. distance along the test section in Figure 31 for 5 different flows. The pressure drop includes both frictional loss and loss due to flow restriction at the spacer pin positions.

The two-phase pressure drop is listed in Table 5B and plotted versus distance along the test section in Figure 32 for 4 different combinations of flow, heat flux, and exit quality. Here again, the loss is due to both channel friction and flow restriction, but the pressure drop as plotted in Figure 32 also includes drop due to acceleration of the flow and hydrostatic drop. The curves through the points of Figure 32 are curved upward in contrast to the straight lines through the points of Figure 31. This is, of course, due to the increasing steam void along the length of the test section and the consequent increasing momentum and higher friction losses.

Comparison with Other Annular Data

Other annular burnout data are available, from Columbia University,[11] Italy (CISE),[12], and Great Britain (AERE),[13] with which the APED results may be compared. All of the data used for comparison were obtained in internally heated annuli, at a pressure of 1000 psia. The salient features of the test equipment and conditions for all three sources, as well as for the APED tests used for comparison, are summarized in Table 6. The Columbia tests were with a 1.375 inch O.D. rod in a 1.745 inch I.D. tube, 42 inch heated length. These data are compared with APED results for the 0.375 inch rod in a 0.710 inch I.D. liner, 70 inch heated length, four different flow rates, in Figures 40 and 41.

The Columbia data, with the exception of the lowest flow condition, shows the same effect of quality and flow which is shown by all the APED data (except rough liner). The best-fit line through the Columbia data at each flow condition has a slightly smaller slope than does the line through the APED data at about the same flow. The Columbia points at $G = 1.9 \times 10^6$ lb/hr-ft^2 average about 15 per cent below the APED points at $G = 2.24 \times 10^6$ lb/hr-ft^2. The Columbia points at $G = 1.4 \times 10^6$ lb/hr-ft^2 average about 10 per cent below the APED points at 1.68×10^6 lb/hr-ft^2. At $G = 1.1 \times 10^6$ lb/hr-ft^2 the best-fit line through the Columbia data intersects the corresponding line through the APED data. It is concluded from the foregoing that although the Columbia data tend to be lower than the APED data at the higher flows, the agreement between the two in generally good at flows in the range 1×10^6 to 2×10^6 lb/hr-ft^2, qualities in the range of 2 to about 16 per cent.

The agreement at lower flows appears not to be so good. The Columbia points at $G = 0.7 \times 10^6$ lb/hr-ft^2 are 30 per cent below the APED points at

TABLE 6 - SINGLE ROD

Salient features of test equipment and conditions, four sources of burnout data for internally heated annulus, forced circulation, vertical upward flow.

Source	D_1 (in.)	t (in.)	D_2 (in.)	D_h (in.)	L (in.)	Material of Rod	Rod Held Concentric By	Power Supply	Conditions at Test Section Inlet	Burnout Detector	Pressure (psia)	Mass Velocity ($lb/hr\text{-}ft^2$)	Quality (Per Cent)
Columbia University[11]	1.375		1.745	0.370	42	304 SS		DC	Subcooled	Change of rod resistance at b.o. position detected by resistance bridge circuit	1000	0.7×10^6 to 1.9×10^6	to 22½
APED	0.375	0.049	0.710	0.335	70	304 SS	Sets of 3 radial pins on 18" centers	AC	Subcooled	"	1000	0.56×10^6 to 2.24×10^6	to 30
Italy (CISE)[12]	0.198	0.016	0.325	0.127	19.7	304 SS	Insulating bushings at ends	DC	Two-Phase	"	1000	1.7×10^6 and 2.15×10^6	24 to 42
Great Britain (AERE)[13]	0.375	0.062	0.546	0.171	29	Stainless Steel	Insulating bushings at ends	AC	Two-Phase	"	1000	1.5×10^6 and 2.2×10^6	9 to 45
APED	0.375	0.049	0.555	0.180	70	304 SS	Sets of 3 radial pins on 18" centers	AC	Subcooled	"	1000	1.68×10^6 and 2.24×10^6	0 to 18

$G = 0.56$ lb/hr-ft^2 in the quality range 18 to 24 per cent. This in itself shows poor agreement, but at qualities below this range, the Columbia data depart from a straight line. A best-fit curve through the Columbia points goes through a maximum at $X = 12$ per cent, implying that burnout can occur at two different qualities for the same heat flux. Moreover, the Columbia points at low flow do not show the flow effect which is shown by the other Columbia data, and by all the APED data (except as previously mentioned). The burnout behavior at low flows is the same as observed by the Russians[14] under hydraulically unstable conditions in their test loop. Unstable conditions may have existed in the Columbia test loop during the tests at the lowest flow condition.

The Italian tests were with a 0.198-inch O.D. rod in a 0.325-inch I.D. tube, 19.7-inch heated length. The British tests were with 0.375-inch O.D. rod in a 0.546-inch I.D. tube, 29-inch heated length. These data are compared with APED results for the 0.375-inch rod in a 0.555-inch I.D. liner, 70-inch heated length, two different flow rates, in Figure 42.

The Italian data are for qualities above 24 per cent. The APED data are for qualities below 18 per cent. Direct comparison is not possible. However, the Italian and British data appear to be in good agreement with each other, and the British data extend down to qualities of 9 per cent. Hence, direct comparison is possible between the British and APED results in the quality range 9 to 18 per cent.

From 9 to 18 per cent quality, neither the British nor the APED data show a significant flow effect.* At about 9 per cent quality, the British and APED

---

* The absence of flow effect is associated with the relatively high flows (of the order of 2×10^6 lb/hr-ft^2), as mentioned in the subsection titled Effect of Flow on Burnout. At higher qualities ($X > 20$ per cent) both the British and Italian data show a strong flow effect.

data are in agreement. As the quality is increased to 18 per cent, the British data changes very little ($0.72 < \Phi_{bo}/10^6 < 0.79$), but appears to go through a maximum at X = 12 per cent. The APED data, on the other hand, decreases monotonically as the quality is increased, and at X = 18 per cent, lies 38 per cent below the British data.

The differences between the British and APED results are not insignificant. There were differences in equipment and procedure as may be noted in Table 6. The British used a 29-inch heated length, and introduced two-phase flow at the inlet end. Even at the lowest quality condition, i.e., exit quality of 9 per cent, the quality at inlet was still about 5 per cent. The APED heated length, on the other hand, was 70 inches; the flow at the inlet end was subcooled liquid for all exit qualities. This is believed to be a major difference between the British and APED experimental conditions. The two-phase flow structure at the British test section inlet had to undergo a transition from an adiabatic to a non-adiabatic channel wall. If this transition was not completed by the exit end of the test section, the formation of a steam blanket (associated with the onset of burnout) tended to be suppressed.

In summary of the comparisons of the APED single rod with results for other internally heated annuli, the following statements are made:

1. The Columbia test section, like the APED test section, was relatively long, and the condition at inlet was always subcooled liquid. The agreement between Columbia and APED results is generally good at flows in the range 1×10^6 to 2×10^6 lb/hr-ft^2, qualities in the range 2 to about 16 per cent. Poor agreement at a lower flow (0.7×10^6 lb/hr-ft^2) may be due to hydraulically unstable conditions in the Columbia loop.

2. The British test section was relatively short, and the condition at inlet was always two-phase. At about 9 per cent quality, the British and APED data are in agreement. As the quality is increased to 18 per cent, the British data changes very little while the APED data decreases monotonically to a value 38 per cent below the British. It is believed that the difference between the APED and British results is due to the difference in two-phase flow structure existing at the British test section inlet compared with the two-phase flow structure existing in the APED test section a comparable distance ahead of the burnout position.

Comparison with Multirod Data

Some multirod burnout data are now available, from Columbia,[19] Hanford,[20] and APED.[21] The salient features of the multirod geometries and test conditions are summarized in Table 7.

The burnout data used for comparison consists, in every case, of the heat flux on the rod whose instrumentation indicated a burnout condition,* versus the bulk, or average, quality at the test section exit.

The Columbia 7-rod data and the APED Multirod data (both 9-rod and 3-rod) all at 1000 psia, are compared with APED single rod data at 1000 psia in Figure 43. There are two categories for the Columbia 7-rod data, depending on the means for maintaining the spacing between adjacent rods. The "non-wrapped" used ceramic ferrules (see Table 7), while the "wrapped" used .083" O.D. tubing wrapped in a helix around each of the outer six rods. At the low flow

* Thus in the case of the Columbia data, for example, the heat flux at burnout is 3 per cent below the average, while in the case of the Hanford data, it is 7 per cent above the average.

TABLE 7 - MULTIROD

Salient features of test equipment and conditions, three sources of burnout data for multirod geometries, forced circulation, vertical upward flow.

Source	Type of Array	No. of Rods	Rod Dia. (in.)	t (in.)	Nom. Spacing Rod-Rod	Nom. Spacing Rod-Channel	D_h* (in.)	L (in.)	Matrl. of Rod Surface	Rod Spacing Held By	Power Supply	Conditions at Test Section Inlet	Heat Flux Distribution	Burnout Detection	P (psia)	G/10^6 (lb/hr-ft^2)	X (Per Cent)
Columbia Univ.[19]	Hexagonal	7	0.550	0.035	0.083	0.089	0.25	37	347 SS	(1) Outer 6 rods wrapped w/.083" O.D. x .010" wall 304 SS tubes, 10" pitch, all 6 rods wrapped in same direction. (2) No wrapping. Spacing held by set of 6 $\frac{1}{2}$-inch long x 0.179" O.D. x 0.092" I.D. ceramic ferrules, placed in spaces between rods, located midway along heated length.	DC	Subcooled	Heat flux for center rod about 3% below average flux.	Change in resistance of segment of center rod at exit end, detected by bridge circuit.	1000	0.5 1.0 1.5	19 to 42
Hanford[20]	Circular	19	0.564	.0095 and .0115	0.074	0.110	0.32	18.5	Inconel	All except center rod & 6 of outer rods wrapped alternately clockwise & counterclockwise w/ceramic bead insulated wire, 10" pitch	DC		Heat flux for outer 12 rods about 7% above average	Thermocouples located 1" before exit end, on 14 of the rods. Each TC connected to strip recorder. Condition identified as burnout when 50°F excursion occurred on one or more traces.**	1215	0.5 1.0 2.0	to 29
APED[21]	Square	9	0.375	0.028, 0.035, and 0.042	0.195	0.172***	0.52	18	304 SS	1st group of sapphire pins w/necessary mounting provisions located 7 dias. ahead of heated length; 2nd group identical to 1st, located 7 dias. after heated length. Also, 1/32" high Rulon buttons on channel walls; located on 4" centers, and Rulon spacers on	AC	Two-Phase	(1,3,4) One corner rod adjacent side rod, and center rod (A, B and C rods, respectively) 25% above flux for remaining 6 rods. (2) A rod 22% above A & B rods which in turn were 25% above flux for remaining 6 rods.	A, B, & C rods instrumented to detect change in resistance in exit half. Also thermocouples located $\frac{1}{4}$" from exit end, distributed circumferentially to determine location of b.o.****	1000 1400	0.56 1.12 0.56 1.12	15 to 33 12 to 34

TABLE 7 (Continued)

Source	Type of Array	No. of Rods	Rod Dia. (in.)	t (in.)	Nom. Spacing Rod - Rod	Nom. Spacing Rod - Channel	D_h * (in.)	L (in.)	Matrl. of Rod Surface	Rod Spacing Held By	Rod Supply	Conditions at Test Section Inlet	Heat Flux Distribution	Burnout Dectection	P (psia)	$G/10^6$ (lb/hr-ft^2)	X (Per Cent)
APED[21]										4 side rods to prevent electrical shorts. Spacers located 19 dias. ahead of & 2 dias. following exit end of heated length.							
APED	Triangular	3	0.250	0.016	0.062	0.132	0.335	54	304 SS	Sets of 3 AC radial pins on 24 in. centers, plus short pieces of .062 SS wire located on 4" centers & kept in place by smaller wire wrapped around & spot welded to rods. Also simulated plate-type spacers shown in Fig. 9B	Subcooled	Uniform	One rod instrumented to detect change in resistance in last 12" before exit end.	1000	0.42 to 0.7	20 to 36

* Based on entire wetted perimeter.

** For all of the runs used for comparison purposes here, burnout occurred on one of the outer rods.

*** For the first assembly (see heat flux distribution column), clearance between B rod and channel reduced to 0.095".

**** For assembly No. 1, three of the burnouts occurred on rod B. For the remaining 19 runs of Assembly No. 1, and for the 11 runs of the remaining assemblies, all burnouts occurred on rod A, the corner rod. Burnout was always on the side of the rod facing the channel.

condition ($G = 0.5 \times 10^6$ lb/hr-ft^2) for the Columbia 7-rod, the one non-wrapped point agrees with a straight line extrapolation of the APED single rod points at 0.56×10^6; at the intermediate flow (1×10^6 lb/hr-ft^2) the two non-wrapped points are about 30 per cent high with respect to an extrapolation of the single rod points at 1.12×10^6 lb/hr-ft^2; and at the high flow (1.5×10^6 lb/hr-ft^2) the one non-wrapped point agrees with an extrapolation of the single rod points at 1.68 lb/hr-ft^2 (and, incidentally, with the single rod points at 1.12×10^6 lb/hr-ft^2). At the low and intermediate flows, the wrapped points are high with respect to the non-wrapped, whereas at the high flow, the wrapped and non-wrapped points agree.

The foregoing comparison of the single rod with the Columbia 7-rod results indicates that the single rod data would predict multirod burnout well at flows from 0.5 to 1.5×10^6 lb/hr-ft^2, but if the rods were wrapped would tend to predict conservatively (i.e., low) at the lower flows.

The APED 9-rod data are mostly at the lower flow ($G = 0.56 \times 10^6$ lb/hr-ft^2) conditions. The two9-rod points at $G = 1.12 \times 10^6$ lb/hr-ft^2 show a reversal of the flow effect observed with the single rod in that they lie above the 9-rod points at the lower flow. A best-fit line through the 9-rod points at $G = 0.56 \times 10^6$ lb/hr-ft^2 has a smaller slope than the corresponding line through the single rod data ($D_h = .335$) at the same flow. At a quality of 20 per cent, the 9-rod points are about 28 per cent low with respect to the single-rod points. At a quality of 30 per cent, the 9-rod points agree with the single rod points.

The same general remarks can be made of the 3-rod points in comparison with the single rod ($D_h = .335$) at the low flow. At a quality of 20 per cent, the 3-rod points are about 46 per cent low; at a quality of 34 per cent, the 3-rod points agree with the single rod.

The foregoing comparison of the APED multirod data (both 9-rod and 3-rod) at 1000 psia with the APED single rod data indicates that the single rod data predict multirod burnout conditions which are optimistic (high) at low flows and qualities of about 20 per cent but which are fairly good at qualities of about 30 to 35 per cent. The results are inconclusive for higher flows.

The APED 9-rod data at 1400 psia are compared with APED single rod data at 1400 and 1450 psia in Figure 44. The 9-rod points at the low flow ($G = 0.56 \times 10^6$ lb/hr-ft^2) lie about 12 per cent below the 9-rod points at $G = 1.12 \times 10^6$ lb/hr-ft^2, showing a reversal of the single rod flow effect. Because of limited data, the comparison of 9-rod with single rod can only be made at the intermediate flow 1.12×10^6 lb/hr-ft^2 A best-fit line through the 9-rod points has a smaller slope than the corresponding line through the single rod data At qualities above 14 per cent, the 9-rod points are high, on the average, with respect to the single rod points. As the quality decreases to values below 14 per cent, the 9-rod data become low with respect to the single rod points.

The foregoing comparison of the single rod with the APED 9-rod results at 1400 psia and $G/10^6 = 1.12$ indicate that the single rod data would predict multirod burnout optimistically at low qualities ($X < 14$ per cent) and conservatively at higher qualities ($X > 14$ per cent). The results are inconclusive at lower and higher flows.

The Hanford 19-rod data at 1215 psia are compared with the APED single rod data at 1200 psia in Figure 45. At low qualities ($X < 8$ per cent) the 19-rod points at the low flow ($G = 0.5 \times 10^6$ lb/hr-ft^2) are low and at the high flow ($G = 1.5 \times 10^6$ lb/hr-ft^2) are high, with respect to the intermediate flow (1.0×10^6 lb/hr-ft^2), showing a reversal of the flow effect observed

with the single rod. At higher qualities, the 19-rod data show no clear flow effect. Because of limited data at 1200 psia, direct comparison of 19-rod with single rod can only be made at the intermediate flow (1×10^6 lb/hr-ft^2 for Hanford, 1.12×10^6 lb/hr-ft^2 for APED), in the range of qualities from 2 to 14 per cent. A best-fit line through the 19-rod points has a smaller slope than the corresponding line through the single rod points. At $X = 2$ per cent, the 19-rod points are 27 per cent below the single rod. At $X = 14$ per cent, the 19-rod and the single rod data agree.

The foregoing comparison of the single rod with the Hanford 19-rod results indicates that the single rod data predict multirod burnout conditions which are optimistic at intermediate flows and low qualities ($X < 14$ per cent), but which are good at qualities in the neighborhood of 14 per cent, and (by extrapolation) would be conservative at higher qualities. The results are inconclusive for low and high flows.

In summary of the comparisons of the APED single rod results with the multirod results from three sources, the following general observations are made:

1. The multirod shows no consistent flow effect (although a few data points suggest a slight effect of higher burnout heat flux with increased flow, which is the reverse of the flow effect observed with the single rod.).
2. Lines through the multirod data have generally smaller slopes than the corresponding lines through the single rod data. Hence, at low qualities, the multirod burnout heat flux is lower than the single rod, but as the quality is increased, the multirod burnout flux first equals and then exceeds that for the single rod.

There are two important differences between the multirod and the single rod test conditions. First, the multirod test sections are generally short (except the Columbia and the APED 3-rod) compared with the APED single rod.

Second, because of the strong electrodynamic forces existing between all the rods in a multirod cluster, extensive provisions must be made to provide radial support for each rod, in order to maintain proper (and controlled) spacing. These provisions for maintaining the spacing disturb the flow pattern, and can so alter the distribution of the liquid phase as to change the burnout characteristics.

It is believed that the provision for maintaining proper spacing, with consequent disturbance of the flow pattern, is probably the more important of the two differences mentioned above. The disturbance to the flow pattern is of the same type (though not necessarily of the same order) as produced by the rough liner. Referring back to the rough liner results (Figures 33, 34, and 35) it will be recalled that:

1. There is little or no flow effect
2. The slope of the ϕ_{bo} vs. X curve is smaller for the rough liner than for the smooth liner at $G = 1.12 \times 10^6$ lb/hr-ft^2.

These two statements correspond to the two general observations made concerning the multirod results. It may also be noted that the Columbia 7-rod results, "non-wrapped" categroy, were probably obtained under the cleanest channel conditions (i.e., least disturbance to flow pattern) and agree quite well with the single rod results.

CORRELATION OF APED SINGLE ROD DATA

Any correlation of the data listed in Table 4, whether empirical or theoretical, should take into account the effects of geometry (i.e., hydraulic diameter), pressure, quality (or enthalpy), and flow to do the data justice. Furthermore, it should show the trends illustrated in Figures 36, 37, and 38. The final check, of course, is the accuracy with which it correlates all applicable data.

Correlation

The correlation developed here employs a method suggested by the method proposed in Reference 22 for subcooled pool boiling. That method consists simply of adding another term to the pool boiling term to account for subcooling. According to the method employed here, the heat flux at burnout is proportional to the sum of (1) the pool boiling heat flux at burnout, plus terms to account for (2) forced convection, and (3) the bulk state of the coolant.

$$\left\{\begin{matrix}\text{Total}\\ \text{heat flux}\\ \text{at burnout}\end{matrix}\right\} \propto \left[\left\{\begin{matrix}\text{Pool boiling}\\ \text{heat flux}\\ \text{at burnout}\end{matrix}\right\} + \left\{\begin{matrix}\text{Added flux}\\ \text{due to forced}\\ \text{convection}\end{matrix}\right\} + \left\{\begin{matrix}\text{Adjustment in flux}\\ \text{depending on state}\\ \text{(quality or subcooled)}\end{matrix}\right\}\right]$$

The first and second terms on the right may be calculated, based on established correlations, and are functions of pressure. The second term is also a function of geometry and flow. The third term may be evaluated in terms of all four parameters, using a strictly empirical approach. The method as used in this report has been modified slightly to evaluate all of the terms at a single pressure and to lump all pressure effects into a single factor.

$$\left\{\begin{matrix}\text{Total}\\ \text{heat flux}\\ \text{at burnout}\end{matrix}\right\} = f(P_o-P)\left[\left\{\begin{matrix}\text{Pool boiling}\\ \text{b.o. heat flux}\\ \text{at 1000 psia}\end{matrix}\right\} + \left\{\begin{matrix}\text{Add. flux due}\\ \text{to forced convection}\\ \text{at 1000 psia}\end{matrix}\right\} + \left\{\begin{matrix}\text{Adjustment in flux}\\ \text{depending on quality,}\\ \text{flow, hydraulic}\\ \text{diameter}\end{matrix}\right\}\right]$$

or

$$\frac{\Phi_{bo}}{10^6} = f(P_o-P)\left[\frac{\Phi_{pb}}{10^6} + \frac{\Phi_{conv.}}{10^6} - \gamma\right] \qquad (11)$$

where

$$f(P_o - P) = 1 + K_1(1000 - P) + K_2(1000 - P)^2 \tag{12}$$

$$\phi_{pb} = 0.131\, h_{fg}\, \rho_v \left[\frac{\sigma g (\rho_\ell - \rho_v)}{\rho_v^2}\right]^{\frac{1}{4}} \quad \left\{\begin{array}{l}\text{Ref. 22,}\\ \text{evaluated at}\\ \text{P = 1000 psia}\end{array}\right\} \tag{13}$$

$$\phi_{conv} = 0.020\left(\frac{D_2}{D_1}\right)^{0.5}\left(\frac{G D_h}{\mu}\right)^{0.8}\frac{k}{D_h}\, Pr^{\frac{1}{3}}\left[T_w - T_s\right] \quad \left\{\begin{array}{l}\text{Ref. 23,}\\ \text{evaluated at}\\ \text{1000 psia}\end{array}\right\} \tag{14}$$

$$T_w - T_s = \frac{60}{e^{\frac{P}{900}}}\left[\frac{\phi}{10^6}\right]^{\frac{1}{4}} \quad \left\{\begin{array}{l}\text{Ref. 9,}\\ \text{evaluated at}\\ \text{1000 psia}\end{array}\right\} \tag{15}$$

$$T_w - T_s \cong 19.75\left[0.682 + 0.318\,\frac{\phi}{10^6}\right] \quad \left\{\begin{array}{l}\text{linear approximation}\\ \text{to (5). Error less}\\ \text{than 7\% in the range}\\ 0.3 < \frac{\phi}{10^6} < 1.7\end{array}\right\} \tag{16}$$

$$\mathcal{F} = f(D_h, G, x) \tag{17}$$

It was found that the function of equation (17) could be closely approximated by

$$\mathcal{F} = a + c(x - b) \tag{18}$$

where a and b are functions of flow, and c is a function of both flow and hydraulic diameter.

$$a = a_{-2}\left(\frac{G}{10^6}\right)^{-2} + a_{-1}\left(\frac{G}{10^6}\right)^{-1} + a_0 + a_1\left(\frac{G}{10^6}\right) + a_2\left(\frac{G}{10^6}\right)^2$$

$$b = b_{-2}\left(\frac{G}{10^6}\right)^{-2} + b_{-1}\left(\frac{G}{10^6}\right)^{-1} + b_0 + b_1\left(\frac{G}{10^6}\right) + b_2\left(\frac{G}{10^6}\right)^2$$

where a_i and b_i; i = -2, -1, 0, 1, and 2; are constants.

It will be noted that

$$c = \frac{\partial \mathcal{F}}{\partial x} = - \frac{\partial \phi_{bo}}{\partial x} \tag{19}$$

which facilitated the calculation of c from the experimental data. An expression which gave a good fit to c was found to be

$$c = c_0 + c_1 D_h + c_2 D_h \frac{G}{10^6} \tag{20}$$

where c_0, c_1, and c_2 are constants.

Values for the coefficients in the pressure term (equation (12)) were selected which would give a close fit to the data. The coefficients in the expression for c (equation (20)) were evaluated giving roughly equal weight to each of the values for D_h and G. The coefficients a_i and b_i, i = -2, -1, 0, 1, 2, were evaluated from 376 representative data points* using the method of least squares.

The correlation expression which finally resulted, using the linear approximation equation (16) for $T_w - T_s$ is

$$\frac{\phi_{bo(c)}}{10^6} = \frac{\left[1 + 0.16\left(\frac{1000-P}{400}\right) - 0.04\left(\frac{1000-P}{400}\right)^2\right]}{1 - 0.008\, B\left(\frac{G}{10^6}\right)^{0.8}} \cdot \left[0.0172\, B\left(\frac{G}{10^6}\right)^{0.8} - \left\{0.3175\left(\frac{G}{10^6}\right)^{-2} - 1.8534\left(\frac{G}{10^6}\right)^{-1}\right\} - \left\{2.4 - 3.2\, D_h + 0.83\, D_h\left(\frac{G}{10^6}\right)\right\} \cdot \left\{ \times \right.\right.$$

$$\left.\left. - 0.0629\left(\frac{G}{10^6}\right)^{-2} + 0.3429\left(\frac{G}{10^6}\right)^{-1} - 0.2494 + 0.0020\left(\frac{G}{10^6}\right)^{2}\right\}\right] \tag{21}$$

---

* Points for D_h = 0.180 inch were excluded from this set. The correlation only applies for $D_h \geq 0.25$ inch. The special geometry, rough liner, and 3-rod points were also excluded.

where $\phi_{bo(c)}$ is in Btu/hr-ft^2; P is in psia; $B = \left(\frac{D_2}{D_1}\right)^{0.5}(D_2 - D_1)^{-0.2}$, D_1 and D_2 in feet; G is in lb/hr-ft^2; D_h is in inches; and X, the quality, is expressed as a decimal fraction.

Check of Correlation: Limits for Which Correlation is Valid

The correlation is superposed on a plot of all burnout data for D_h = 0.50 inch, P = 1000 psia, and $G/10^6$ = 0.56, 1.12, and 1.68 lb/hr-ft^2, in Figure 46. Two different rod diameters (D_1 = 0.375 inch and 0.500 inch) and three different heated lengths (L = 36 inches, 70 inches, and 108 inches) are represented by these data.

From an inspection of Figure 46, the following general observations can be made:

1. The correlation shows the same trend with quality as is shown by all the APED burnout data, namely, that the heat flux at burnout decreases with increase in quality. $\frac{d\phi_{bo}}{dx} < 0$

2. The relationship of $\phi_{bo(c)}$ with X is linear. Extrapolation to qualities higher than the highest quality for which there are data results in values of $\phi_{bo(c)}$ which are much too low. For example, extrapolation of the correlation line for $G/10^6$ = 1.68, to 29.4 per cent quality results in a burnout heat flux of zero. The correlation does not apply if the calculated heat flux is less than 0.35 x 10^6 Btu/hr-ft^2.

Considering specifically the data of Figure 46, at the two higher flows the data (except for 3 points) agree with the correlation to within $\pm$ 15 per cent. At the low flow the data (except for 1 point) agree with the correlation to within $\pm$ 10 per cent. These data are considered typical, although agreement with the correlation is not necessarily as good for other combinations of hydraulic diameter and flow.

As noted earlier, the correlation should show the same trends with flow as is shown by the test results in Figure 36. $\phi_{bo(c)}$ has been calculated for the conditions of Figure 36, and is plotted versus flow in Figure 47. The curves of Figure 36 are superposed for comparison.*

Inspection of Figure 47 reveals that for each given quality the calculated burnout heat flux $\phi_{bo(c)}$ decreases with increase in flow, to a flow of about 2×10^6 lb/hr-ft^2. As the flow is increased further $\phi_{bo(c)}$ starts to increase again. Thus, the correlation shows the same trends as the curves of Figure 36, over the range of test conditions.

The correlation should show the same trends with hydraulic diameter as is shown by the test results in Figure 37. $\phi_{bo(c)}$ has been calculated for three of the flow-quality combinations of Figure 37, and is plotted versus hydraulic diameter in Figure 48. The points from Figure 37 are superposed for comparison.

The correlation predicts a linear relationship between ϕ_{bo} and D_h, with ϕ_{bo} increasing to a maximum as D_h decreases to zero. This is in contrast to the trends shown by the points of Figure 37, which indicate that a maximum exists somewhere in the range 0.25 inch $< D_h <$ 0.50 inch.

The poor agreement between $\phi_{bo(c)}$ and the data point at D_h = 0.180 inch is to be expected; the correlation does not apply in the range $D_h <$ 0.25 inch.

In the range 0.25 inch $< D_h <$ 0.5 inch the correlation shows a decrease in $\phi_{bo(c)}$ with increase in D_h, as already noted. This is a contrast to the data, which do not show a consistent trend in ϕ_{bo} vs. D_h. However, the change in $\phi_{bo(c)}$ over this range of D_h is small. The greatest difference

* It will be noted that the calculated curves average about 15 per cent high with respect to the curves of Figure 36, over the range of flows covered by the tests. The purpose here, however, is to compare relative trends with flow, not absolute values.

between calculated curve and data point in Figure 47, 0.25 inch $< D_h <$ 0.5 inch, is 8 per cent.

For $D_h > 0.5$ the trend shown by the correlation, i.e., decrease in $\phi_{bo(c)}$ with increase in D_h, is in good agreement with the trend shown by the data. The calculated values are within 6 per cent of the data points.

In summary of the foregoing, the trends with hydraulic diameter shown by the correlation agree well with the trends shown by Figure 37, for $D_h > 0.5$ inch. The difference between calculated and measured is small (~ 8 per cent max.) for 0.25 inch $< D_h <$ 0.5 inch. The correlation does not apply for $D_h <$ 0.25 inch.

The correlation should show the same trends with pressure as is shown by the curves of Figure 38. ϕ_{bo} has been calculated for the conditions of Figure 38, and is plotted versus pressure in Figure 49. The curves of Figure 38 are superposed for comparison.

Inspection of Figure 49 reveals that for each given quality, $\phi_{bo(c)}$ decreases with increase in pressure. This trend is invariant in the range of pressures from 600 to 1450 psia. Thus, the correlation shows the same trend as the curves of Figure 38, over the range of test conditions.

It is concluded from the foregoing comparisons that the correlation shows essentially the same trends with the four parameters X, G, D_h, and P, as are shown by the data.

The last check which will be made here is to see how well the correlation predicts each of the 362 APED data points upon which it is based,* and also each of 20 Columbia data points.[11]

---

* and for which $\phi_{bo(c)}$ is greater than 0.35 x 10^6 Btu/hr-ft^2.

A plot of $\phi_{bo(c)}$ versus measured ϕ_{bo} for the APED data appears in Figure 50. These points are for the following range of conditions (taken also to be the range of conditions for which the correlation is considered valid):

Quality:	$-0.12 < X < .44$
Flow:	$0.14 < G/10^6 < 6.2$, lb/hr-ft^2
Hydraulic diameter:	$0.25 \leq D_h \leq 0.875$, inch
Pressure:	$600 \leq P \leq 1450$, psia
Heat Flux:	$.35 \times 10^6 < \phi_{bo}/10^6$, Btu/hr-ft^2

Seventy-five per cent of the calculated values $\phi_{bo(c)}$ lie within $\pm$ 10 per cent of the measured values ϕ_{bo}; 95 per cent of the calculated values lie within $\pm$ 20 per cent of the measured; and 99 per cent of the calculated lie within $\pm$ 30 per cent of the measured.

The only other annular data which fall within the range of conditions for which this correlation is considered valid are the Columbia points. A plot of $\phi_{bo(c)}$ versus measured ϕ_{bo} appears in Figure 51, for the three flows $G = 1.1$, 1.4, and 1.9×10^6 lb/hr-ft^2.

Of the 20 points plotted in Figure 51, just six (30 per cent) fall within $\pm$ 10 per cent, but 19 (95 per cent) fall within $\pm$ 20 per cent, and all points fall within $\pm$ 30 per cent. The points average about 12 per cent high, i.e., the average value of burnout heat flux predicted by the correlation for the Columbia test conditions is about 12 per cent higher than the average measured burnout heat flux.

The correlation developed in this section checks 95 per cent of all applicable data to $\pm$ 20 per cent. It is believed that this correlation provides a useful tool for the prediction of burnout, for any combination of conditions which fall within the range for which the correlation is considered valid.

REFERENCES

1. E.E. Polomik, S. Levy, and S.G. Sawochka, "Heat Transfer Coefficients with Annular Flow during Once-Through Boiling of Water to 100% Quality at 800, 1100, and 1400 psia," GEAP-3703, May 1961.

2. H.L. McGill and W.L. Sibbett, "Heat Transfer and Pressure Drop of Water Flowing in a Small Tube," ANL-4603, February 1951.

3. H. Buchberg, et al., "Final Report on Studies in Boiling Heat Transfer," COO-24, March 1951.

4. J. A. Clark and W.M. Rohsenow, "Local Boiling Heat Transfer to Water at Low Reynolds Numbers and High Pressure," M.I.T. Tech. Rept. No. 4 (D.I.C. Project No. 6627) July 1, 1952.

5. J. M. Reynolds, "Burnout in Forced Convection Nucleate Boiling of Water," M.I.T. Tech. Rept. No. 10, NONR-1848(39), (D.S.R. Project No. 7-7673) July 1, 1957.

6. W. H. Lowdermilk and W. F. Weiland, "Some Measurements of Boiling Burnout," NACA RM-E 54 K 10, February 23, 1955.

7. D.A. Dingee, H.M. Epstein, J.W. Chastain, and S.L. Fawcett, "Burnout Heat Flux in a Rectangular Channel," BMI 1065, January 10, 1956.

8. H. M. Epstein, J. W. Chastain, and S. L. Fawcett, "Heat Transfer and Burnout to Water at High Subcritical Pressures," BMI-1116, July 20, 1956.

9. W. H. Jens and P. A. Lottes, "Analysis of Heat Transfer Burnout Pressure Drop and Density Data for High Pressure Water," ANL-4627, May 1, 1951.

10. R.A. DeBortoli, S.J. Green, B.W. LeTourneau, M. Troy, and A. Weiss, "Forced Convection Burnout Studies for Water in Rectangular Channels and Round Tubes at Pressures above 500 psia," WAPD-188, October 1958.

11. D. Blackford and B. Matzner, "Basic Experimental Studies on Boiling Fluid Flow and Heat Transfer at Elevated Pressures," Monthly Progress Report MPR-X-8-61, Engineering Research Laboratories, Columbia University, August 31, 1961

12. N. Adorni, S. Bertoletti, J. Lesage, C. Lombardi, G. Peterlongo, G. Soldaini, F.J. Weckerman, R. Zavattarelli, "Results of Wet Steam Cooling Experiments: Pressure Drop, Heat Transfer and Burnout Measurements in Annular Tubes with Internal and Bilateral Heating," CISE Report R-31, Milano, Italy, Jan. 1961.

13. A.W. Bennett, J.G.Collier, P.M.C. Lacey, "Heat Transfer to Mixtures of High Pressure Steam and Water in an Annulus; Part II: The Effect of Steam Quality and Mass Velocity on the 'Burnout' Heat Flux," AERE-R3804, Harwell, Berkshire, England, August 1961.

14. I.T. Aladyev, Z.L. Miropolsky, V.E. Doroshchuk, M.A. Styrikovich, "Boiling Crisis in Tubes," International Heat Transfer Conference Paper No. 28, Boulder, Colorado, August 28 - September 1, 1961.

15. "A Boiling Water Research and Development Program, First Quarterly Progress Report, Aug. 1960 - Sept. 1960, GEAP-3558, prepared under USAEC Contract No. AT(04-3)-189, P.A. No. 11.

16. S. Levy, E.E. Polomik, C.L. Swan, and A.W. McKinney, "Eccentric Rod Burnout at 1000 psia with Net Steam Generation," GEAP-3148, April 6, 1959.

17. E. Janssen, J.A. Kervinen, S. Levy, "Single Rod Burnout Tests with Simulated Spacers and Net Steam Generation at 1000 psia," GEAP-3491, July 15, 1960.

18. E. Janssen, "Effect of Instrument Tube on Burnout Limit, Dresden First Load," GEAP-3473, July 12, 1960.

19. B. Matzner, "Basic Experimental Studies on Boiling Fluid Flow and Heat Transfer at Elevated Pressures," Monthly Progress Report MPR-X-5-61, Engineering Research Laboratories, Columbia University, May 31, 1961.

20. G. M. Hesson, D.E. Fitzsimmons, E.D. Waters, and J.M. Batch, "Preliminary Boiling Burnout Experiments with a 19-rod Bundle Geometry in Axial Flow," Hanford Document No. HW-73395, April 17, 1962.

21. E.E. Polomik and E.P. Quinn, "Multirod Burnout at High Pressure," GEAP-3940, September 1962.

22. N. Zuber, M. Tribus, and J.W. Westwater, "The Hydrodynamic Crisis in Pool Boiling of Saturated and Subcooled Liquids," International Heat Transfer Conference Paper No. 27, Boulder, Colorado, Aug. 26 - Sept. 1, 1961.

23. R. P. Stein, and W. Begell. "Heat Transfer to Water in Turbulent Flow in Internally Heated Annuli," A.I.Ch.E. Journal, V. 4, No. 2, June 1958, pp. 127-131.

NOTATION

a	Coefficient
A	Flow area, ft^2
A_o	Orifice area, ft^2
A	Heat transfer area, ft^2
b	Coefficient
B	$= (D_2/D_1)^{0.5} (D_2 - D_1)^{-0.2}$
c	Coefficient
D_1	Rod O.D., inches or feet
D_2	Tube I.D., inches or feet
D_h	Hydraulic diameter, inches
f	Function
$\mathcal{F}$	Term in correlation expression for ϕ_{bo} which depends on the bulk state of the coolant.
g	Gravitational constant, ft/sec^2
G	Mass velocity, $lb/hr\text{-}ft^2$
Δh	Head difference across orifice, ft.
$\Delta h'$	Orifice manometer deflection, inches
Δh_s	Subcooling at test section inlet, Btu/lb
h_{fg}	Latent heat of vaporization, Btu/lb
k	Thermal conductivity, Btu/hr-ft ^oF
K	Orifice discharge coefficient
K	Constant
L	Heated length, inches
N_R	Reynolds number
P	Pressure, psia
Pr	Prandtl number
q	Heat transfer rate, Btu/sec

T_1 Temperatures at test section inlet, ^{o}F

T_{13} Temperatures at orifice, ^{o}F

T_r Room temperature, ^{o}F

T_s Saturation temperature, ^{o}F

T_w Temperature of heat transfer surface, ^{o}F

w Density of water at temp T_{13}, lb/ft^3

w_r Density of water at temp T_r , lb/ft^3

w_{man} Density of manometer fluid at temp T_r, lb/ft^3

$\dot{W}$ Mass flow rate, lb/sec

X Quality = $\dot{W}g/\dot{W}$

X_e Quality at test section exit

α Thermal coefficient at expansion, $^{o}F^{-1}$

μ Viscosity, lb/hr-ft

ρ_l Density of liquid phase, lb/ft^3

ρ_v Density of vapor phase, lb/ft^3

σ Surface tension, lb/ft

ϕ Heat flux, $Btu/hr\text{-}ft^2$

ϕ_{bo} Burnout heat flux, $Btu/hr\text{-}ft^2$

TABLE 4

OLD TEST SECTION

UNIFORM HEAT FLUX DISTRIBUTION

RUN NO.	P PSIA	$G/10^6$ LB/HR FT^2	Δh_s BTU/LB	$\Phi_{bo}/10^6$ BTU/HR FT^2	X PER CENT
D_1 = 0.540"		D_2 = 0.875 "		D_h = 0.335"	L = 102"
(The following data taken using the variable flow procedure)					
Single Rod Concentric,		Minimum Annular Clearance		0.167"	
1.	1003	.261	70.7	.263	61.5
2.	1002	.337	60.1	.296	53.6
3.	1006	.559	63.8	.375	38.1
4.	1004	.909	60.9	.454	27.6
5.	1007	.997	165.0	.647	21.0
6.	997	1.14	266.6	.892	14.8
7.	1002	1.19	54.9	.513	22.3
8.	1001	.955	82.3	.513	25.9
9.	1012	.742	172.0	.514	23.1
10.	999	1.17	72.9	.528	20.8
11.	1002	1.16	71.9	.524	21.3
Single Rod Eccentric,		Minimum Annular Clearance		0.096"	
12.	1000	1.07	126.0	.606	21.1
13.	993	1.19	238.0	.840	13.6
14.	998	.764	60.0	.439	31.8
15.	1002	.747	60.6	.429	31.8
16.	1003	.422	83.8	.359	48.1
17.	1023	.999	74.1	.505	24.8
18.	1012	1.17	184.0	.752	16.2
19.	1006	.767	63.8	.436	30.4
Single Rod Eccentric,		Minimum Annular Clearance		0.061"	
20.	1001	.815	96.2	.479	27.3
21.	990	.442	51.9	.332	45.9
22.	975	1.29	263.0	.938	11.5
23.	1027	.922	216.0	.663	18.6
24.	1000	.819	101.0	.471	25.6
Single Rod Eccentric,		Minimum Annular Clearance		0.033"	
25.	1002	.811	101.0	.443	23.5
26.	1010	.553	51.3	.354	38.1
27.	1014	.248	186.0	.275	65.5
28.	1001	1.23	284.0	.616	8.5
29.	1001	.809	208.0	.446	24.2
30.	1005	1.15	25.3	.427	22.6
31.	1022	1.14	107.0	.539	17.7
32.	985	.835	194.0	.580	19.8
33.	1004	.81	30.1	.397	30.7
34.	1000	.535	39.2	.348	40.5

TABLE 4 (CONT.)

RUN NO.	P PSIA	$G/10^6$ LB/HR FT^2	Δh_s BTU/LB	$\Phi_{bo}/10^6$ BTU/HR FT^2	x PER CENT
D_1 = 0.250"(3 rods)	D_2 = 0.875"	D_h = 0.355"	L = 54"		
Cluster of three rods in single rod test section, with two simulated spacers. (The following data taken using the variable flow procedure).					
Pressure shown is nominal; actual pressure varied $\pm$ 10 psi.					
35.	1000	.700	54.5	.484	20.5
36.	1000	.628	59.8	.453	21.0
37.	1000	.741	56.3	.500	19.6
38.	1000	.707	53.9	.503	21.4
39.	1000	.398	71.5	.391	30.7
40.	1000	.501	63.9	.437	26.6
41.	1000	.571	132.2	.578	22.0
42.	1000	.574	143.2	.594	21.1
43.	1000	.476	36.2	.414	30.8
44.	1000	.420	34.9	.416	35.1
45.	1000	.378	37.0	.391	37.5
46.	1000	.329	63.9	.359	35.9
47.	1000	.329	69.2	.359	35.1
48.	1000	.426	47.4	.437	35.6
49.	1000	.460	87.6	.497	31.6
D_1 = 0.540"	D_2 = 0.875"	D_h = 0.335"	L = 102"		
Jacket at top end of single concentric rod to simulate flow conditions past spacer. (The following data taken using the variable flow procedure.)					
Jacket No. 1 - Concentric					
50.	1024	.646	57.5	.404	35.4
51.	990	.885	44.7	.448	28.5
52.	1020	1.27	39.0	.512	22.4
53.	997	1.08	120.	.632	22.7
54.	1019	1.09	129.	.646	21.9
55.	1004	.929	40.0	.523	33.4
Jacket No. 1 - 0.015" Eccentric					
56.	1004	.793	52.4	.426	29.7
57.	1004	1.00	46.9	.466	25.4
58.	994	1.17	39.0	.468	22.0
59.	1002	1.26	38.9	.477	20.7
60.	998	1.41	41.2	.490	18.1
61.	1000	1.45	119.	.668	14.0

TABLE 4 (CONT.)

RUN NO.	P PSIA	$G/10^6$ LB/HR FT^2	Δh_s BTU/LB	$\Phi_{bo}/10^6$ BTU/HR FT^2	X PER CENT
	Jacket No. 2 - Concentric				
62.	999	1.28	51.4	.471	17.9
63.	1001	1.14	54.3	.460	20.1
64.	1001	.997	56.9	.443	22.4
65.	998	.848	60.4	.443	27.4
66.	1000	.745	67.7	.420	29.2
67.	998	.584	77.2	.388	34.8
68.	1000	1.38	73.1	.491	13.7
D_1 = 0.540"	D_2 = 0.875"	D_h = 0.335"	L = 102"		
(The following data taken using the variable flow procedure)					
* 69.	1000	.416	89.0	.346	44.8
70.	1009	.534	80.1	.386	38.5
71.	1006	.534	74.5	.386	39.3
72.	1000	.537	73.6	.392	39.9
73.	1000	.713	64.3	.415	31.0
74.	1016	.871	57.9	.443	26.9
75.	1004	1.03	53.4	.454	22.8
76.	1006	1.19	44.5	.466	20.5
77.	1008	1.35	42.2	.477	18.4
78.	998	.423	81.0	.346	45.0
79.	609	.404	56.4	.357	47.4
80.	599	.495	58.0	.395	41.8
81.	601	1.04	43.5	.500	23.9
82.	599	1.15	41.6	.517	22.3
83.	598	.831	47.9	.470	28.7
84.	598	.695	47.6	.437	32.7
85.	599	.744	52.6	.460	31.3
86.	599	1.01	40.1	.517	26.4
87.	599	1.26	40.6	.566	22.4
88.	601	1.33	37.1	.568	21.6
89.	597	1.53	155.7	.586	2.60
90.	596	1.50	35.0	.590	19.8
91.	598	1.15	37.9	.547	24.5
92.	593	.753	44.8	.462	32.1
93.	1000	.806	136.4	.569	28.6
94.	999	.588	146.0	.483	35.1
95.	1004	.630	221.9	.608	33.6
96.	1002	.784	247.1	.694	24.1
97.	1001	.808	278.0	.743	21.7

* Only a simple concentric annular geometry is used for these and all subsequent runs, except for the rough liner runs Nos. 606 through 630.

TABLE 4 (CONT.)

RUN NO.	P PSIA	$G/10^6$ LB/HR FT^2	Δh_s BTU/LB	$\phi_{bo}/10^6$ BTU/HR FT^2	X PER CENT
98.	1004	1.16	237.0	.850	14.8
99.	999	1.29	221.6	.873	13.4
100.	998	1.38	225.6	.902	11.3
101.	998	1.46	217.4	.902	9.79
102.	999	1.54	215.9	.940	9.65
103.	998	1.03	60.4	.443	20.9
104.	1001	1.19	52.5	.453	18.6
105.	998	1.35	76.1	.454	11.8
106.	998	.768	248.8	.693	25.0
107.	1002	.801	291.8	.751	20.9
108.	997	.980	253.8	.789	17.5
109.	999	.894	243.4	.687	16.5
110.	1000	.642	251.9	.616	28.5
111.	1001	.534	273.9	.574	33.3
D_1 = 0.540"	D_2 = 0.875"		D_h = 0.335"	L = 102"	
SAND BLASTED (Approximately 300 microinch rms roughness) (The following data taken using the variable flow procedure)					
112.	999	.697	64.9	.386	28.9
113.	1004	.872	58.2	.403	23.5
114.	1001	1.01	53.0	.409	20.2
115.	1002	1.17	49.2	.411	17.1
116.	999	.385	100.2	.321	43.2
117.	1004	.474	84.5	.360	40.4
118.	999	.551	78.6	.386	37.1
119.	1009	1.20	51.6	.454	18.7
120.	1009	1.32	51.6	.438	15.5
121.	1012	1.39	44.1	.440	15.5
122.	1009	1.48	43.7	.440	14.1
123.	1001	.839	215.5	.647	21.0
124.	1000	.940	215.9	.717	20.3
125.	1001	1.12	215.5	.761	14.7
126.	1011	1.21	220.6	.841	14.7
127.	996	1.33	227.6	.870	10.9
D_1 = 0.540"	D_2 = 0.875"		D_h = 0.335"	L = 102"	
(The following data taken using the constant-flow procedures)					
128.	999	1.11	13.6	.432	25.1
129.	999	1.12	121.4	.617	20.0
130.	999	1.14	162.9	.729	19.7
131.	999	1.12	159.3	.722	20.6
132.	996	1.12	203.9	.810	19.2
133.	1009	1.12	250.1	.846	14.7
134.	1001	1.13	226.8	.841	17.3
135.	1008	1.12	124.1	.660	22.1

RUN NO.	P PSIA	$G/10^6$ LB/HR FT^2	Δh_s BTU/LB	$\Phi_{bo}/10^6$ BTU/HR FT^2	X PER CENT
136.	1000	1.12	183.2	.761	19.4
137.	997	1.12	100.7	.603	22.3
138.	989	1.12	73.2	.559	23.6
139.	999	1.12	53.2	.505	23.5
140.	999	.564	23.4	.374	42.9
141.	999	.564	65.8	.392	38.6
142.	1000	.560	109.4	.436	37.8
143.	999	.550	132.7	.450	36.9
144.	999	.565	161.5	.468	33.2
145.	1001	.571	186.1	.500	32.8
146.	1000	.553	174.2	.488	35.2
147.	1001	.565	210.9	.522	32.4
148.	1004	.555	244.2	.547	31.6
149.	992	.565	306.1	.591	26.1
150.	998	.574	343.2	.627	23.7
151.	1002	1.13	20.1	.454	25.1
152.	997	1.13	48.6	.512	24.3
153.	1003	1.12	76.7	.551	22.9
154.	1003	1.12	99.4	.594	22.1
155.	1000	1.13	118.1	.633	21.2
156.	999	1.11	113.3	.625	22.1
157.	998	1.13	149.0	.681	19.4
158.	996	1.13	182.5	.745	18.2
159.	997	1.13	223.3	.838	17.8
160.	993	1.13	267.0	.920	15.9
161.	994	1.11	245.5	.879	17.5
162.	1012	1.13	215.8	.829	18.5
163.	1001	1.12	309.0	.977	13.5
164.	995	1.11	352.7	1.088	14.3
165.	999	1.55	10.0	.510	21.5
166.	1001	1.55	62.2	.616	18.4
167.	1009	1.55	101.6	.704	16.2
168.	992	1.55	128.7	.750	14.0
169.	1003	1.55	148.6	.797	13.3
170.	997	1.55	173.7	.886	13.3
171.	1009	1.56	221.2	1.013	11.5
172.	999	1.55	261.1	1.090	9.2
173.	992	1.58	285.1	1.149	7.3
174.	994	1.54	300.9	1.181	7.3
175.	996	1.53	246.2	1.049	10.1
176.	992	1.54	334.9	1.249	5.5
177.	999	1.54	298.5	1.204	8.8
178.	998	1.55	282.3	1.162	9.2
179.	1017	1.55	189.7	.913	12.2
180.	999	1.55	254.3	1.084	9.9
181.	994	1.55	291.7	1.158	7.6
182.	994	1.53	344.8	1.274	5.4

TABLE 4 (CONT.)

RUN NO.	P PSIA	$G/10^6$ LB/HR FT^2	Δh_s BTU/LB	$\phi_{bo}/10^6$ BTU/HR FT^2	X PER CENT
183.	999	1.54	299.5	1.186	7.8
184.	1004	1.54	267.6	1.127	10.1
185.	999	1.55	218.5	1.024	12.7
186.	995	1.56	199.3	.972	13.2
187.	998	1.56	174.6	.902	13.7
188.	997	1.55	150.3	.836	14.7
189.	1006	1.55	129.6	.773	15.0
190.	993	1.55	98.9	.694	16.1
191.	994	1.55	64.5	.625	18.4
192.	999	1.54	12.5	.499	20.8
193.	999	.845	11.4	.430	33.9
194.	1001	.845	60.9	.488	31.2
195.	999	.846	92.5	.524	29.2
196.	1004	.845	137.9	.580	27.0
197.	1005	.850	179.7	.671	27.8
198.	999	.845	217.4	.716	26.0
199.	1001	.837	255.7	.800	27.6
200.	996	.845	317.2	.856	22.3
201.	999	.846	362.2	.904	19.2
202.	1005	.835	412.2	.977	18.7
203.	1007	.827	381.7	.950	21.8
204.	1001	.840	360.3	.920	21.4
205.	1001	.840	316.6	.863	23.4
206.	999	.839	263.4	.813	27.5
207.	996	.845	231.5	.731	25.0
208.	1001	.849	201.8	.680	25.2
209.	1002	.835	162.7	.646	29.2
210.	998	.849	127.9	.596	29.6
211.	1003	.840	87.6	.525	30.4
212.	1449	1.14	12.9	.374	23.9
213.	1449	1.13	56.5	.437	20.9
214.	1449	1.13	93.6	.511	19.6
215.	1449	1.13	122.2	.585	20.0
216.	1452	1.14	159.2	.625	15.9
217.	1452	1.14	186.4	.692	15.9
218.	1451	1.13	212.1	.747	15.6
219.	1452	1.12	237.8	.795	15.1
220.	1449	1.15	16.4	.352	21.7
221.	1449	1.13	97.6	.525	20.0
222.	1452	1.13	123.3	.562	18.1
223.	1447	1.13	139.7	.592	17.3
224.	1447	1.13	147.3	.603	16.9
225.	1447	1.13	161.0	.627	16.3
226.	1451	1.12	176.4	.684	17.6
227.	1443	1.14	169.7	.681	18.2
228.	1446	1.14	169.8	.670	17.2
229.	1444	1.13	162.6	.666	18.5
230.	1443	1.13	158.5	.666	19.3
231.	1448	1.13	155.2	.636	17.6

TABLE 4 (CONT.)

RUN NO.	P PSIA	$G/10^6$ LB/HR FT^2	Δh_s BTU/LB	$\Phi_{bo}/10^6$ BTU/HR FT^2	X PER CENT
232.	1447	1.13	152.3	.625	17.5
233.	1448	1.13	143.1	.613	18.3
234.	1447	1.13	183.0	.666	14.8
235.	599	1.13	11.5	.492	25.5
236.	599	1.13	46.8	.545	23.7
237.	599	1.12	91.8	.618	21.7
238.	599	1.13	120.2	.704	22.5
239.	598	1.12	170.1	.804	21.5
240.	599	1.13	188.7	.822	19.7
241.	597	1.12	208.2	.863	19.3
242.	597	1.12	233.7	.909	18.6
243.	593	1.11	247.5	.950	19.3
244.	599	1.13	14.1	.488	25.1
245.	607	1.13	92.3	.636	22.6
246.	609	1.11	271.4	.956	16.6

TABLE 4 (CONT.)

NEW TEST SECTION

UNIFORM HEAT FLUX DISTRIBUTION

RUN NO.	P PSIA	$G/10^6$ LB/HR FT^2	Δh_s BTU/LB	$\Phi_{bo}/10^6$ BTU/HR FT^2	X PER CENT
D_1 = .540"		D_2 = .875"	D_h = .355"	L = 108"	
(The following data taken using constant flow procedure)					
.875" I.D. Riser (Loop Configuration No. 1)					
247.	999	1.13	33.1	.451	24.6
248.	999	1.13	75.5	.511	22.0
249.	999	1.13	113.8	.576	20.3
250.	999	1.13	143.1	.633	19.6
251.	999	1.12	176.4	.708	19.6
252.	999	1.12	219.7	.788	18.2
253.	999	1.12	261.3	.882	18.0
254.	999	1.12	355.3	1.030	13.6
.875" I.D. Riser, 25 feet of 1/4 Inch Pipe Ahead of Test Section (Configuration No. 2)					
255.	999	.565	58.0	.355	37.8
256.	999	.561	86.2	.376	36.4
2" Schedule 80 Pipe Riser, Restriction in Test Section Inlet (Configuration No. 3)*					
257.	999	1.13	38.4	.452	23.7
258.	1003	1.13	69.0	.495	22.0
259.	995	1.13	123.0	.588	19.7
260.	1009	1.13	151.9	.642	18.9
261.	1000	1.13	170.6	.687	19.0
262.	1004	1.13	192.5	.753	20.1
263.	1002	1.13	223.4	.811	18.9
264.	1003	1.12	257.2	.837	15.7
265.	994	1.13	297.4	.910	14.0
266.	995	1.12	327.4	.966	13.5
267.	997	1.11	349.7	1.005	13.2
268.	1003	1.12	169.2	.708	20.9
269.	1004	1.13	119.5	.624	22.7
270.	1002	1.14	33.3	.458	24.7
271.	1000	1.12	408.4	1.088	9.4

*The restriction was in place for all subsequent runs except as noted. The two riser sizes were used interchangeably, no effect due to riser size being discernible.

TABLE 4 (CONT.)

RUN NO.	P PSIA	$G/10^6$ LB/HR FT^2	Δh_s BTU/LB	$\phi_{bo}/10^6$ BTU/HR FT^2	X PER CENT
272.	1001	.565	70.0	.354	35.7
273.	1006	.569	102.4	.386	34.8
274.	999	.565	123.9	.406	34.2
275.	999	.562	150.4	.438	34.7
276.	999	.562	184.9	.494	36.8
277.	997	.574	60.3	.365	37.9
278.	997	.571	217.1	.506	32.3
279.	994	.562	254.9	.530	30.8
280.	1000	.562	292.4	.563	29.5
281.	999	.560	376.1	.641	27.0
282.	1000	1.67	23.8	.510	19.0
283.	999	1.68	57.3	.589	17.3
284.	1002	1.68	95.7	.700	16.3
285.	1004	1.65	125.6	.783	16.0
286.	999	1.68	158.7	.859	13.6
287.	999	1.67	208.5	.968	10.9
288.	994	1.67	242.0	1.035	8.6
289.	994	1.67	284.2	1.146	7.2
290.	1004	1.67	164.2	.880	13.8
(The following data taken using the variable flow procedure)					
291.	1004	.294	47.1	.252	56.6
292.	1000	.440	28.4	.317	49.1
293.	994	.558	18.3	.358	44.9
294.	999	.712	15.5	.399	39.3
295.	994	.837	13.9	.416	34.8
296.	1002	1.01	16.0	.440	30.1
297.	1003	1.25	14.7	.466	25.3
298.	992	1.13	13.0	.458	28.0
299.	999	1.28	15.5	.462	24.4
300.	999	1.41	12.7	.473	23.0
301.	999	1.55	15.5	.504	21.8
302.	999	1.68	12.7	.488	19.7
D_1 = .540" D_2 = .875" D_h = .335" L = 72"					
(The following data taken using the constant flow procedure)					
303.	999	1.13	37.6	.580	19.6
304.	995	1.14	37.8	.605	20.5
305.	1004	1.13	97.1	.736	17.3
306.	1009	1.13	170.8	.934	14.7
307.	990	1.13	244.4	1.112	11.2
308.	997	1.13	42.0	.597	19.7
309.	999	1.12	78.6	.694	18.5
310.	999	1.12	113.8	.781	17.0
311.	999	1.12	190.5	.966	13.2

TABLE 4 (CONT.)

RUN NO.	P PSIA	$G/10^6$ LB/HR FT^2	Δh_s BTU/LB	$\phi_{bo}/10^6$ BTU/HR FT^2	X PER CENT
312.	999	.565	58.8	.483	33.2
313.	999	.561	157.5	.605	29.1
314.	1004	.561	261.9	.786	29.0
315.	999	.559	305.1	.827	26.4
316.	999	1.73	19.6	.646	15.5
317.	999	1.13	41.0	.592	19.5
318.	999	1.13	70.9	.660	18.0
319.	999	1.13	72.2	.663	17.9
320.	999	1.13	40.8	.597	19.8
321.	994	1.74	31.5	.644	13.5
322.	1002	1.73	74.7	.805	11.5
323.	999	1.71	124.9	1.000	9.7
324.	964	1.69	178.1	1.230	8.5
	(The following data taken using the variable flow procedure)				
325.	999	1.42	30.4	.699	15.9
326.	999	.570	51.5	.488	34.4
327.	997	.300	88.4	.351	44.5
D_1 = .375"	D_2 = .875"		D_h = .500"	L = 106 3/4"	
	(The following data taken using the constant flow procedure)*				
328.	994	1.12	31.0	.610	16.3
329.	999	1.13	70.9	.703	13.3
330.	999	1.14	98.6	.785	11.4
331.	1004	1.12	163.2	1.000	9.4
D_1 = .375"	D_2 = .875"		D_h = .500"	L = 108"	
332.	999	1.12	30.9	.591	15.9
333.	996	1.12	65.1	.694	14.3
334.	1000	1.12	108.2	.835	12.5
335.	999	1.12	133.0	.915	11.5
336.	1005	1.12	178.0	1.079	10.2
337.	999	1.14	182.5	1.082	8.94
338.	999	1.13	196.4	1.116	8.61
339.	999	1.12	219.0	1.181	7.61
340.	1004	1.14	177.4	1.051	8.90
341.	999	1.12	119.9	.866	11.9
342.	999	1.12	30.1	.592	16.1

*All subsequent data also taken using the constant flow procedure.

TABLE 4 (CONT.)

RUN NO.	P PSIA	$G/10^6$ LB/HR FT^2	Δh_s BTU/LB	$\phi_{60}/10^6$ BTU/HR FT^2	X PER CENT
343.	999	1.69	23.7	.679	12.1
344.	999	1.69	55.4	.804	10.1
345.	999	1.69	81.1	.897	8.33
346.	1004	1.68	110.8	.971	5.53
347.	999	1.69	130.5	1.095	5.20
348.	999	1.69	152.6	1.175	3.72
349.	984	1.69	158.7	1.237	4.13
350.	1009	1.67	131.5	1.119	5.95
351.	999	1.69	79.9	.903	8.63
352.	998	1.69	24.9	.686	12.1
353.	995	.532	49.4	.492	28.5
354.	994	.540	104.0	.563	24.7
355.	1006	.539	149.0	.640	23.6
356.	994	.547	191.	.711	21.6
357.	1006	.545	239.2	.804	21.0
358.	1006	.548	299.6	.946	21.5
359.	999	.548	243.0	.819	21.1
360.	999	.542	159.4	.671	24.0
361.	999	.531	47.6	.479	28.1
362.	999	.859	36.8	.557	19.7
363.	989	.86	87.2	.677	17.4
364.	1004	.857	142.7	.804	14.8
365.	994	.859	186.7	.921	13.3
366.	999	.856	235.9	1.085	13.3
D_1 = .375"	D_2 = .875"		D_h = .500"	L = 70"	
367.	999	1.12	25.0	.851	15.4
368.	999	1.12	52.8	.930	12.9
369.	999	1.12	86.2	1.052	10.6
370.	999	1.12	122.4	1.140	6.98
371.	999	1.11	140.7	1.199	5.66
372.	999	1.12	149.4	1.240	5.23
373.	999	1.12	163.9	1.285	3.81
374.	999	1.12	189.4	1.362	1.74
375.	1001	1.12	216.5	1.450	- 0.45
376.	999	1.69	20.9	.904	10.4
377.	999	1.69	55.4	1.073	7.53
378.	999	1.67	96.3	1.216	3.65
379.	999	1.68	126.1	1.335	0.73
380.	1004	1.69	165.3	1.502	- 2.83
381.	1004	1.69	176.4	1.540	- 3.98
382.	1004	1.69	113.3	1.266	1.74
383.	999	1.69	93.8	1.221	3.91
384.	999	1.69	19.6	.930	10.9

TABLE 4 (CONT.)

RUN NO.	P PSIA	$G/10^6$ LB/HR FT^2	Δh_s BTU/LB	$\phi_{60}/10^6$ BTU/HR FT^2	X PER CENT
385.	999	.533	45.0	.668	24.8
386.	999	.530	71.9	.703	22.6
387.	999	1.12	245.1	1.560	- 2.29
388.	1002	1.12	266.1	1.631	- 3.85
389.	599	1.10	29.3	.906	14.7
390.	599	1.12	59.1	1.006	12.3
391.	599	1.13	83.0	1.083	10.3
392.	599	1.11	103.7	1.149	9.20
393.	599	1.12	144.4	1.295	6.24
394.	599	1.12	185.3	1.467	4.24
395.	599	1.69	15.4	.992	11.1
396.	599	1.67	78.1	1.288	6.68
397.	604	1.68	96.4	1.371	5.22
398.	599	1.68	107.2	1.430	4.55
399.	599	.535	39.3	.701	24.2
400.	604	.535	80.9	.792	22.3
401.	599	.539	119.0	.870	20.1
402.	599	.555	198.3	1.075	16.6
403.	599	.550	251.0	1.168	13.5
404.	604	.550	134.9	.930	19.7
405.	603	.552	240.6	1.121	12.8
406.	804	1.12	79.5	1.030	10.6
407.	804	1.12	129.4	1.269	8.30
408.	809	1.11	168.5	1.407	5.91
409.	809	1.12	197.4	1.478	3.01
410.	799	1.12	25.8	.847	14.3
411.	799	1.09	196.8	1.364	1.43
412.	799	1.12	210.2	1.443	0.48
413.	799	1.12	232.2	1.574	0.05
414.	799	1.12	259.5	1.741	- 0.29
415.	1199	1.12	31.3	.763	13.2
416.	1199	1.12	144.1	1.168	4.61
417.	1199	1.12	180.6	1.312	2.14
418.	1204	1.12	201.4	1.354	- 0.40
419.	1204	1.12	175.3	1.269	1.79
420.	1199	1.12	199.0	1.362	0.24
421.	1399	1.12	104.3	.954	6.20
422.	1404	1.12	153.5	1.128	2.09
423.	1399	1.12	182.0	1.216	- 0.59
424.	1399	1.12	194.6	1.252	- 1.67

TABLE 4 (CONT.)

RUN NO.	P PSIA	$G/10^6$ LB/HR FT^2	Δh_s BTU/LB	$\phi_{bo}/10^6$ BTU/HR FT^2	X PER CENT
425.	1379	1.69	137.5	1.226	- 3.02
426.	1404	1.69	108.1	1.121	0.24
427.	1404	1.71	91.7	1.106	2.65
428.	1409	1.69	71.8	1.023	4.90
429.	1409	1.69	36.9	.885	8.59
430.	1404	1.68	24.5	.835	9.95
431.	1404	1.69	93.3	1.097	2.41
432.	1404	1.69	110.2	1.164	0.63
D_1 = .375"	D_2 = .710"		D_h = .335"	L = 70"	
433.	1004	2.24	155.9	1.297	1.21
434.	999	2.25	193.6	1.455	- 1.62
D_1 = .375"	D_2 = 1.250"		D_h = .875"	L = 70"	
435.	994	.568	24.2	.799	11.9
436.	1004	.564	149.2	1.288	2.44
437.	989	.562	177.0	1.412	0.70
438.	1004	.284	40.5	.649	19.2
439.	984	.286	55.5	.715	19.3
440.	1004	.284	34.6	.668	20.9
441.	1004	.281	138.1	.906	14.7
442.	999	.284	35.7	.649	19.9
443.	1014	.282	102.3	.811	16.4
444.	996	.281	135.4	.901	14.9
445.	1004	.281	186.6	1.052	13.0
446.	1004	.284	215.8	1.123	10.8
447.	999	.286	265.5	1.290	9.35
448.	1004	.282	299.3	1.338	6.81
449.	1002	.141	54.1	.541	34.5
450.	994	.140	82.9	.579	33.3
451.	1004	.144	145.4	.687	30.6
452.	1004	.142	177.2	.739	30.7
453.	1004	.142	251.6	.858	28.8
454.	1004	1.12	57.0	1.176	2.98
D_1 = .375"	D_2 = .710"		D_h = .335"	L = 70"	
455.	999	2.25	16.0	.808	13.2
456.	999	2.27	43.7	.918	10.9
457.	1004	2.26	63.7	.954	8.65
458.	1004	2.28	99.6	1.075	5.18
459.	1004	2.26	135.4	1.192	2.12
460.	997	2.24	165.4	1.312	.015
461.	984	2.25	204.6	1.467	- 3.08

TABLE 4 (CONT.)

RUN NO.	P PSIA	$G/10^6$ LB/HR FT^2	Δh_s BTU/LB	$\Phi_{bo}/10^6$ BTU/HR FT^2	X PER CENT
462.	999	1.70	23.1	.744	15.6
463.	999	1.68	79.9	.932	11.9
464.	999	1.68	122.4	1.052	8.54
465.	1009	1.68	169.6	1.195	4.85
466.	1014	1.70	209.4	1.312	1.48
467.	1004	1.69	242.4	1.433	- .24
468.	1004	1.68	171.9	1.207	4.79
469.	1004	1.68	83.9	.918	10.9
470.	1004	1.69	26.3	.742	15.1
471.	1004	1.12	34.6	.649	19.9
472.	1004	1.13	70.7	.727	17.3
473.	1004	1.12	115.8	.816	13.9
474.	999	1.13	159.9	.918	10.9
475.	999	1.13	188.2	.992	9.28
476.	999	1.12	222.0	1.075	7.61
477.	994	1.13	250.5	1.149	5.74
D_1 = .375"	D_2 = .555"		D_h = .180"	L = 70"	
478.	1000	2.23	92.2	.633	13.2
479.	1000	2.26	104.0	.645	11.5
480.	1000	2.24	137.9	.693	8.56
481.	1000	2.25	182.1	.783	5.45
482.	995	2.25	218.6	.864	3.37
483.	1000	2.27	284.4	1.041	.475
484.	1000	1.70	52.7	.455	17.8
485.	1000	1.70	157.2	.615	10.8
486.	1000	1.71	203.2	.705	8.45
487.	1001	1.70	238.2	.761	6.60
488.	1003	1.69	274.7	.833	5.29
489.	997	1.70	296.4	.880	4.41
490.	1003	1.68	335.5	.966	3.85
D_1 = 0.500"	D_2 = 1.00"		D_h = .50"	L = 29"	
(No restriction in test section inlet)					
491.	999	4.36	6.0	1.110	2.14
492.	1004	2.02	13.0	1.060	4.21
493.	1004	2.04	29.8	1.140	2.03
494.	979	2.05	43.2	1.110	- .257

TABLE 4 (CONT.)

RUN NO.	P PSIA	$G/10^6$ LB/HR FT^2	Δh_s BTU/LB	$\phi_{60}/10^6$ BTU/HR FT^2	X PER CENT
D_1 = 0.500"	D_2 = 1.00"		D_h = .50"	L = 36"	
(No restriction in test section inlet)					
495.	1004	2.04	10.8	.958	5.23
496.	999	2.05	25.3	1.050	3.64
497.	999	2.04	46.6	1.151	1.14
498.	999	2.04	55.2	1.193	.085
499.	999	2.04	68.4	1.280	- 1.32
500.	999	2.04	86.2	1.363	- 3.48
501.	999	2.04	100.3	1.426	- 5.21
502.	999	2.04	112.3	1.464	- 6.73
503.	1004	2.04	133.0	1.544	- 9.41
504.	994	1.72	9.2	.939	6.58
505.	994	1.71	33.6	1.087	4.17
506.	994	1.71	63.7	1.252	.914
507.	999	1.71	79.9	1.329	- .858
508.	999	1.71	91.3	1.391	- 2.14
509.	999	1.71	115.0	1.513	- 4.73
D_1 = 0.500"	D_2 = 0.75"		D_h = .25"	L = 36"	
(No restriction in test section inlet)					
510.	999	4.12	11.4	.957	6.50
511.	999	4.12	37.1	1.113	3.89
512.	999	4.14	68.4	1.259	.286
513.	999	4.12	102.6	1.363	- 4.03
514.	999	4.16	130.5	1.496	- 7.33
515.	994	2.07	24.5	.890	11.5
516.	992	2.08	50.5	.974	8.81
517.	1006	2.07	72.0	1.026	6.52
518.	999	2.07	88.7	1.085	4.91
519.	1001	2.07	107.9	1.151	3.11
520.	999	2.07	128.6	1.231	1.35
521.	999	2.06	141.9	1.280	.162
522.	999	2.06	156.3	1.325	- 1.24
523.	999	2.07	172.8	1.374	- 3.05
524.	999	2.07	184.9	1.391	- 4.61
525	999	2.06	204.6	1.454	- 6.39
526.	1406	4.18	14.3	.800	5.17
527.	1404	4.17	26.6	.838	3.42
528.	1405	4.14	42.7	.911	1.40
529.	1404	4.14	58.0	.981	- .576
530.	1404	4.13	74.4	1.078	- 2.44
531.	1399	4.13	99.4	1.183	- 5.76

TABLE 4 (CONT.)

RUN NO.	P PSIA	$G/10^6$ LB/HR FT^2	Δh_s BTU/LB	$\phi_{bo}/10^6$ BTU/HR FT^2	X PER CENT
532.	1399	4.14	118.2	1.287	- 8.03
533.	1394	4.14	130.1	1.374	- 9.21
534.	1399	4.14	149.9	1.482	- 11.60
D_1 = 0.500"		D_2 = 1.00"		D_h = .50"	L = 36"
	(No restriction in test section inlet)				
535.	999	4.08	3.0	1.082	3.43
536.	1002	4.08	24.1	1.200	.596
537.	999	4.09	31.7	1.235	- .455
538.	1004	4.07	48.4	1.357	- 2.57
539.	999	4.07	59.1	1.454	- 3.86
540.	999	6.14	0.47	1.082	2.51
541.	999	6.10	20.7	1.294	- .074
542.	1004	6.10	37.0	1.450	- 2.22
543.	999	6.13	44.2	1.506	- 3.20
544.	1404	4.14	13.1	1.009	1.75
545.	1399	4.09	28.3	1.110	- .420
546.	1409	4.10	46.1	1.249	- 2.95
547.	1404	4.09	55.3	1.353	- 4.11
548.	1410	4.07	63.0	1.426	- 5.12
549.	1399	4.10	7.2	.974	2.67
D_1 = 0.500"		D_2 = 0.75"		D_h = .25"	L = 36"
	(No restriction in test section inlet)				
550.	1009	6.01	8.2	1.031	4.85
551.	1009	6.17	22.5	1.092	2.83
552.	1009	6.18	41.5	1.176	.371
553.	1009	6.18	53.1	1.224	- 1.14
554.	1009	6.19	65.5	1.308	- 2.59
555.	1009	6.20	78.8	1.398	- 4.14
556.	1009	6.20	92.3	1.496	- 5.65
D_1 = .500"		D_2 = 1.00"		D_h = .50"	L = 29"
	(No restriction in test section inlet)				
557.	1000	.405	51.6	.841	17.0
558.	1010	.408	133.3	1.061	10.98
559.	1013	.408	178.2	1.292	10.7
560.	1000	.405	47.2	.823	18.3
561.	1000	.405	47.2	.809	16.8
562.	1000	.408	105.0	.975	12.6

TABLE 4 (CONT.)

RUN NO.	P PSIA	$G/10^6$ LB/HR FT^2	Δh_s BTU/LB	$\phi_{60}/10^6$ BTU/HR FT^2	X PER CENT
563.	1001	.405	51.8	.861	17.7
564.	1003	.408	95.2	.970	14.0
565.	1000	.408	146.6	1.165	11.8
566.	1003	.409	200.2	1.360	9.30
567.	1005	.205	93.0	.690	26.4
568.	1005	.206	148.4	.811	24.8
569.	1005	.204	185.2	.868	22.7
570.	1005	.204	237.5	.950	19.5
571.	1005	.203	280.7	1.023	17.7
572.	1005	.203	354.7	1.165	14.7
573.	1000	.608	36.6	.932	12.8
574.	1000	.612	60.3	1.016	10.8
575.	1000	.610	113.4	1.235	6.95
576.	1000	.614	153.6	1.418	4.22
577.	1000	.611	185.6	1.429	- 0.36
578.	1000	.614	241.3	1.532	- 6.98
579.	1000	.614	254.5	1.690	- 5.94
580.	1000	.609	274.3	1.733	- 7.83
581.	1000	.601	298.0	1.848	- 8.77
582.	1000	.615	326.0	1.899	- 12.9
583.	1010	.406	54.4	.868	17.4
D_1 = 0.375"		D_2 = 0.710"		D_h = 0.335"	L = 70"
584.	999	2.26	23.1	.780	11.5
585.	994	2.24	143.0	1.242	2.05
586.	994	2.25	159.5	1.328	1.15
587.	999	2.25	98.7	1.078	5.66
588.	999	2.24	164.5	1.357	1.04
589.	1014	1.68	171.5	1.164	3.71
590.	994	1.69	195.5	1.257	2.29
591.	999	1.70	37.0	.799	14.8
592.	999	1.13	43.7	.687	19.65
593.	1004	1.14	44.4	.672	18.9
594.	1004	1.13	135.4	.835	11.3
595.	1004	1.12	187.6	.968	8.75
596.	999	.565	109.5	.589	28.5
597.	999	.565	108.8	.594	29.0
598.	999	.559	145.2	.653	28.5
599.	1004	.565	171.7	.708	28.2
600.	999	.573	226.8	.782	24.5
601.	999	.573	279.3	.858	22.1
602.	1004	.578	286.8	.856	20.3

TABLE 4 (CONT.)

RUN NO.	P PSIA	$G/10^6$ LB/HR FT^2	Δh_s BTU/LB	$\phi_{bo}/10^6$ BTU/HR FT^2	X PER CENT
603.	1004	.556	340.4	.935	20.8
604.	999	.565	399.6	1.051	19.3
605.	1004	.569	60.3	.520	30.5
D_1 = 0.375"		D_2 = 0.875"		D_h = .500"	L = 70"
		ROUGH LINER			
606.	994	.546	49.5	.861	32.3
607.	999	.549	54.4	.856	31.2
608.	1004	.536	112.0	.911	26.0
609.	999	.541	141.2	.966	23.6
610.	1004	.542	145.8	.966	22.8
611.	1004	.540	167.7	1.013	21.8
612.	1004	1.12	30.4	1.030	18.7
613.	1004	1.12	54.7	1.092	16.4
614.	1004	1.12	57.5	1.087	15.8
615.	1004	1.12	79.4	1.154	14.0
616.	1004	1.12	118.0	1.242	10.0
617.	1004	1.12	114.5	1.242	10.6
618.	1004	1.12	166.3	1.426	6.61
619.	1004	1.12	166.5	1.388	5.73
620.	1004	1.15	185.4	1.481	4.29
621.	999	1.65	18.2	1.173	15.3
622.	999	1.69	54.1	1.292	11.1
623.	999	1.69	51.5	1.240	10.8
624.	999	1.69	84.9	1.383	7.76
625.	1009	1.69	115.3	1.507	4.94
626.	999	1.69	113.8	1.512	5.23
627.	999	1.68	138.3	1.674	4.01
628.	999	1.68	138.3	1.679	4.06
629.	999	1.69	183.5	1.955	1.18
630.	994	1.69	222.4	2.146	- 1.97

TABLE 5-A

SINGLE PHASE PRESSURE DROP

OLD TEST SECTION

D_1 = 0.540" D_2 = 0.875" D_h = 0.335"

(Rod Concentric)

RUN NO.	P PSIA	$\frac{G}{10^6}$ LB/HR FT^2	T_{in} °F	$\frac{N_R}{10^4}$	V FT/SEC	ΔP * (inches of water) y = 36"	72"	108"
1.	65	1.39	81	1.87	6.20	27	54	81.3
2.	65	1.11	83	1.54	4.96	18.0	36	54.4
3.	65	0.833	93	1.30	3.73	10.0	20.5	31.7
4.	65	0.695	94	1.09	3.11	7.0	15.0	22.5
5.	65	0.556	94	0.88	2.49	4.2	9.4	14.8

* includes channel friction and spacer losses.

TABLE 5-B

TWO-PHASE PRESSURE DROP WITH HEAT ADDITION

OLD TEST SECTION

D_1 = 0.540" D_2 = 0.875" D_h = 0.335" L = 102"

(Rod Concentric)

RUN NO.	P PSIA	$\frac{G}{10^6}$ LB/HR FT^2	Δh_s BTU/LB	$\frac{\Phi}{10^6}$ BTU/HR FT^2	X_e PER CENT	ΔP * (Inches of Water) y = 36"	72"	108"
22.	1000	0.473	56.6	0.331	40.5	- 2.6	1.6	17.5
23.	986	1.22	282.5	0.899	9.1	15.1	34.7	84.
24.	1000	1.23	89.7	0.513	16.1	17.5	59.5	165.
25.	1000	0.742	190.4	0.493	18.2	1.9	10.8	40.5

* Includes channel friction and spacer, acceleration, and hydrostatic pressure drops.

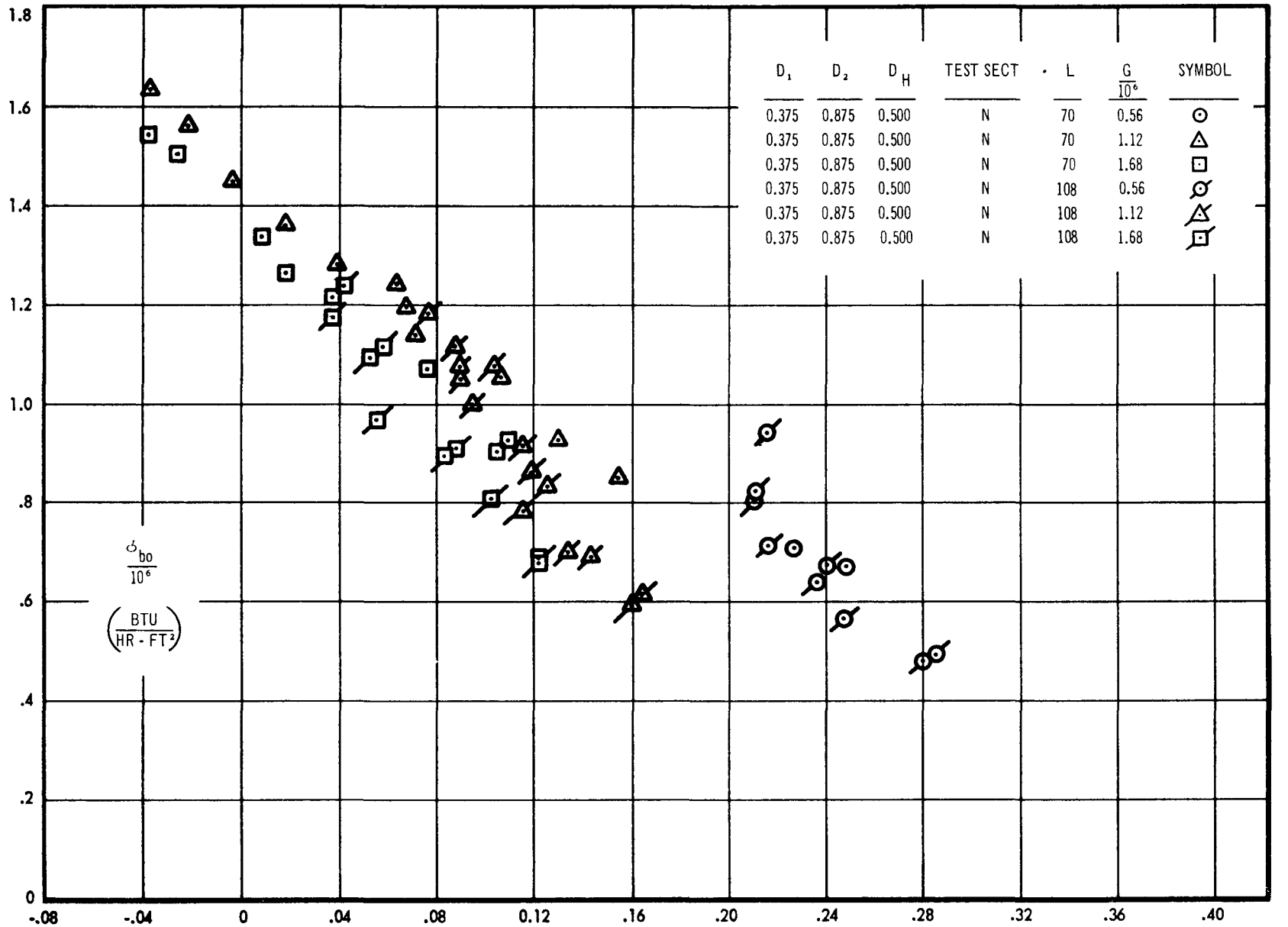

FIGURE 16A EFFECT OF FLOW ON BURNOUT – 1000 PSIA

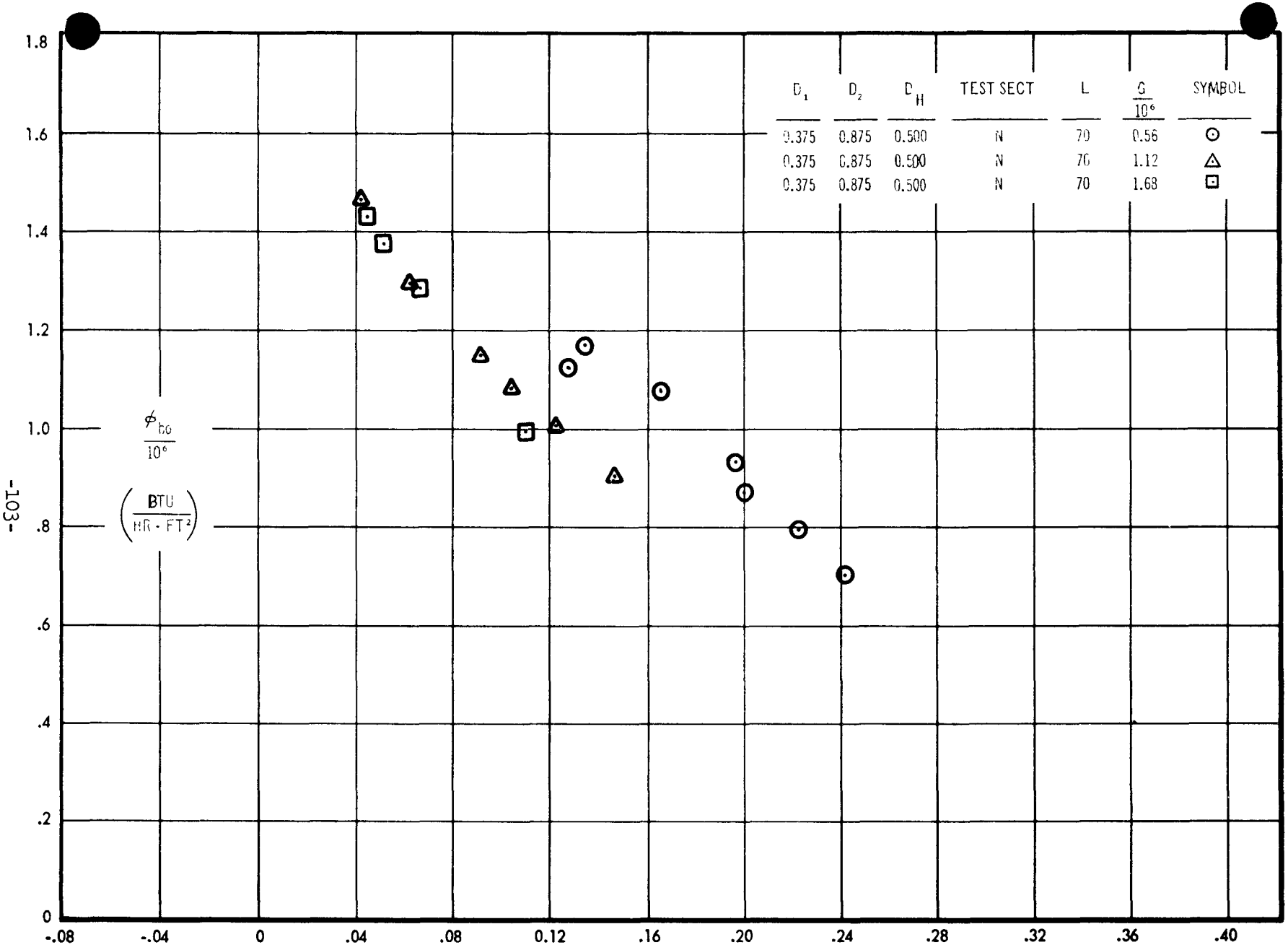

FIGURE 16B EFFECT OF FLOW ON BURNOUT – 600 PSIA

1075–3

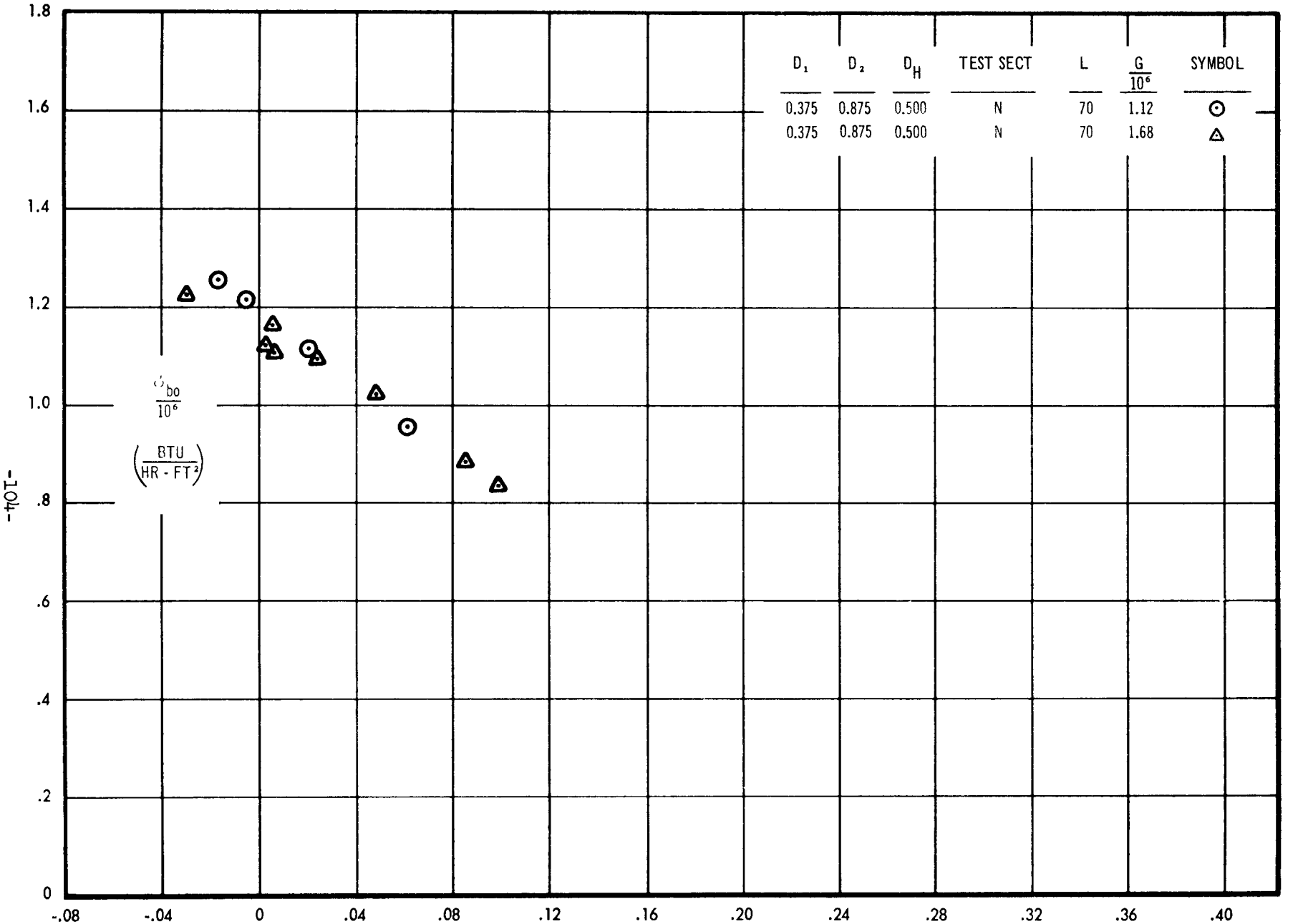

FIGURE 16C EFFECT OF FLOW ON BURNOUT – 1400 PSIA

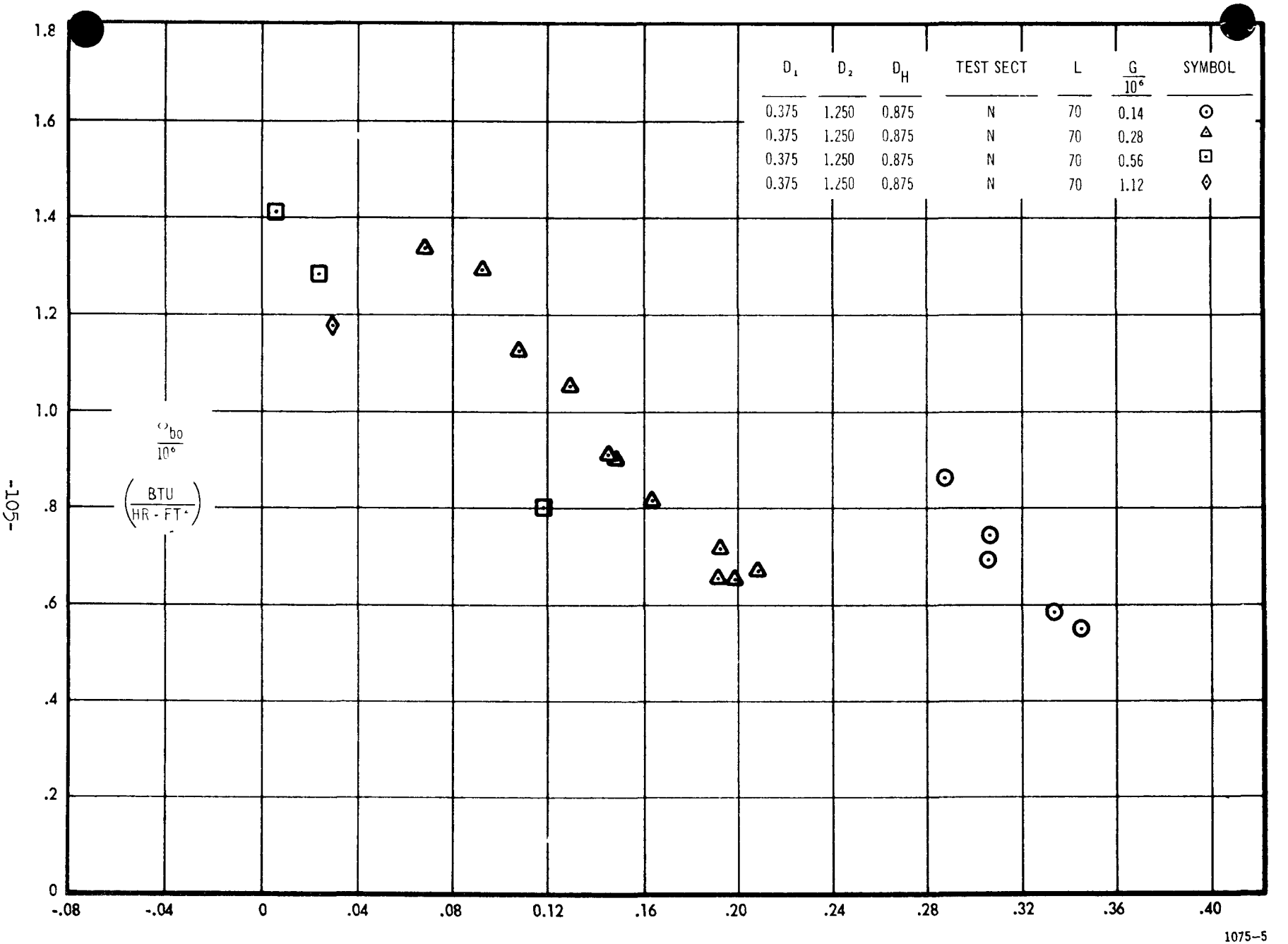

FIGURE 17 A EFFECT OF FLOW ON BURNOUT - 1000 PSIA

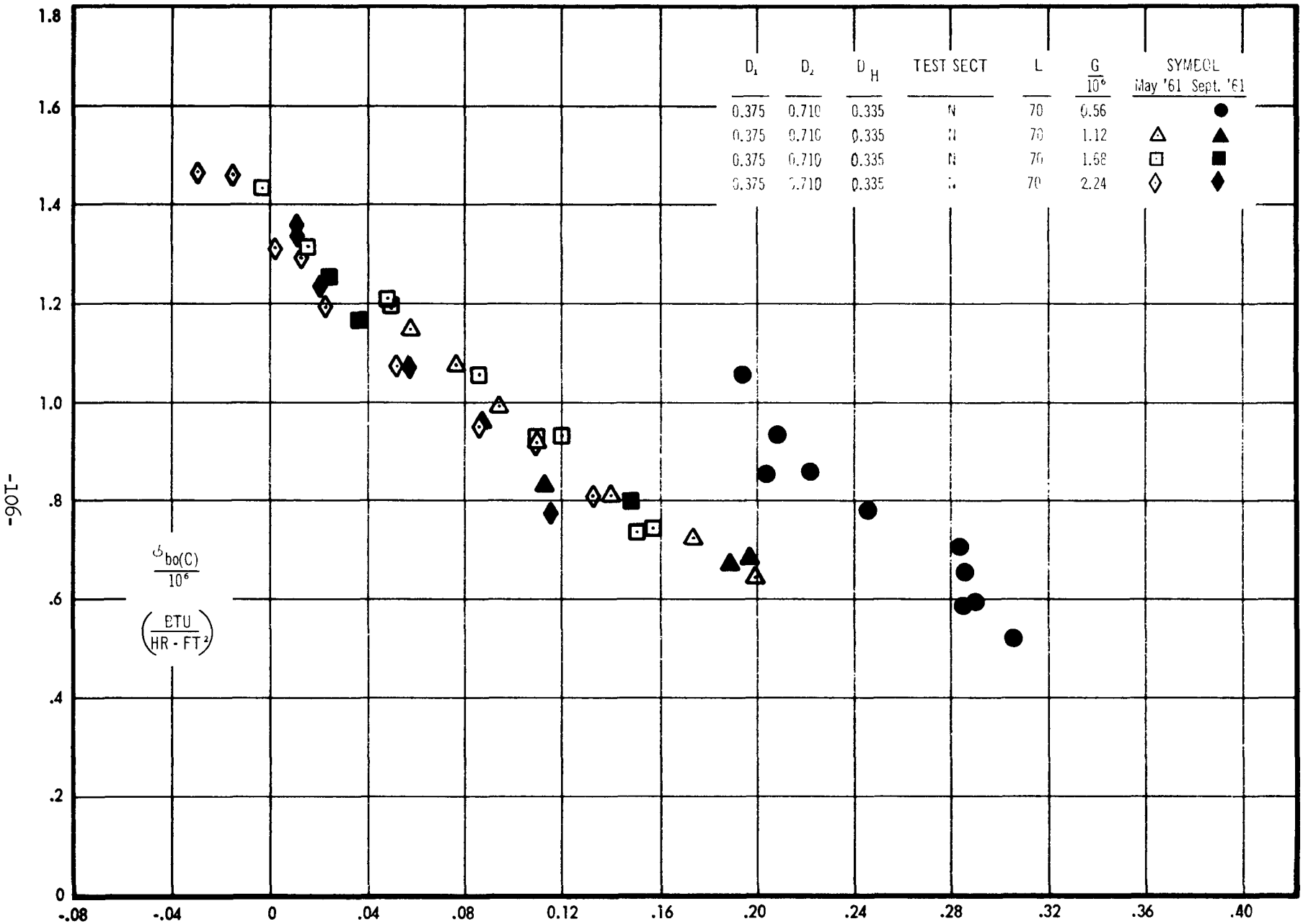

1075-6

FIGURE 17B EFFECT OF FLOW IN BURNOUT – 1000 PSIA

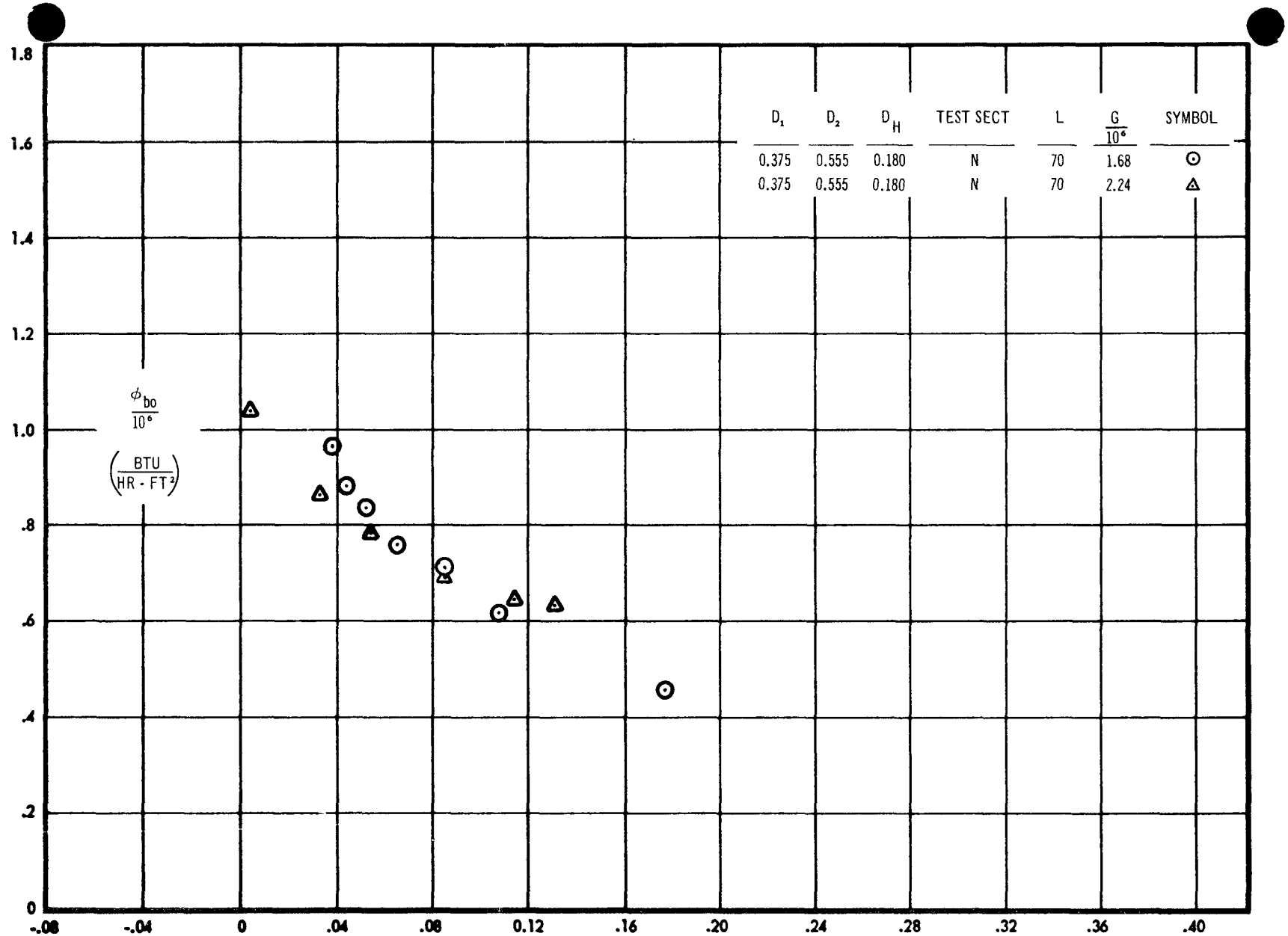

FIGURE 17C EFFECT OF FLOW ON BURNOUT – 1000 PSIA

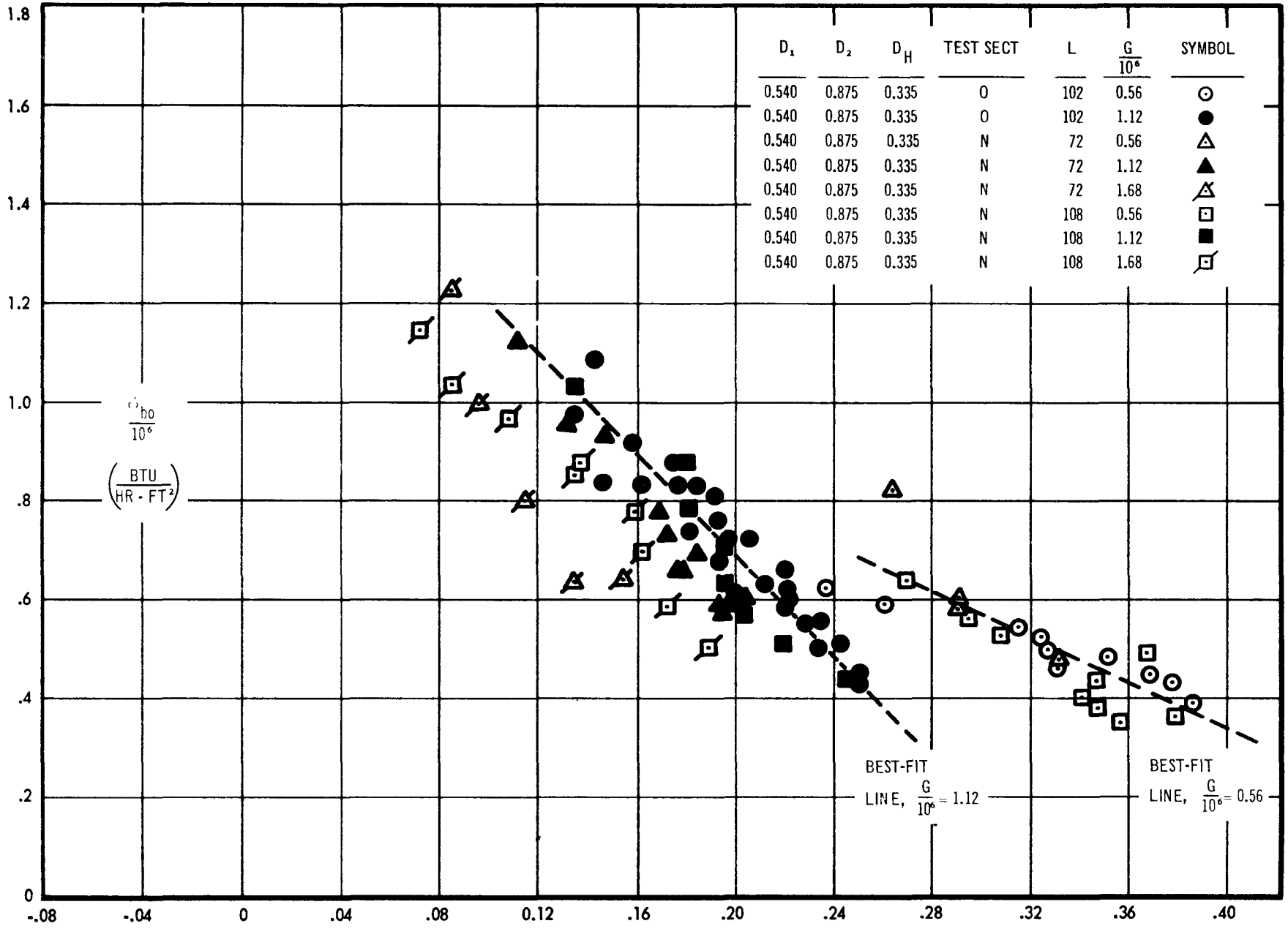

FIGURE 18A EFFECT OF FLOW ON BURNOUT 1000 PSIA

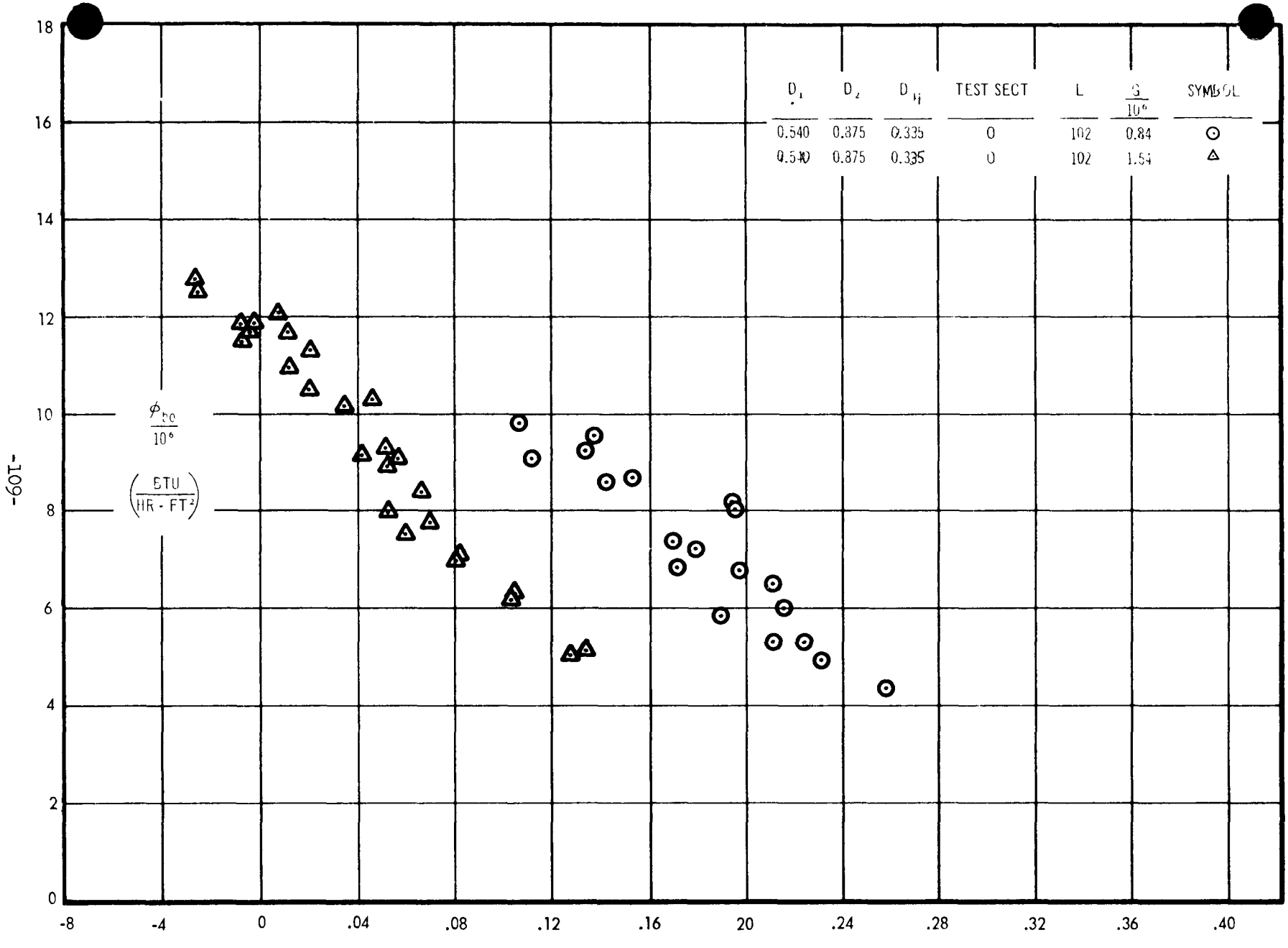

1075-9

FIGURE 18B EFFECT OF FLOW ON BURNOUT – 1000 PSIA

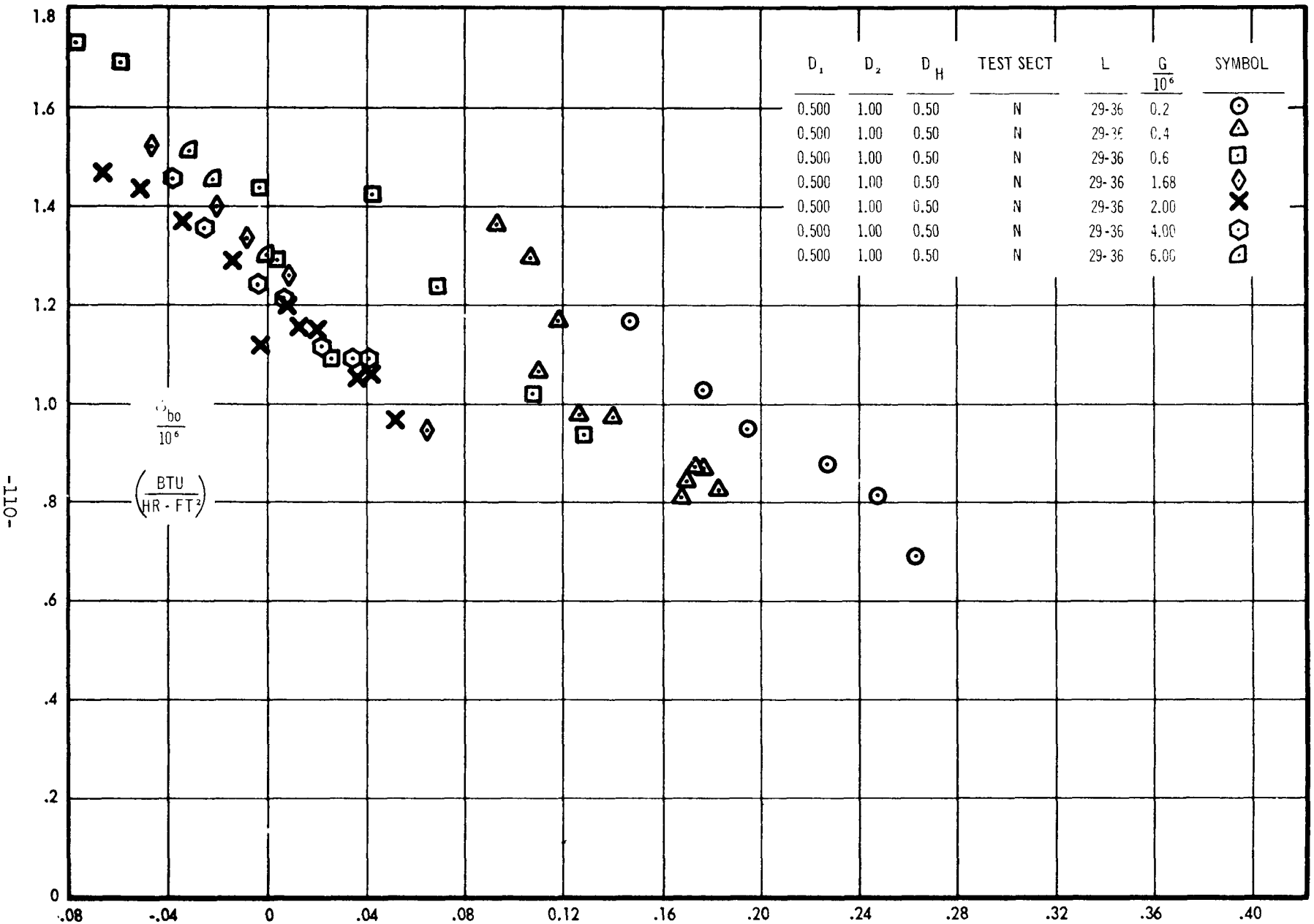

1075-10

FIGURE 19A EFFECT OF FLOW ON BURNOUT – 1000 PSIA

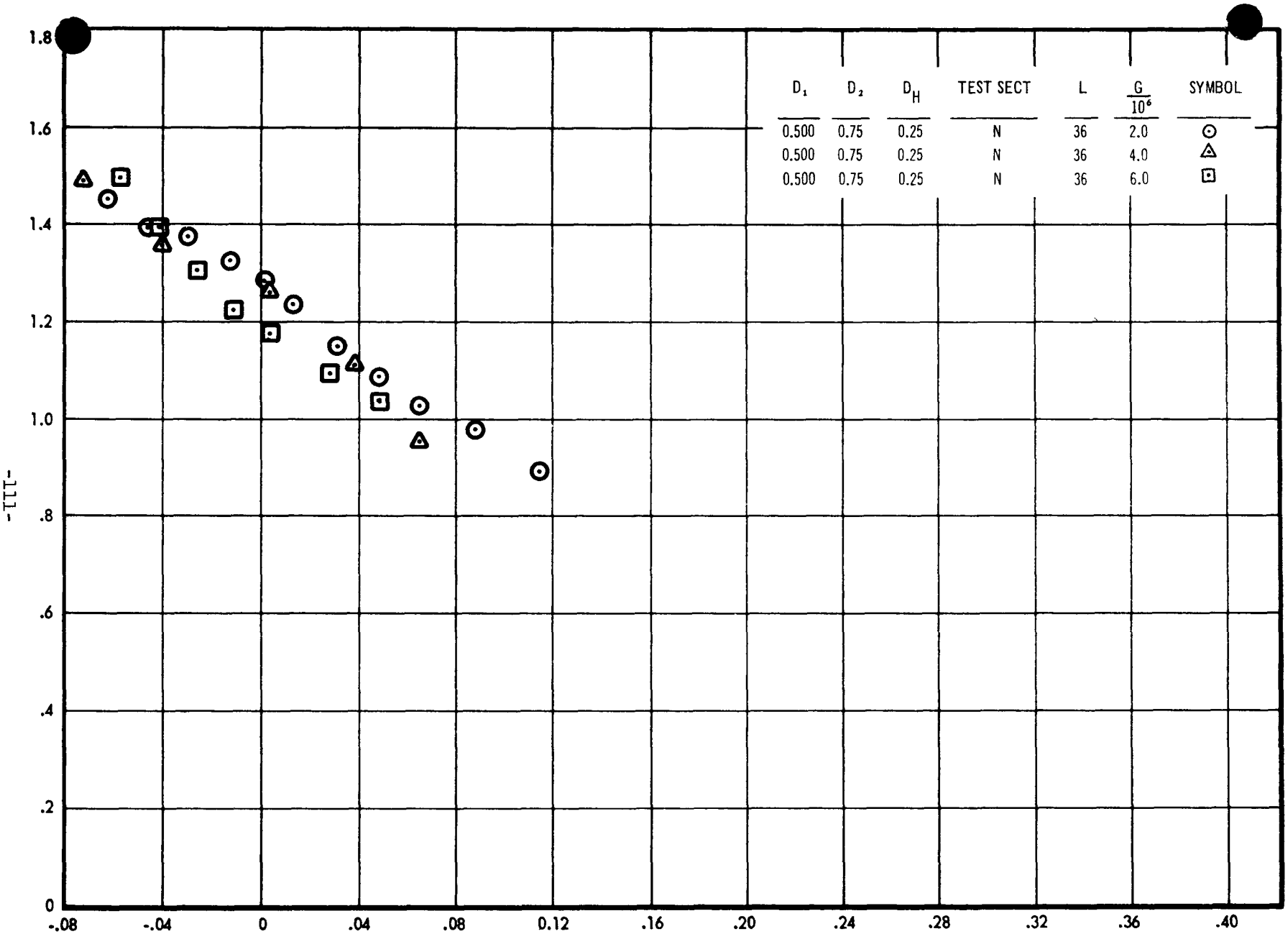

1075-11

FIGURE 19B EFFECT OF FLOW ON BURNOUT - 1000 PSIA

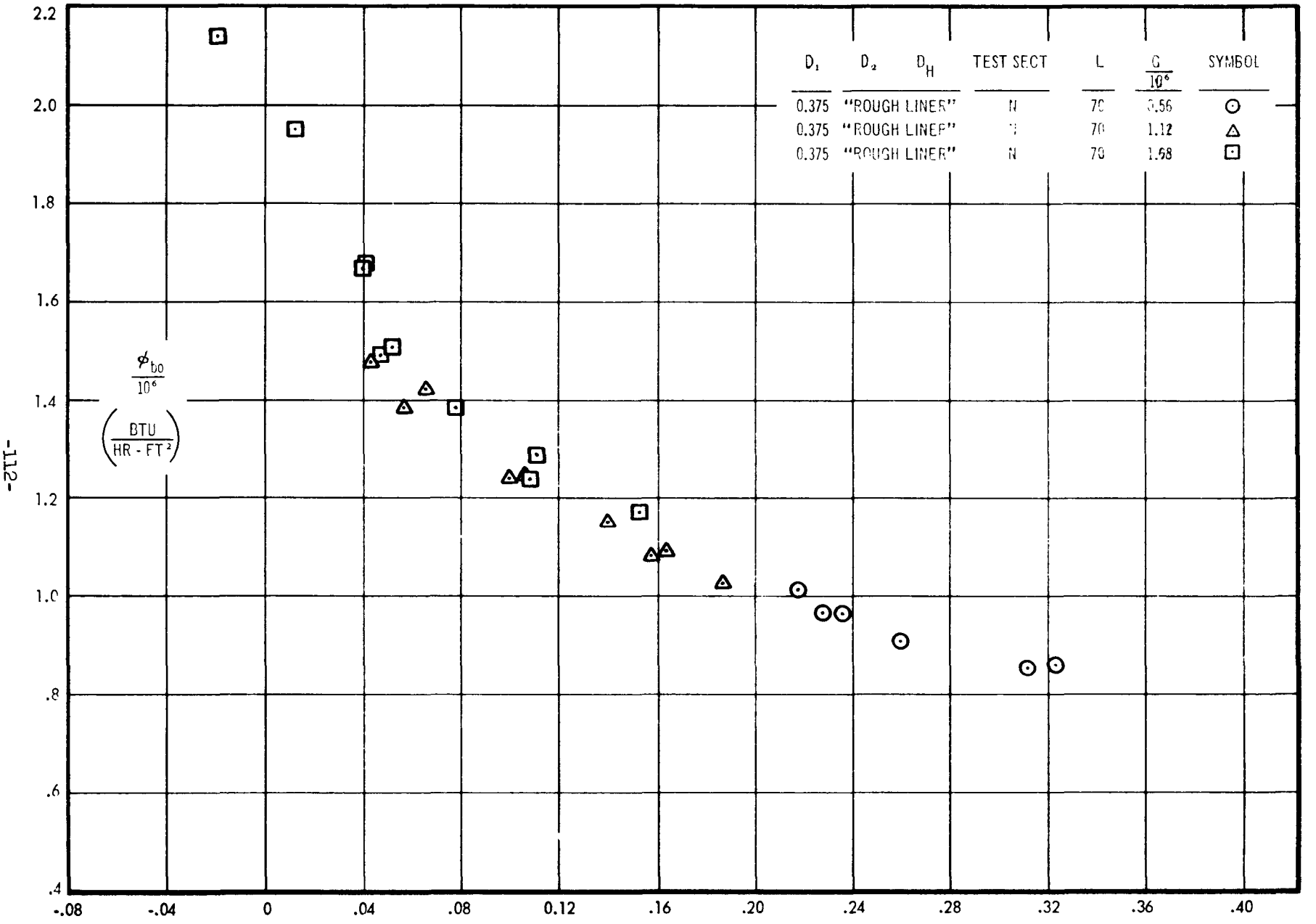

1075-12

FIGURE 20 EFFECT OF FLOW ON BURNOUT – 1000 PSIA

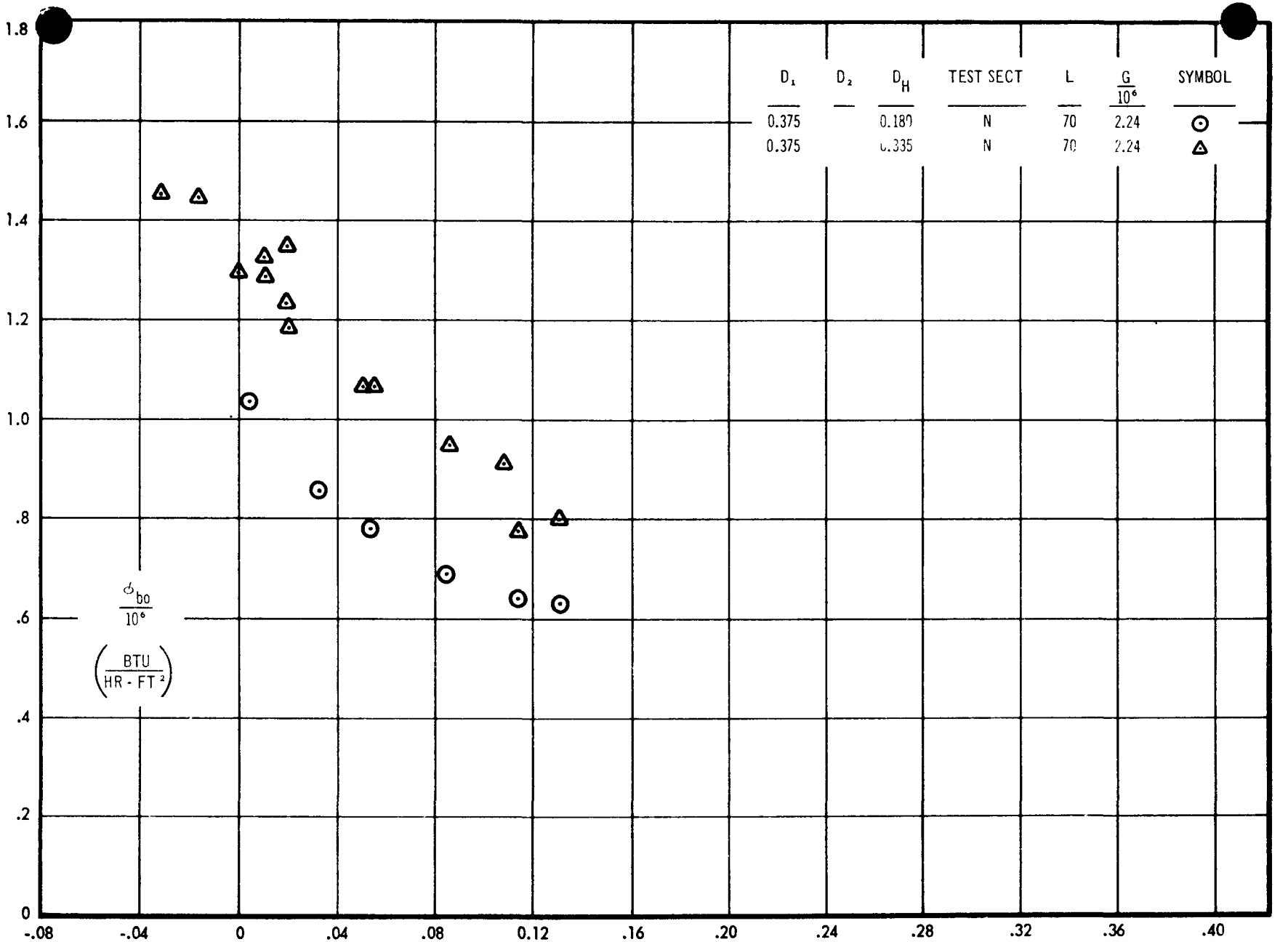

1075-13

FIGURE 21A EFFECT OF HYDRAULIC DIAMETER ON BURNOUT – 1000 PSIA

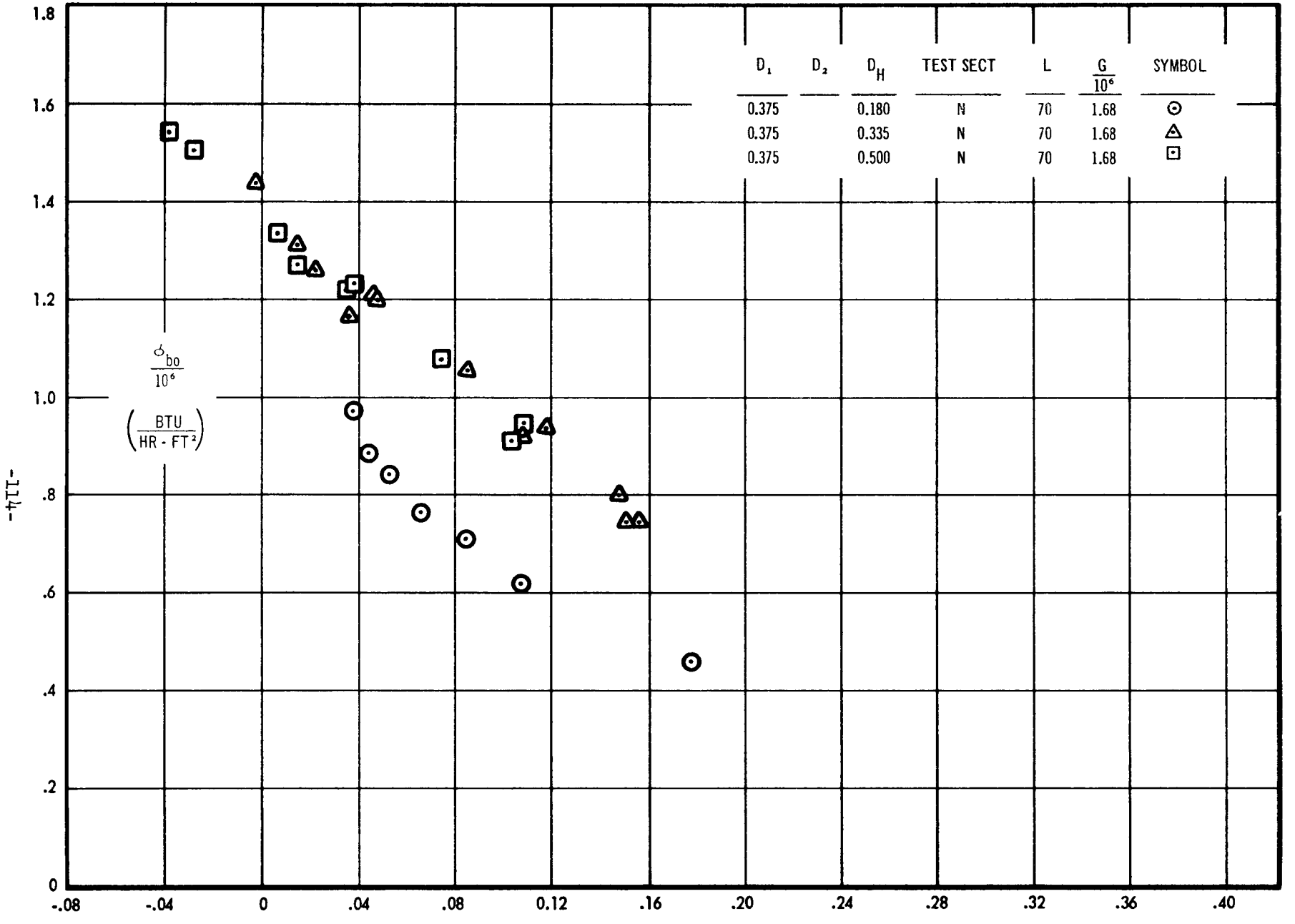

1075-14

FIGURE 21B EFFECT OF HYDRAULIC DIAMETER ON BURNOUT – 1000 PSIA

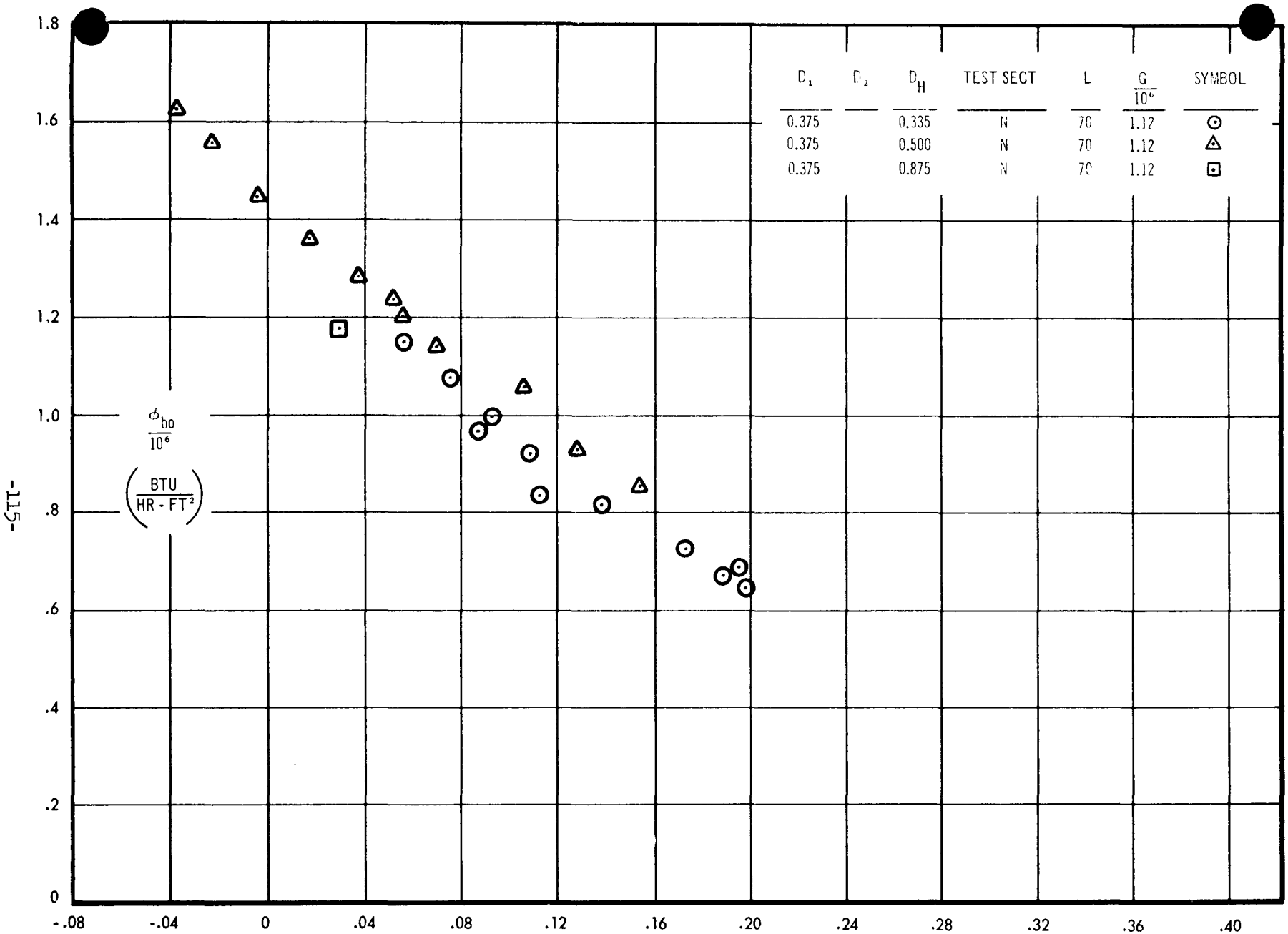

1075-15

FIGURE 21C EFFECT OF HYDRAULIC DIAMETER ON BURNOUT – 1000 PSIA

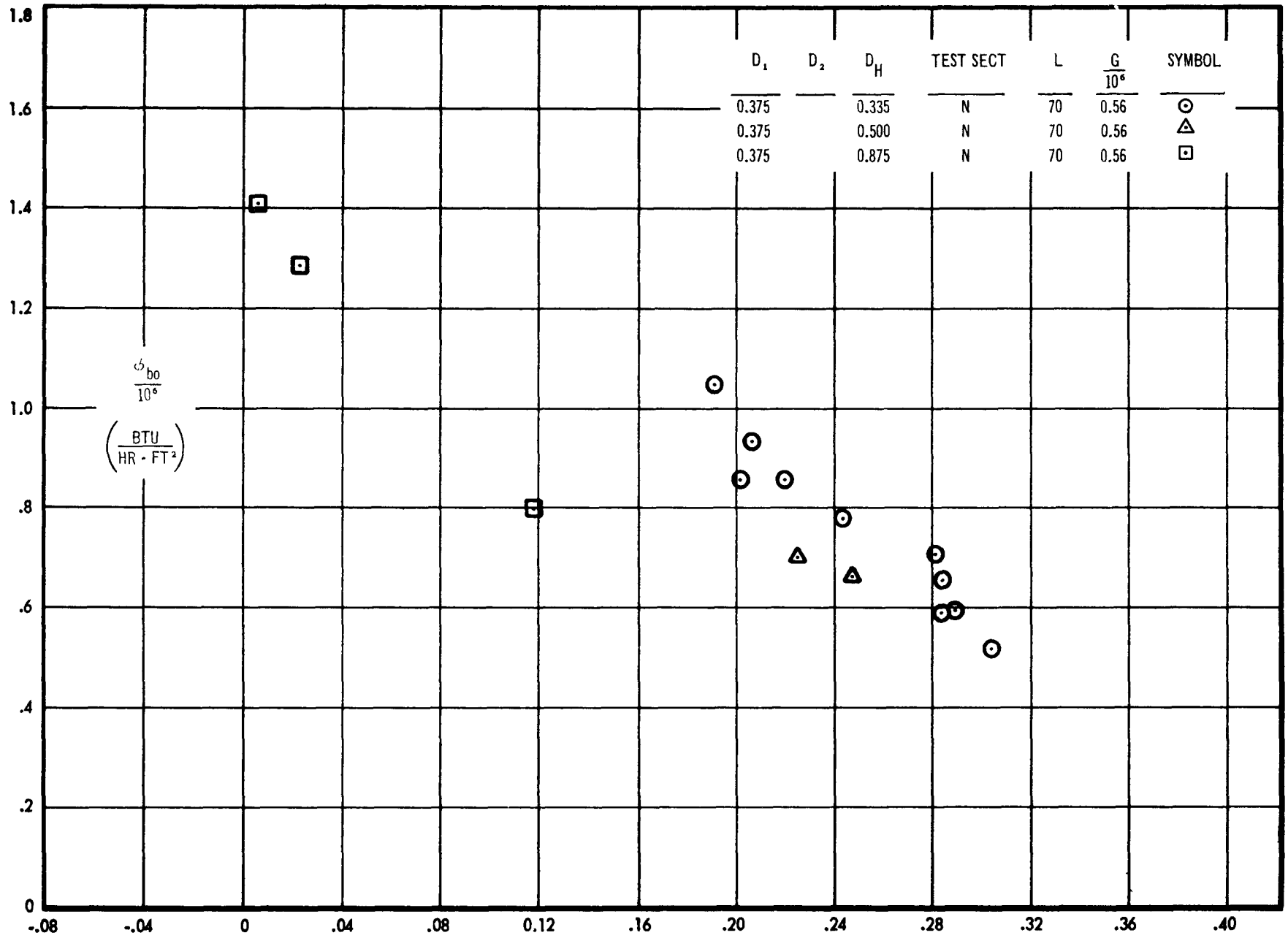

FIGURE 21D EFFECT OF HYDRAULIC DIAMETER ON BURNOUT – 1000 PSIA

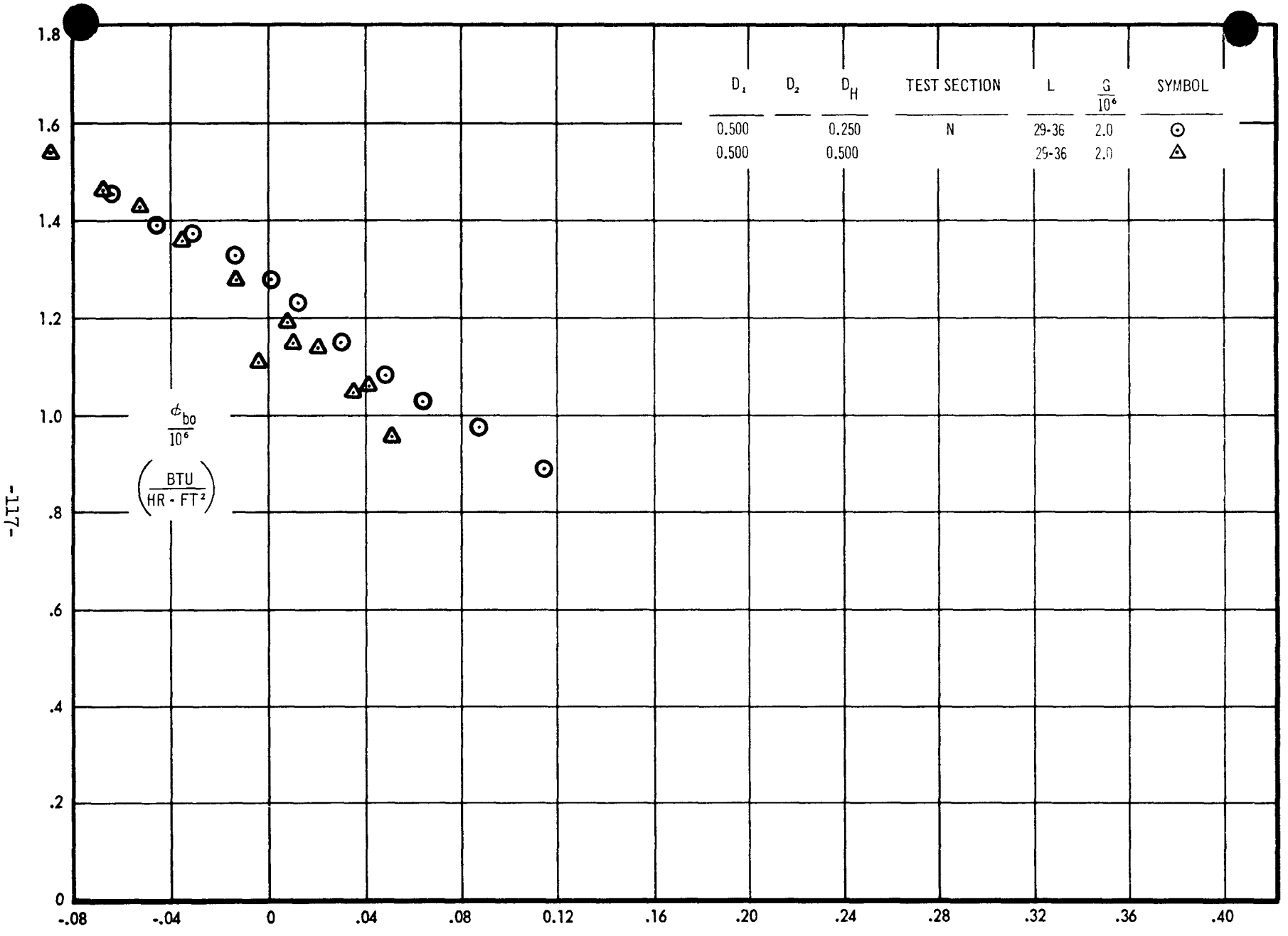

1075-17

FIGURE 22A EFFECT OF HYDRAULIC DIAMETER ON BURNOUT – 1000 PSIA

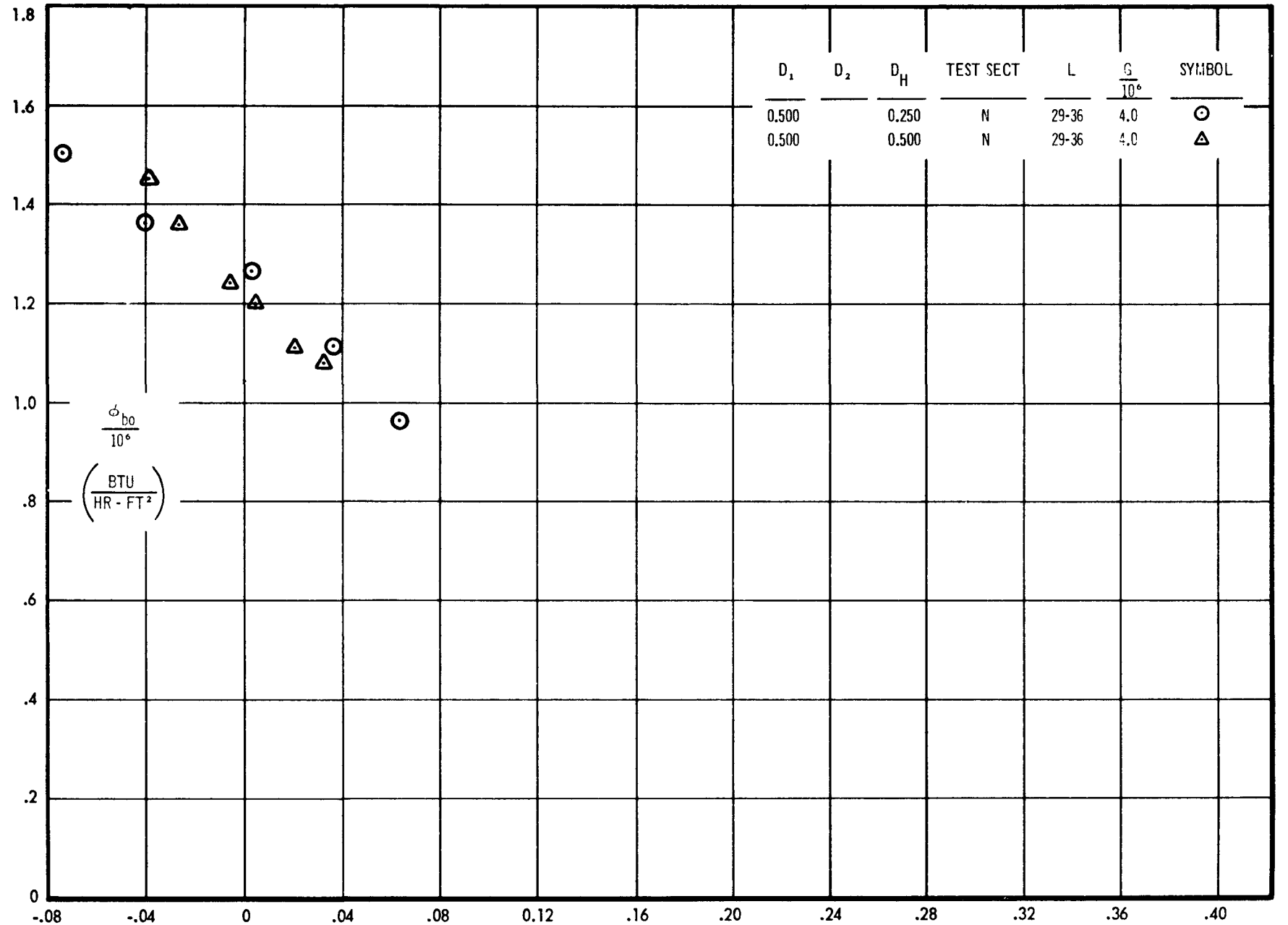

1075-18

FIGURE 22B EFFECT OF HYDRAULIC DIAMETER ON BURNOUT – 1000 PSIA

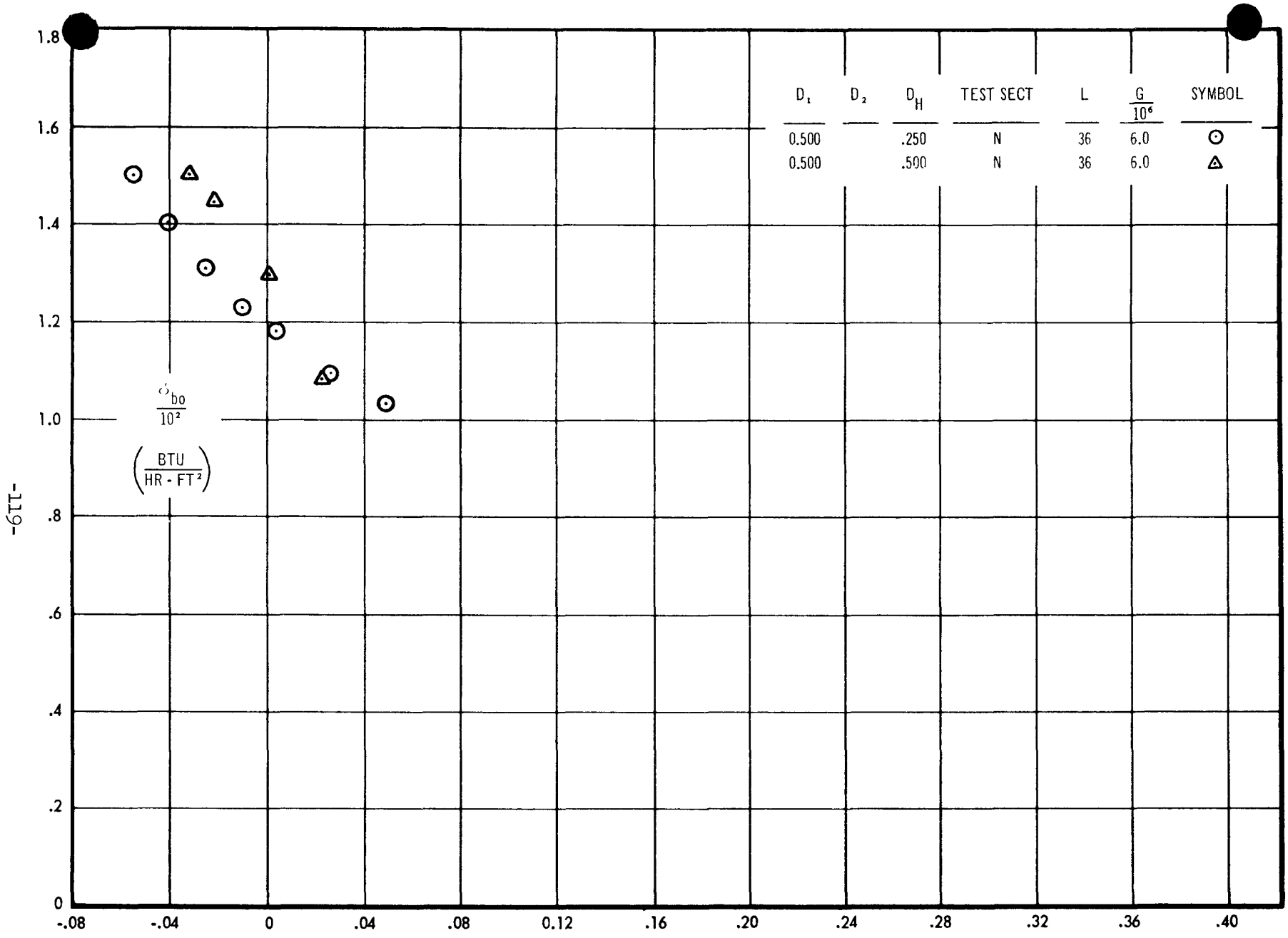

1075–19

FIGURE 22C EFFECT OF HYDRAULIC DIAMETER ON BURNOUT – 1000 PSIA

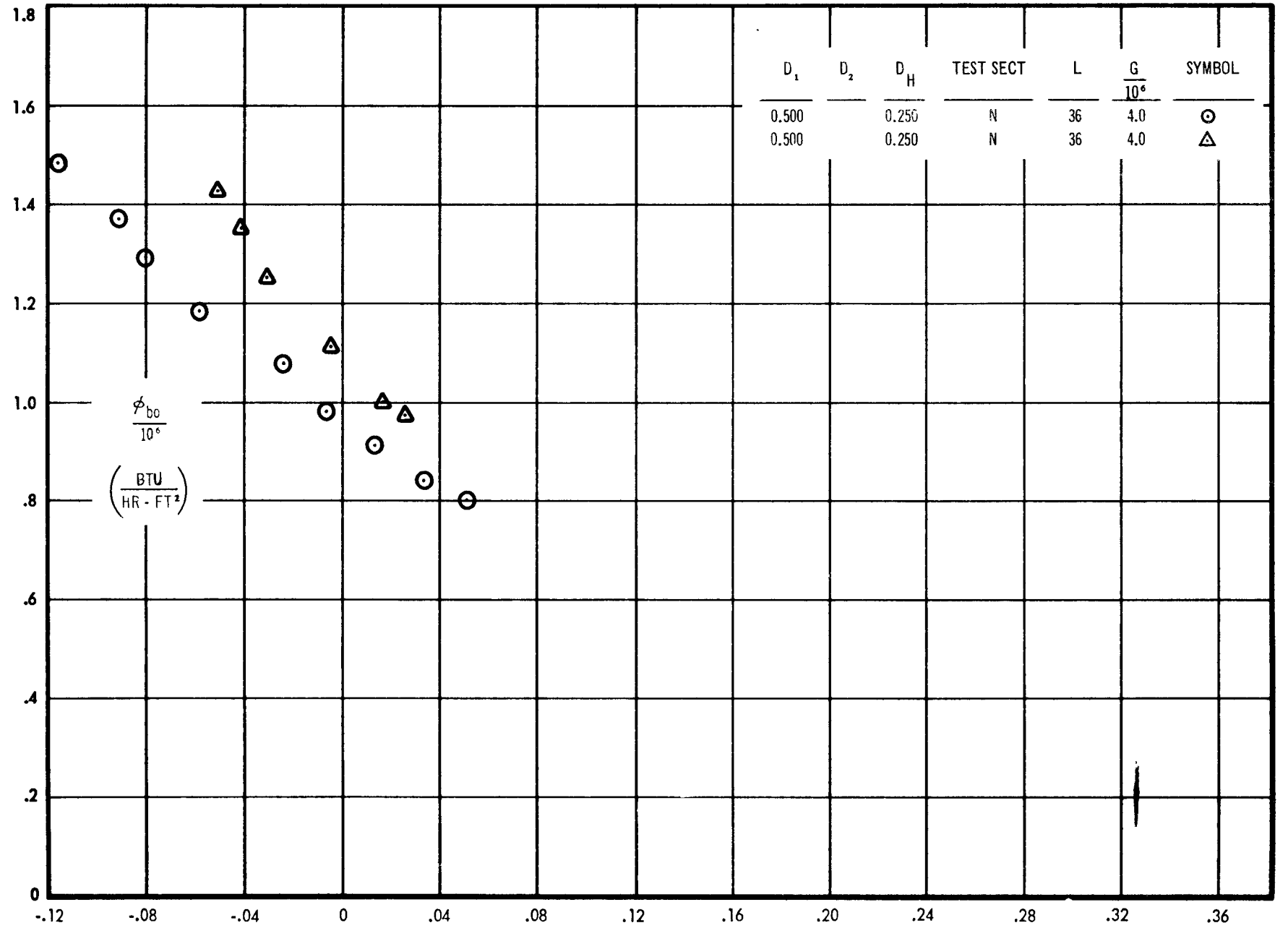

FIGURE 22D EFFECT OF HYDRAULIC DIAMETER ON BURNOUT – 1400 PSIA

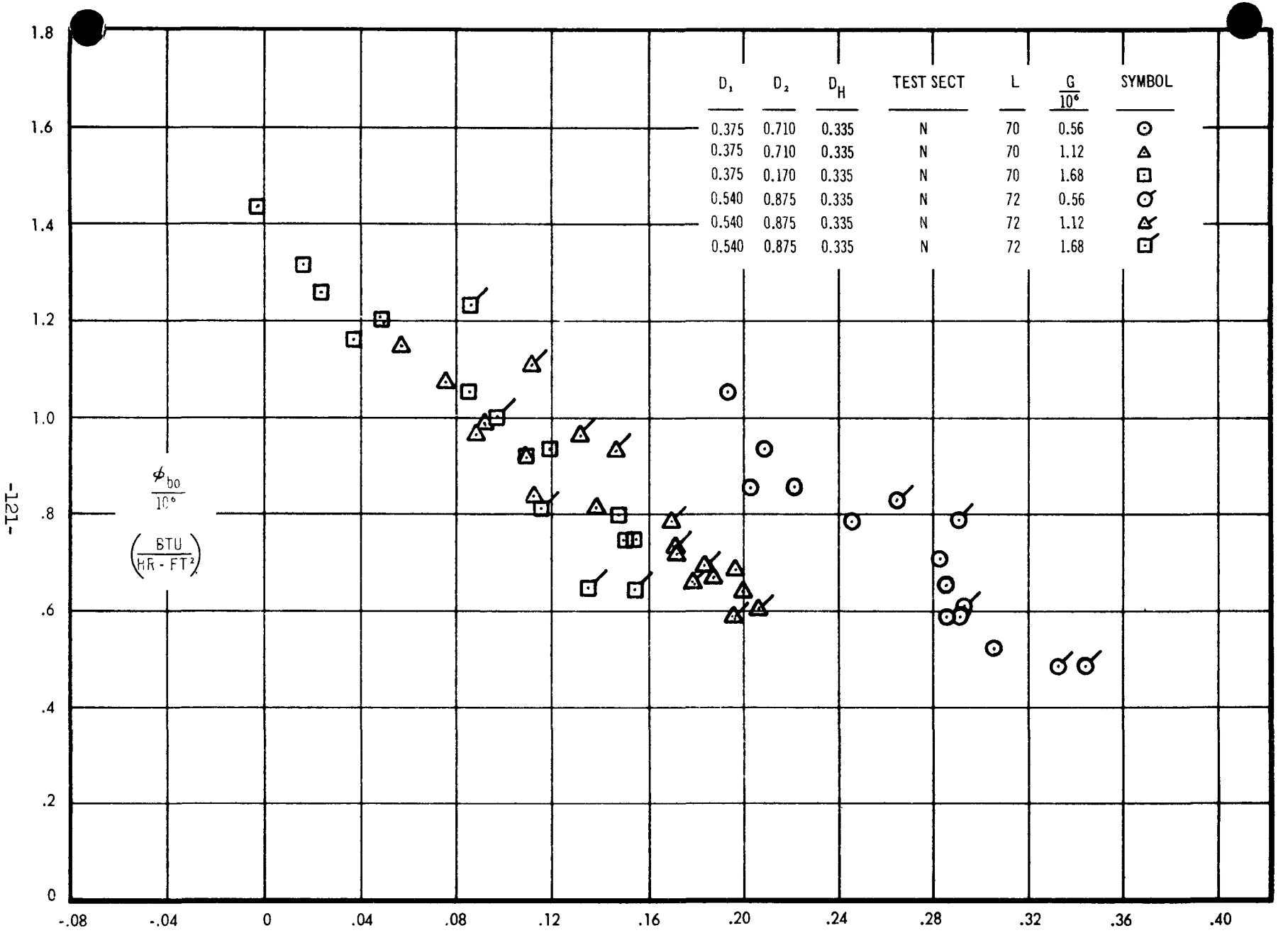

1075-21

FIGURE 23A EFFECT OF ROD DIAMETER ON BURNOUT -- 1000 PSIA

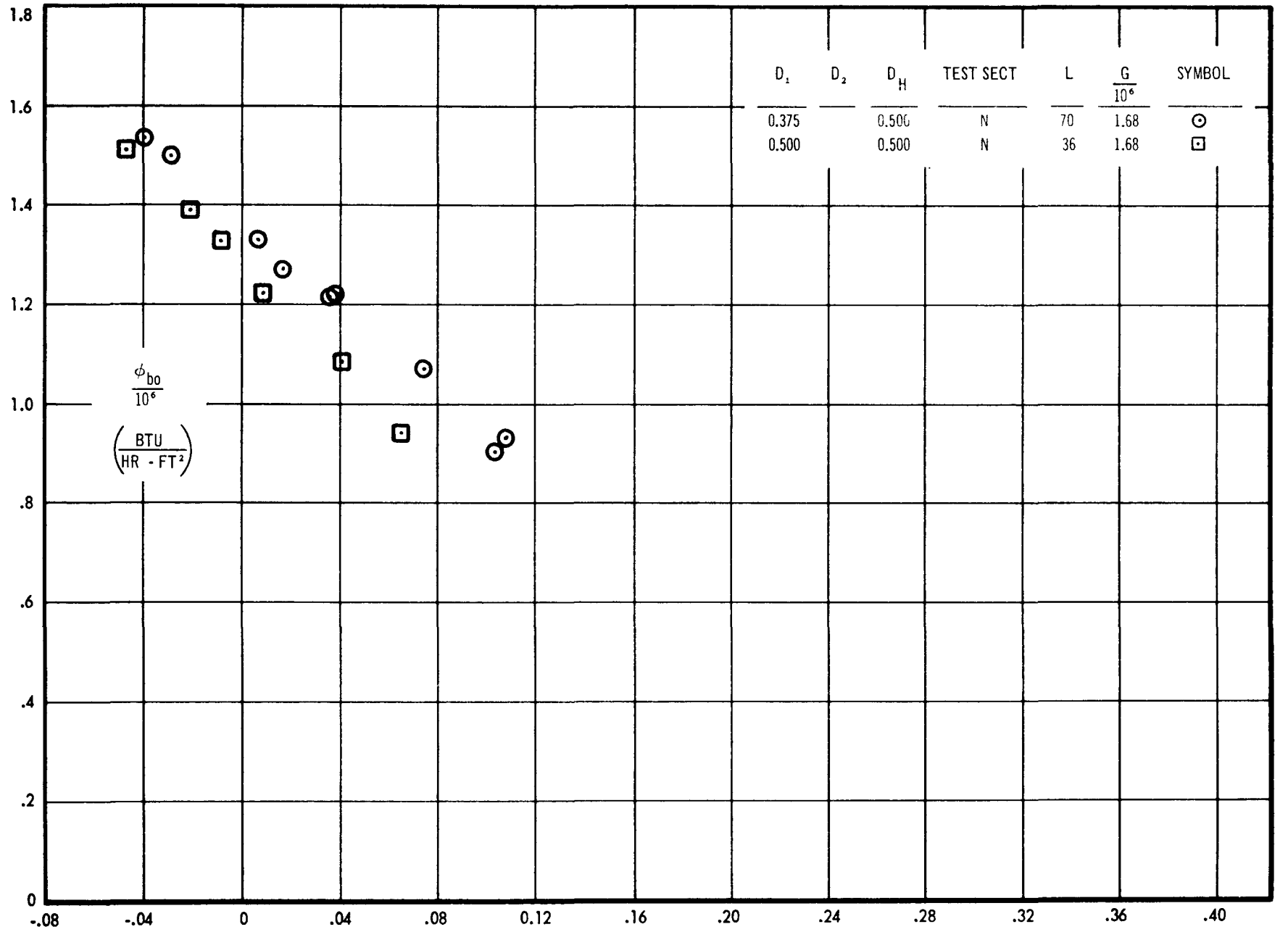

1075-22

FIGURE 23B EFFECT OF ROD DIAMETER ON BURNOUT – 1000 PSIA

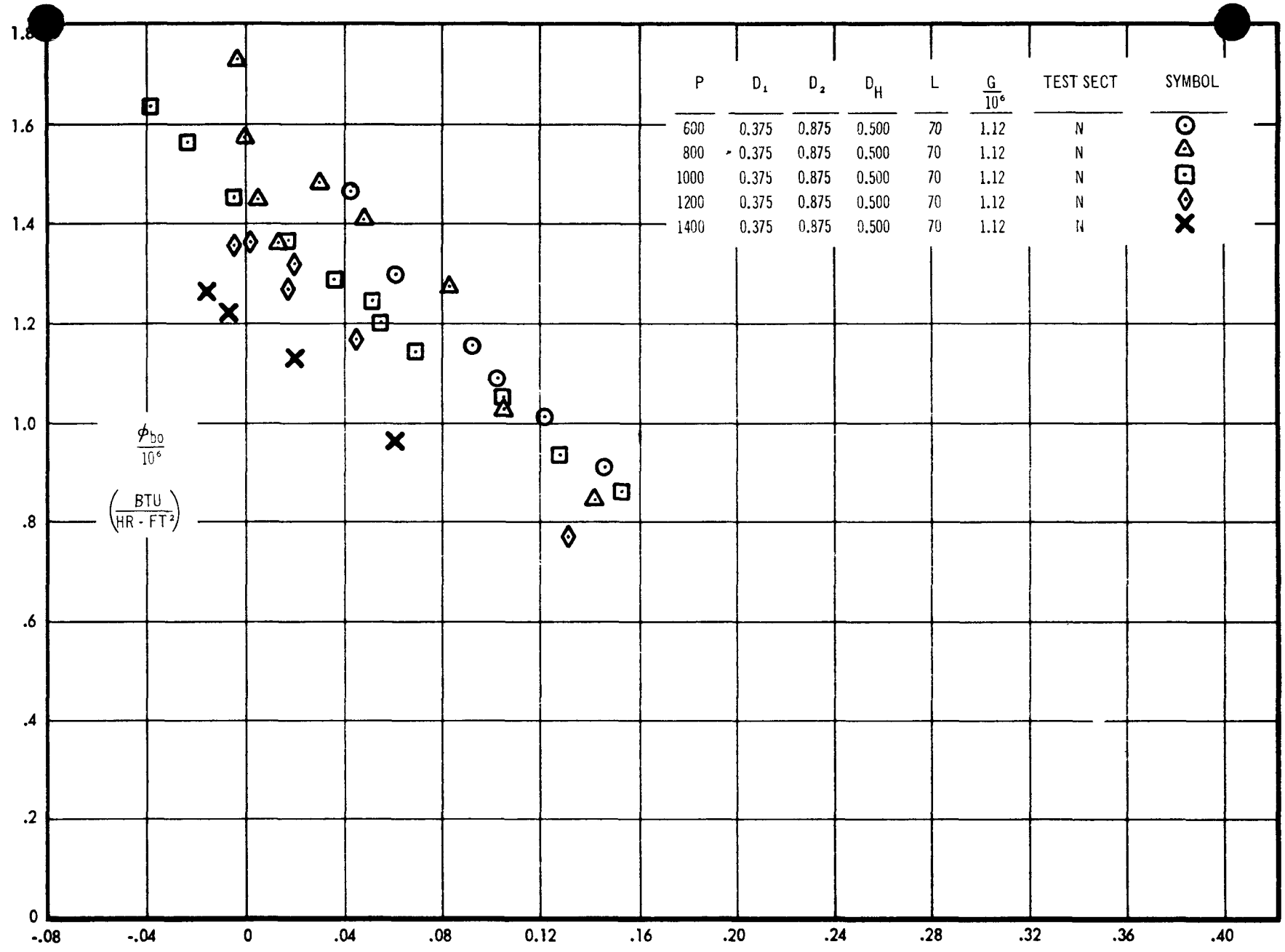

FIGURE 24A EFFECT OF PRESSURE ON BURNOUT

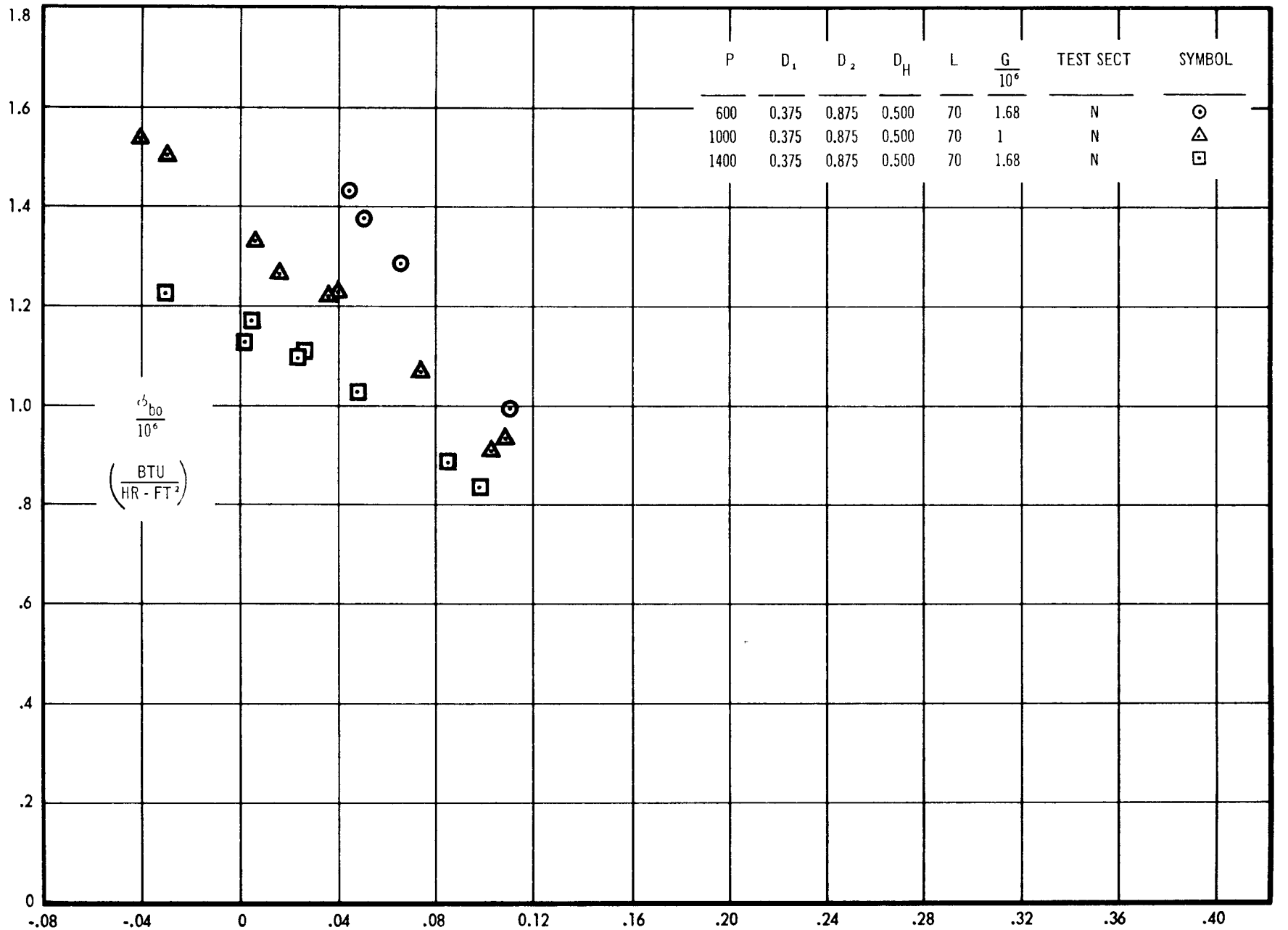

FIGURE 24B EFFECT OF PRESSURE ON BURNOUT

1075-24

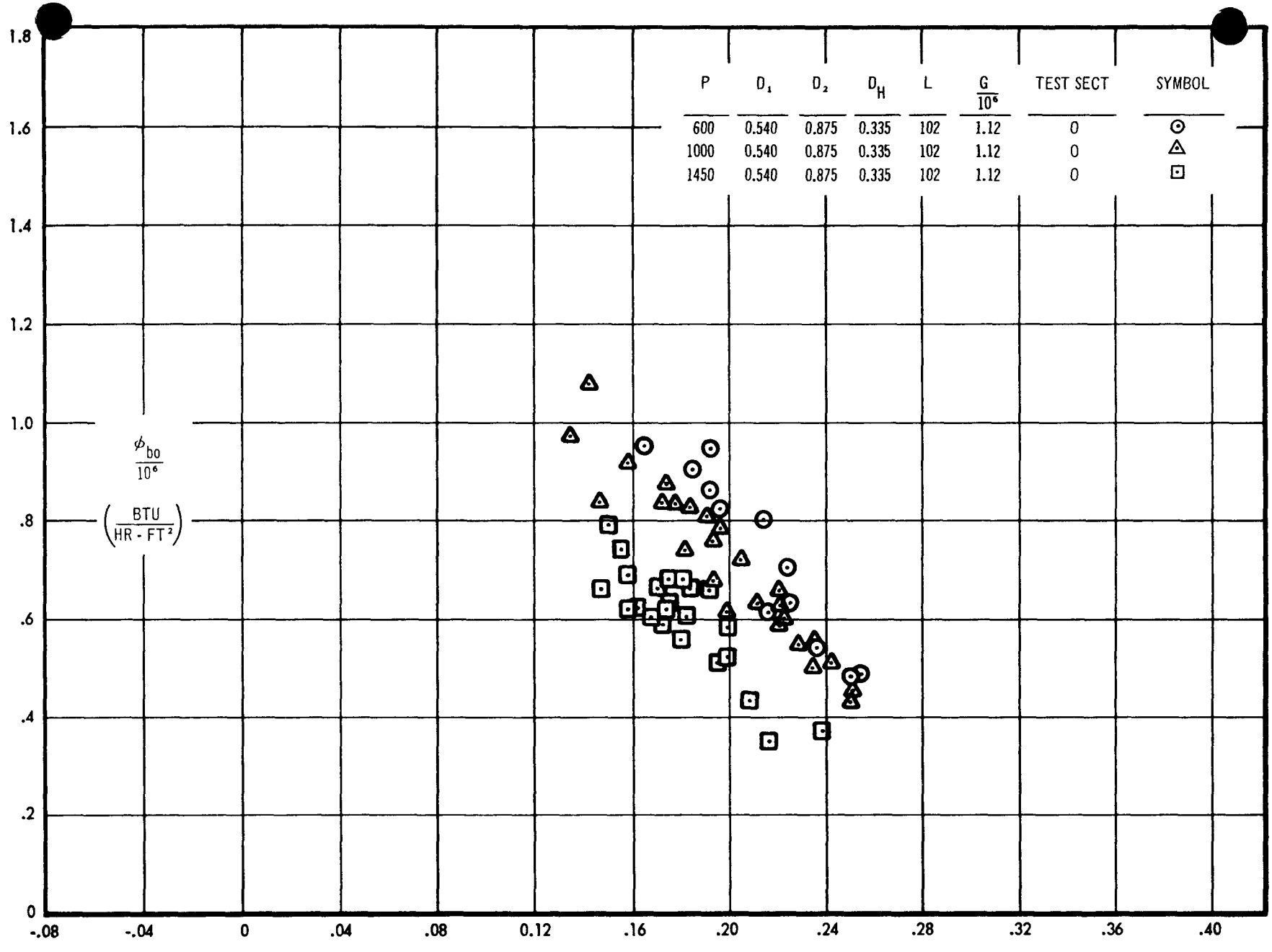

1075–25

FIGURE 25A EFFECT OF PRESSURE ON BURNOUT

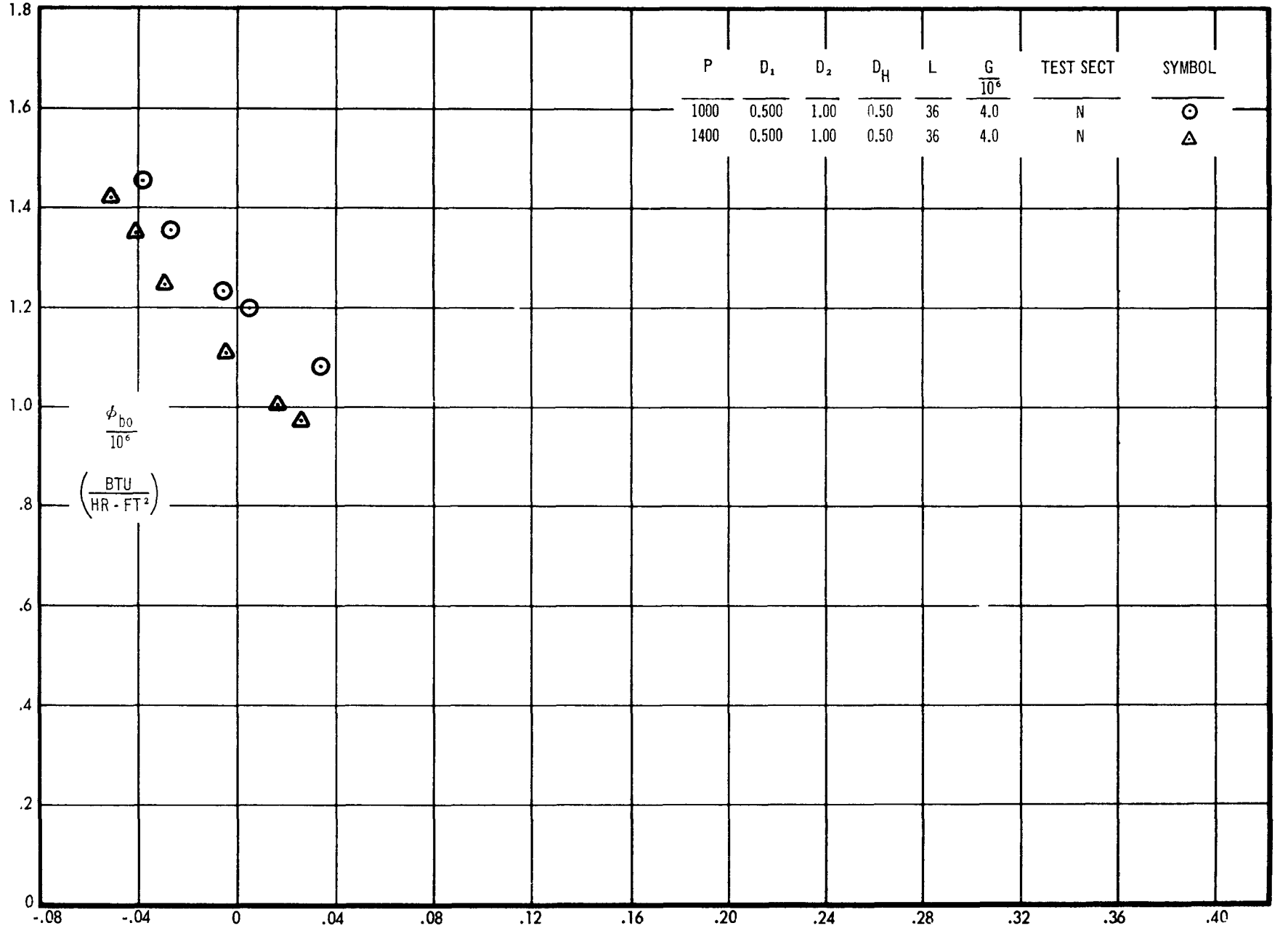

FIGURE 25B EFFECT OF PRESSURE ON BURNOUT

1075–26

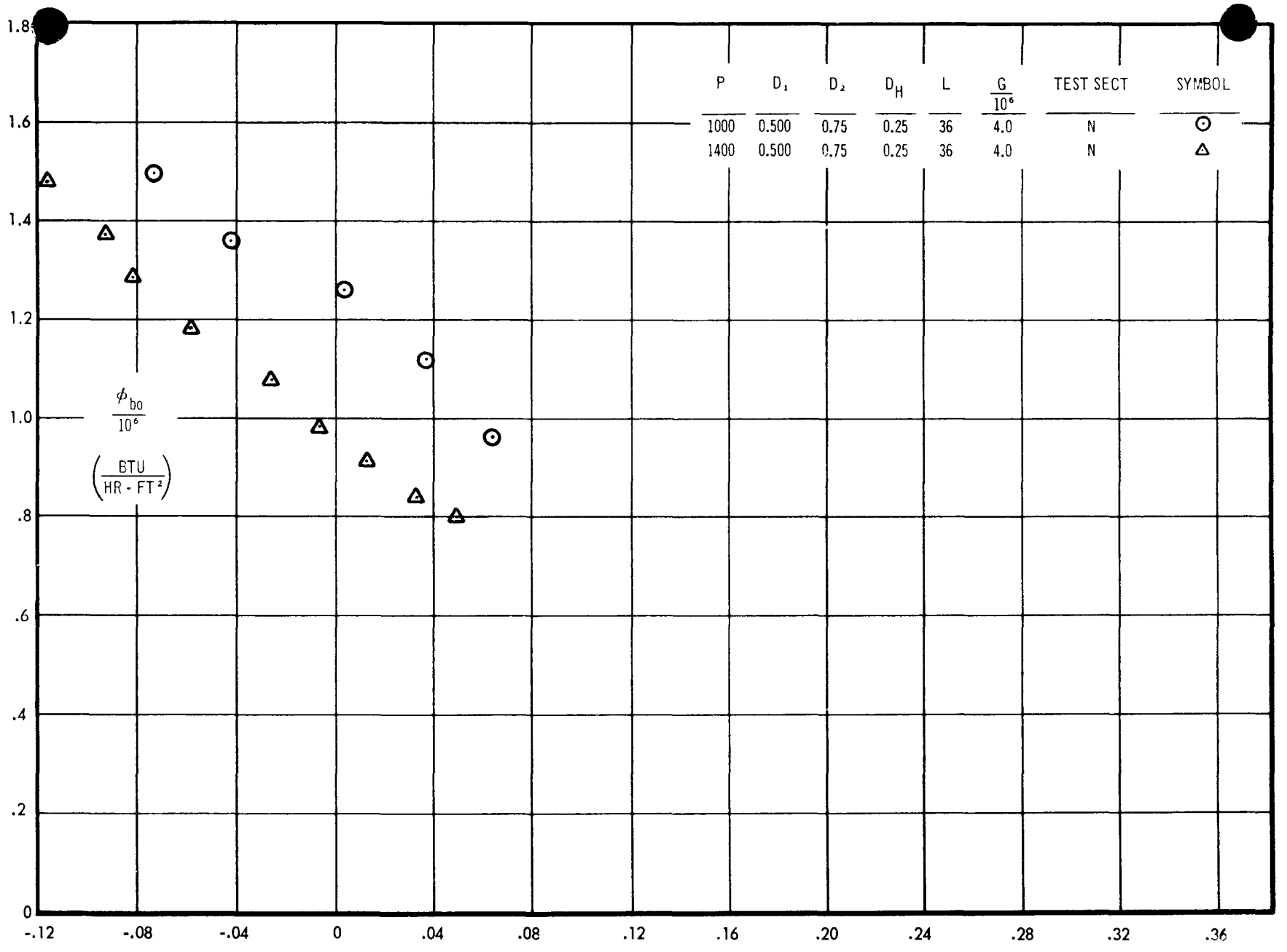

1075–27

FIGURE 25C EFFECT OF PRESSURE ON BURNOUT

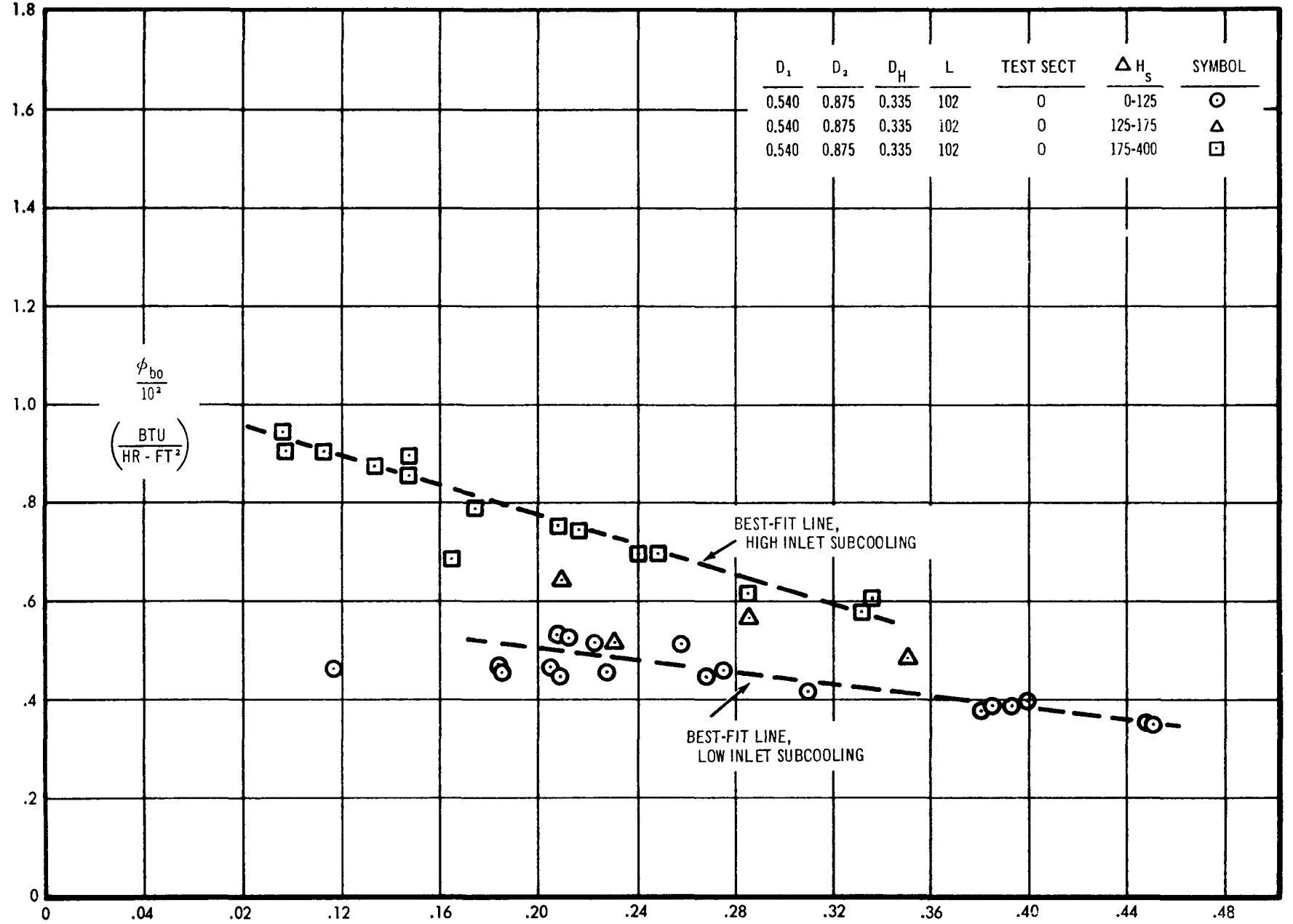

1075-28

FIGURE 26 EFFECT OF INLET SUBCOOLING ON BURNOUT – 1000 PSIA

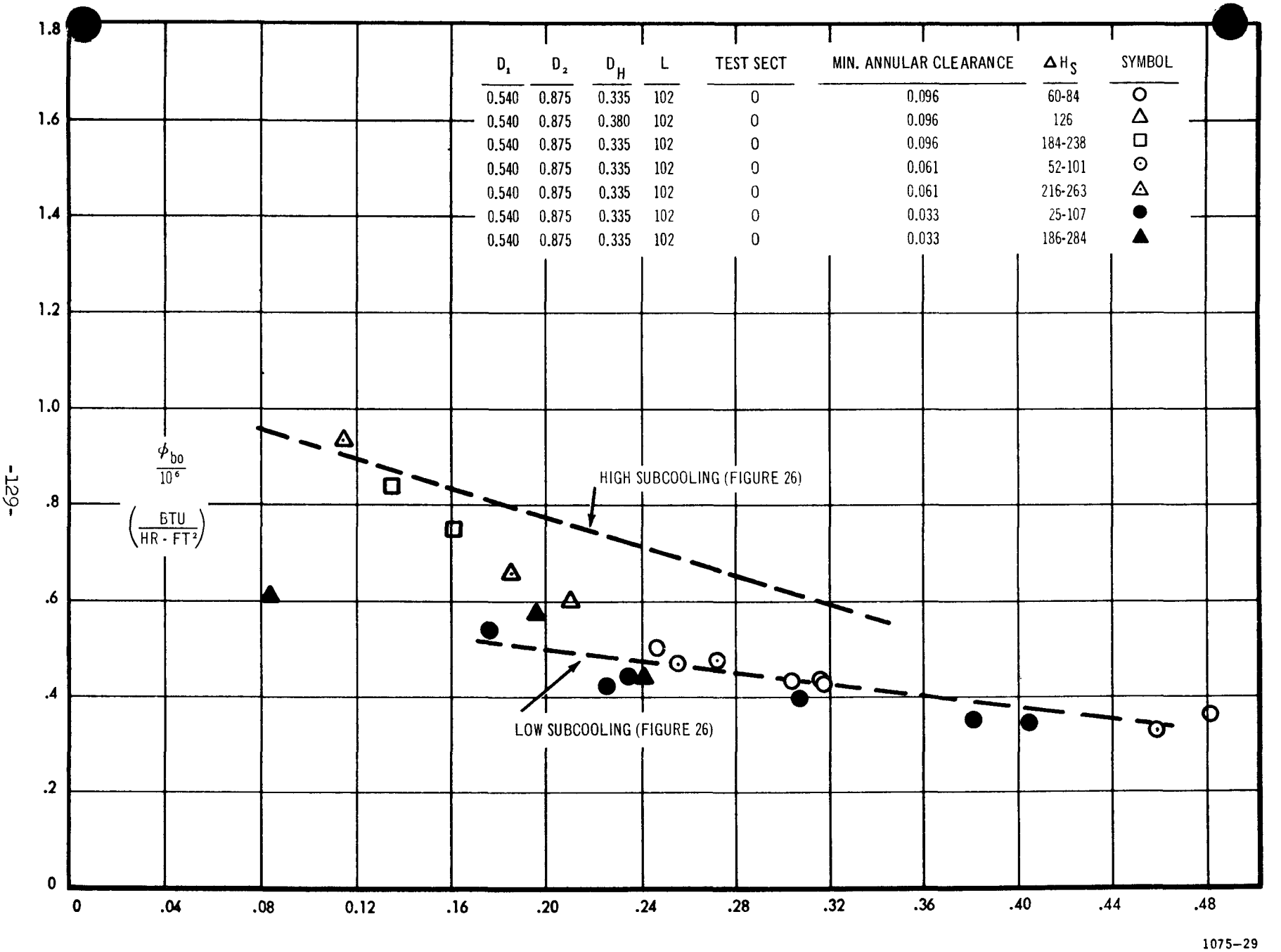

D_1	D_2	D_H	L	TEST SECT	MIN. ANNULAR CLEARANCE	ΔH_S	SYMBOL
0.540	0.875	0.335	102	0	0.096	60-84	○
0.540	0.875	0.380	102	0	0.096	126	△
0.540	0.875	0.335	102	0	0.096	184-238	□
0.540	0.875	0.335	102	0	0.061	52-101	⊙
0.540	0.875	0.335	102	0	0.061	216-263	⊿
0.540	0.875	0.335	102	0	0.033	25-107	●
0.540	0.875	0.335	102	0	0.033	186-284	▲

FIGURE 27 EFFECT OF ROD ECCENTRICITY ON BURNOUT – 1000 PSIA

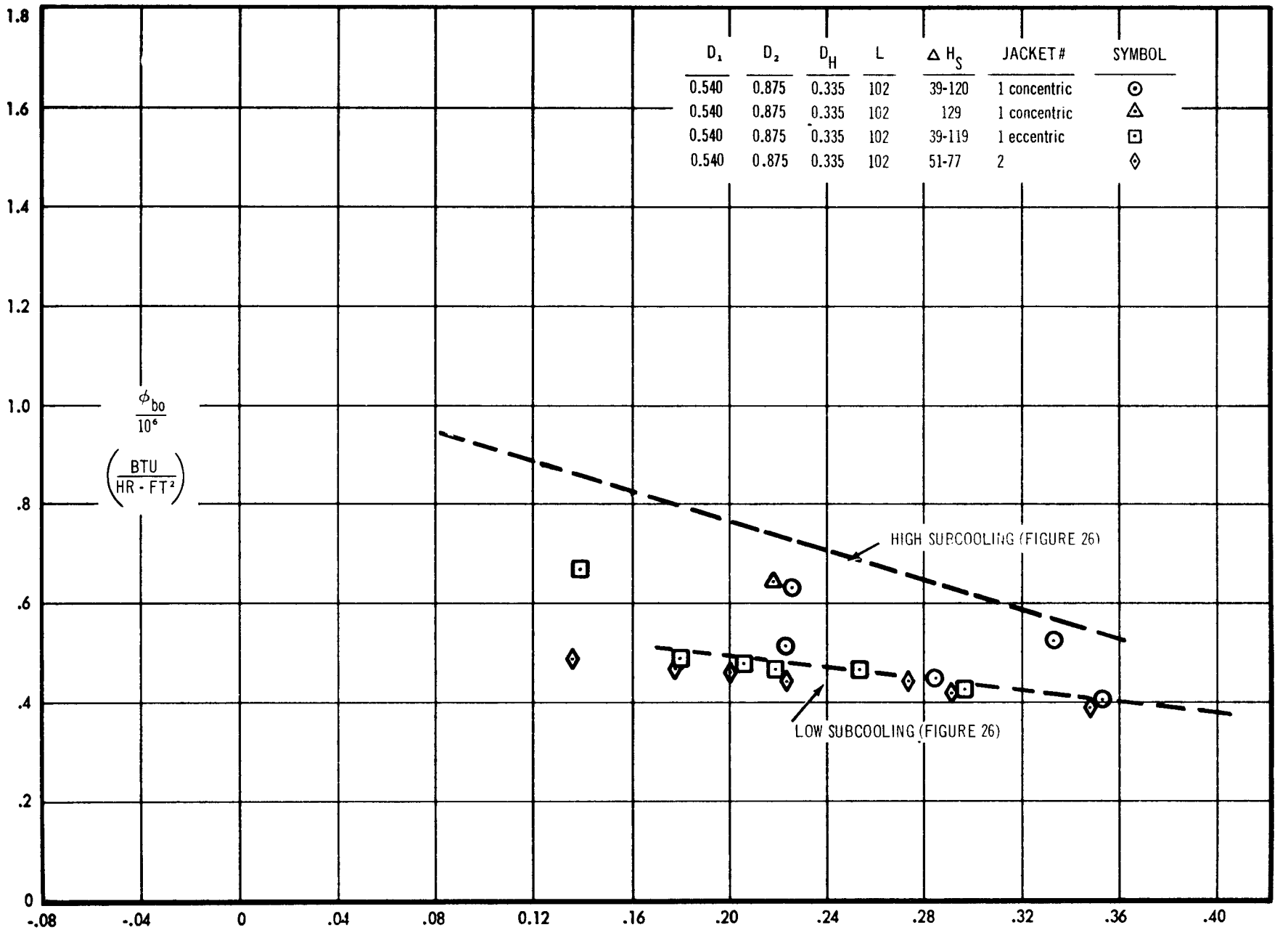

1075-3

FIGURE 28 EFFECT OF SIMULATED SPACER ON BURNOUT – 1000 PSIA

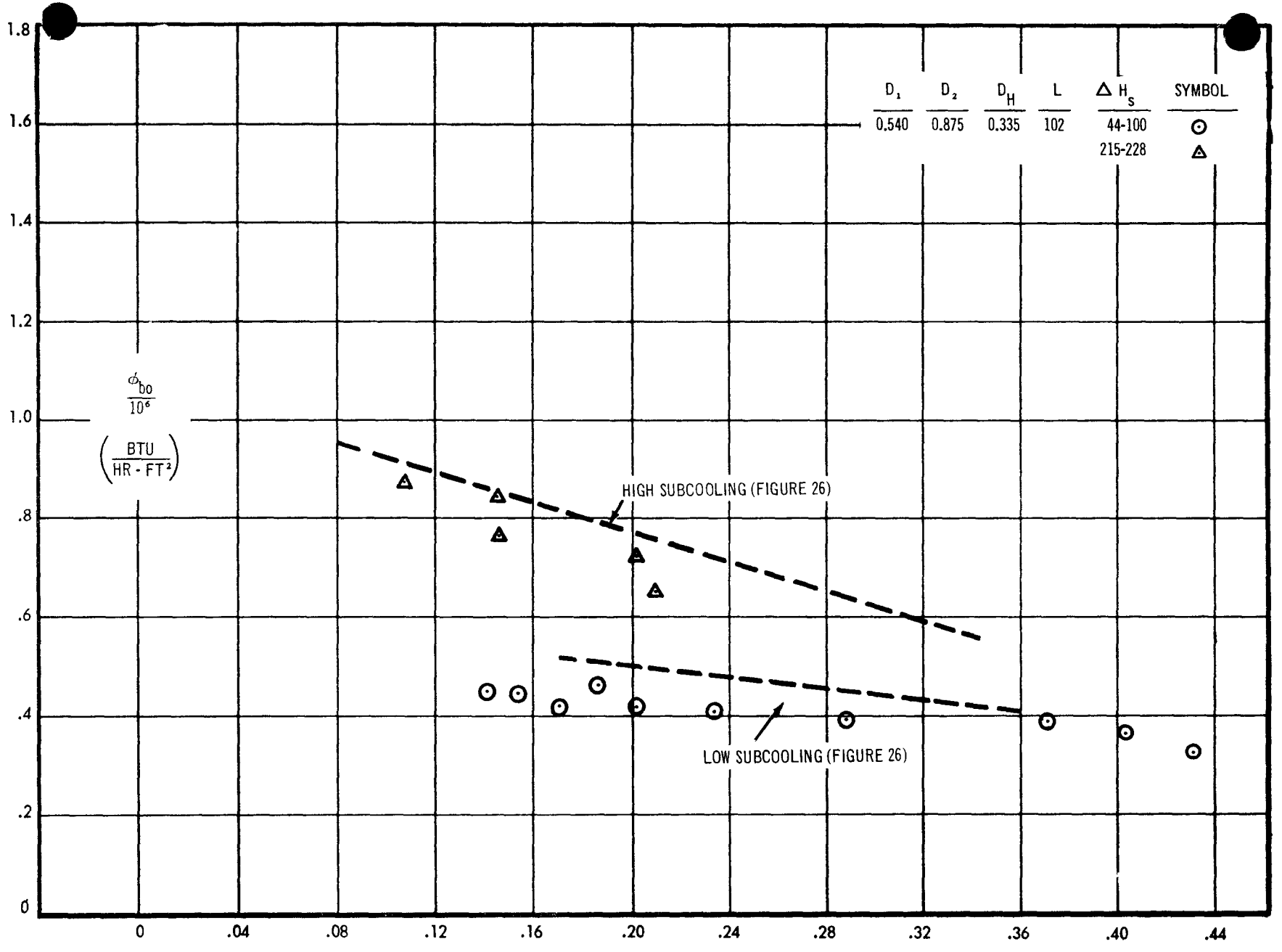

1075–31

FIGURE 29 EFFECT OF SANDBLASTING ON BURNOUT ROUGHNESS OF ROD SURFACE 300 INCH RMS – 1000 PSIA

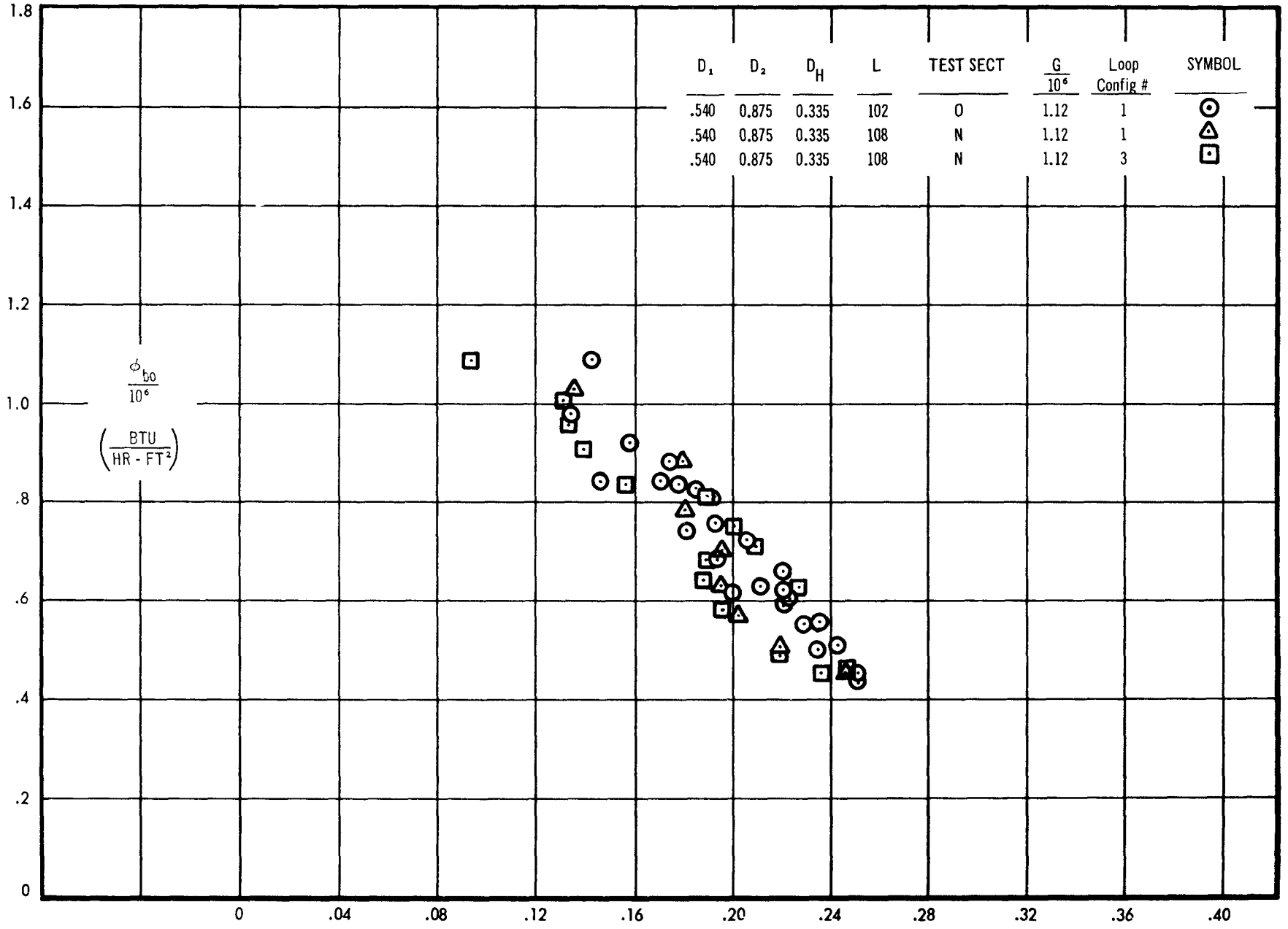

1075–32

FIGURE 30A EFFECT OF LOOP CHARACTERISTICS ON BURNOUT – 1000 PSIA

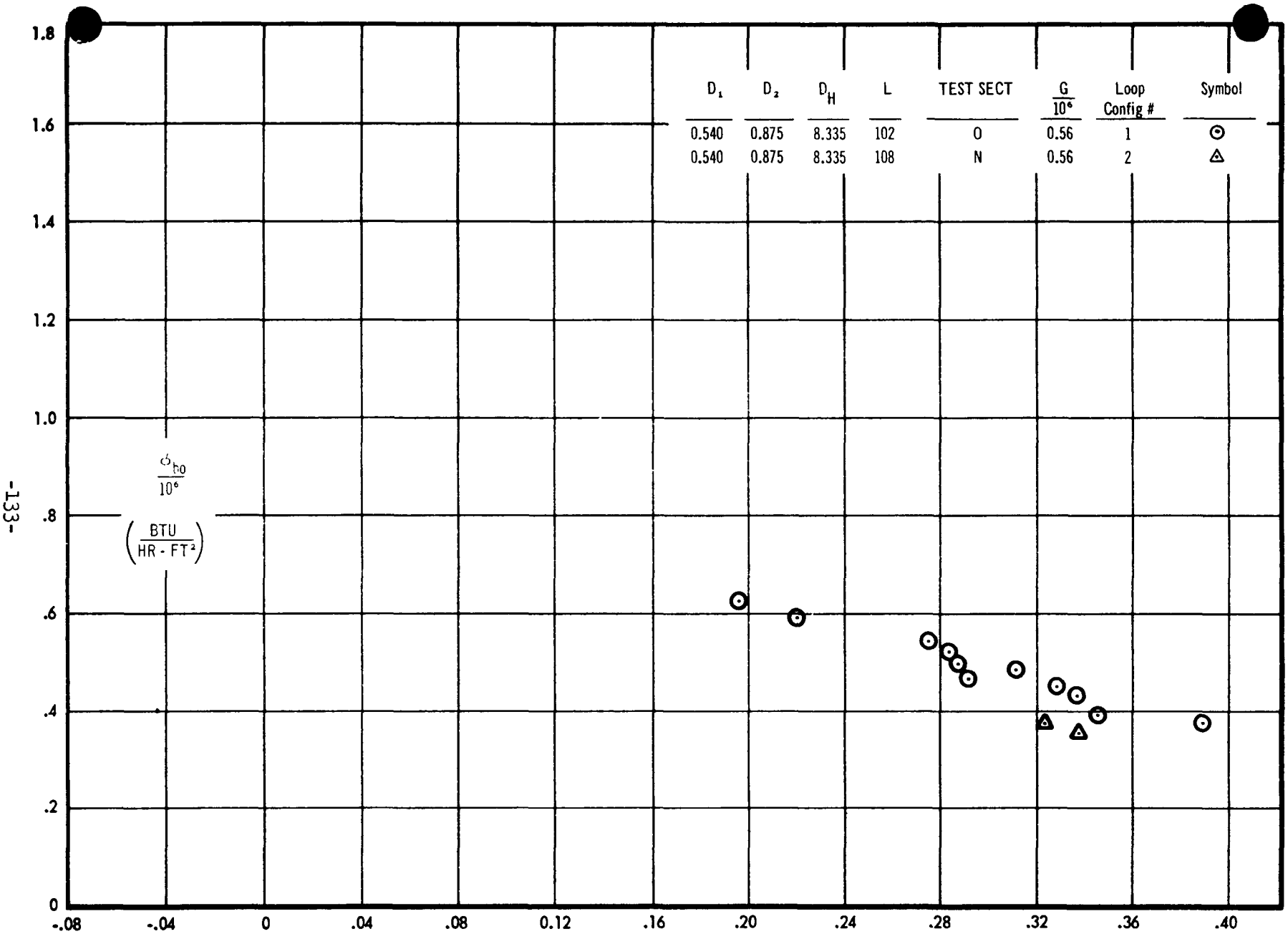

1075-33

FIGURE 30B EFFECT OF LOOP CHARACTERISTICS ON BURNOUT – 1000 PSIA

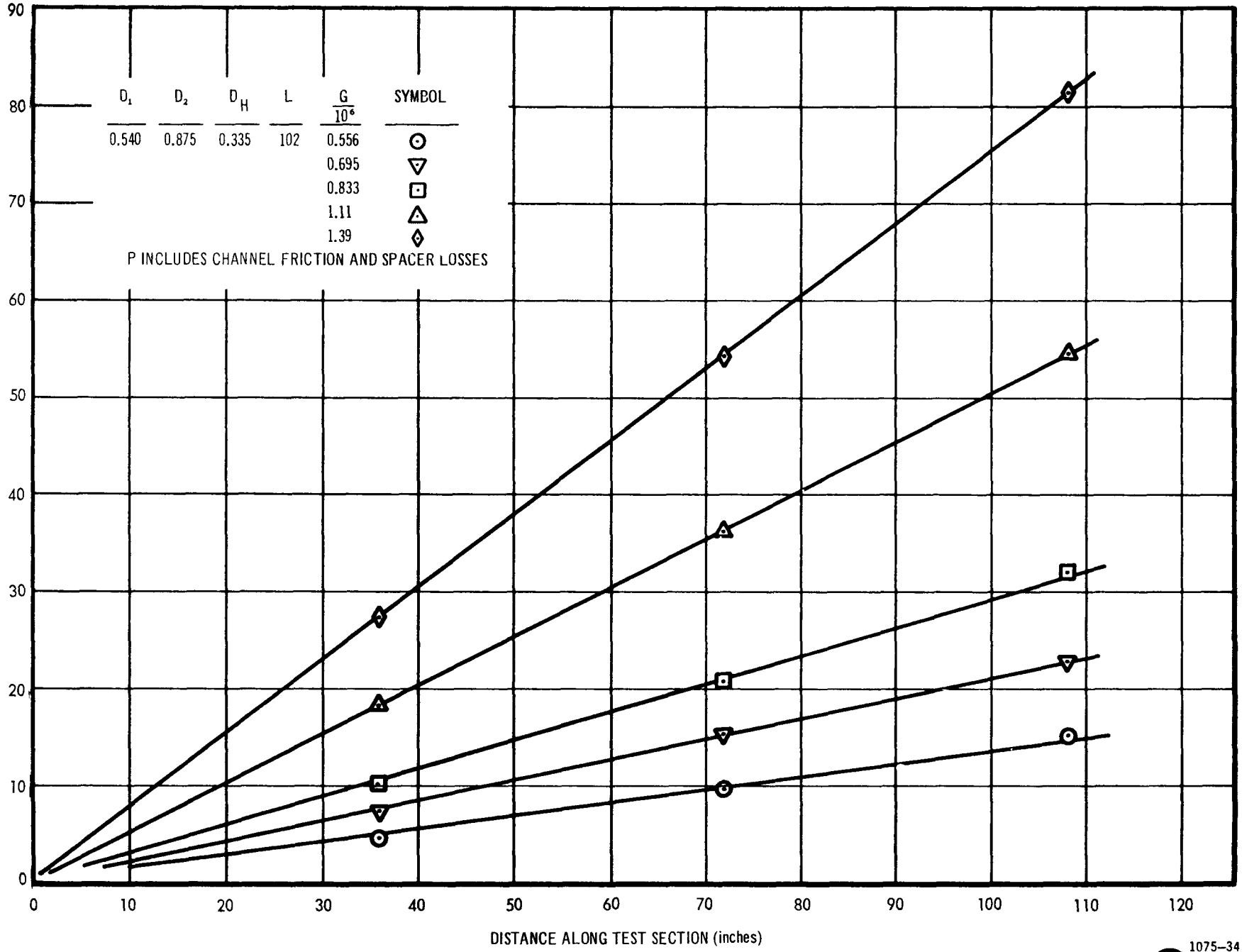

1075–34

FIGURE 31 SINGLE PHASE PRESSURE DROP

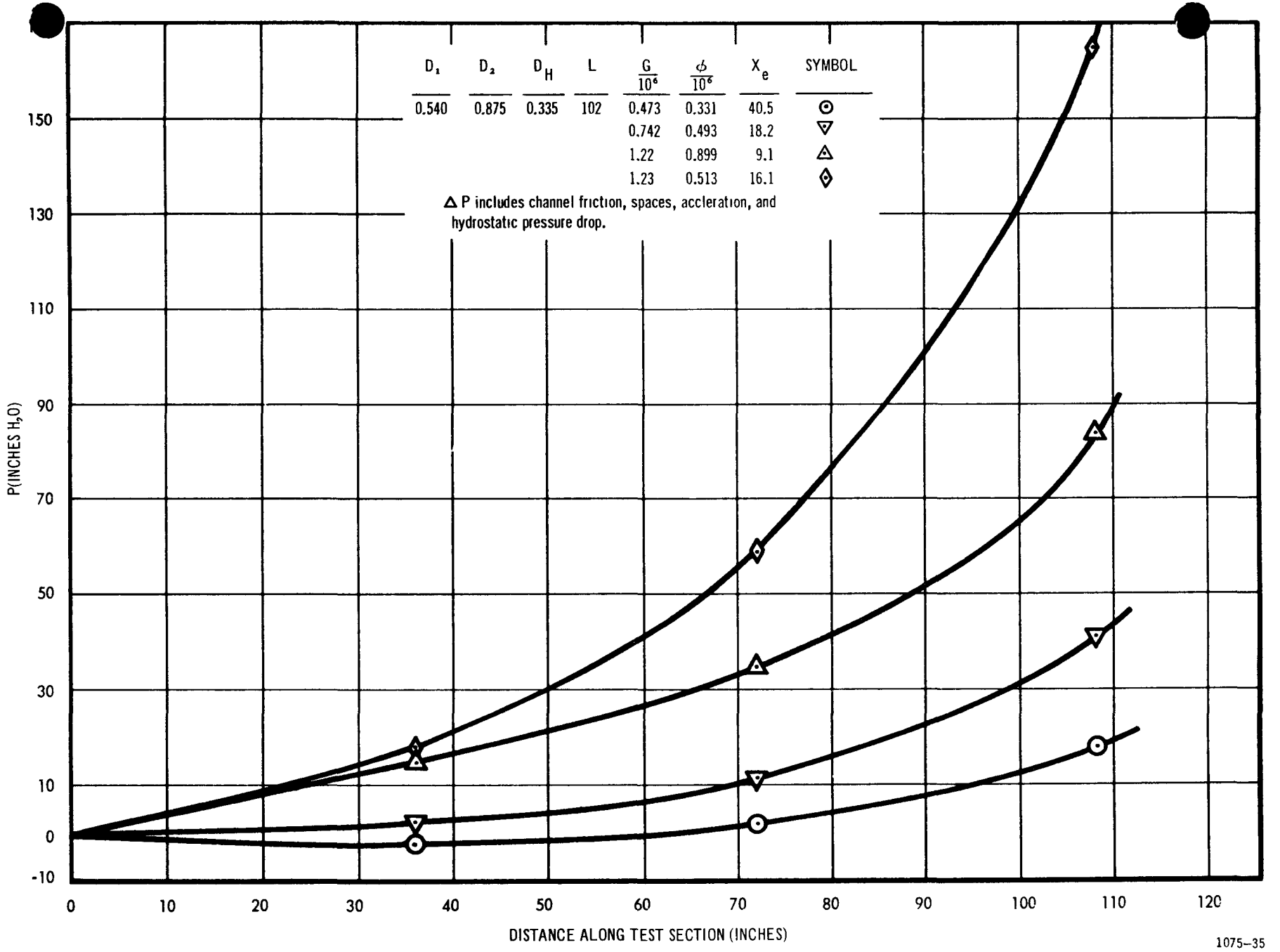

1075-35

FIGURE 32 TWO PHASE PRESSURE DROP WITH HEAT ADDITION

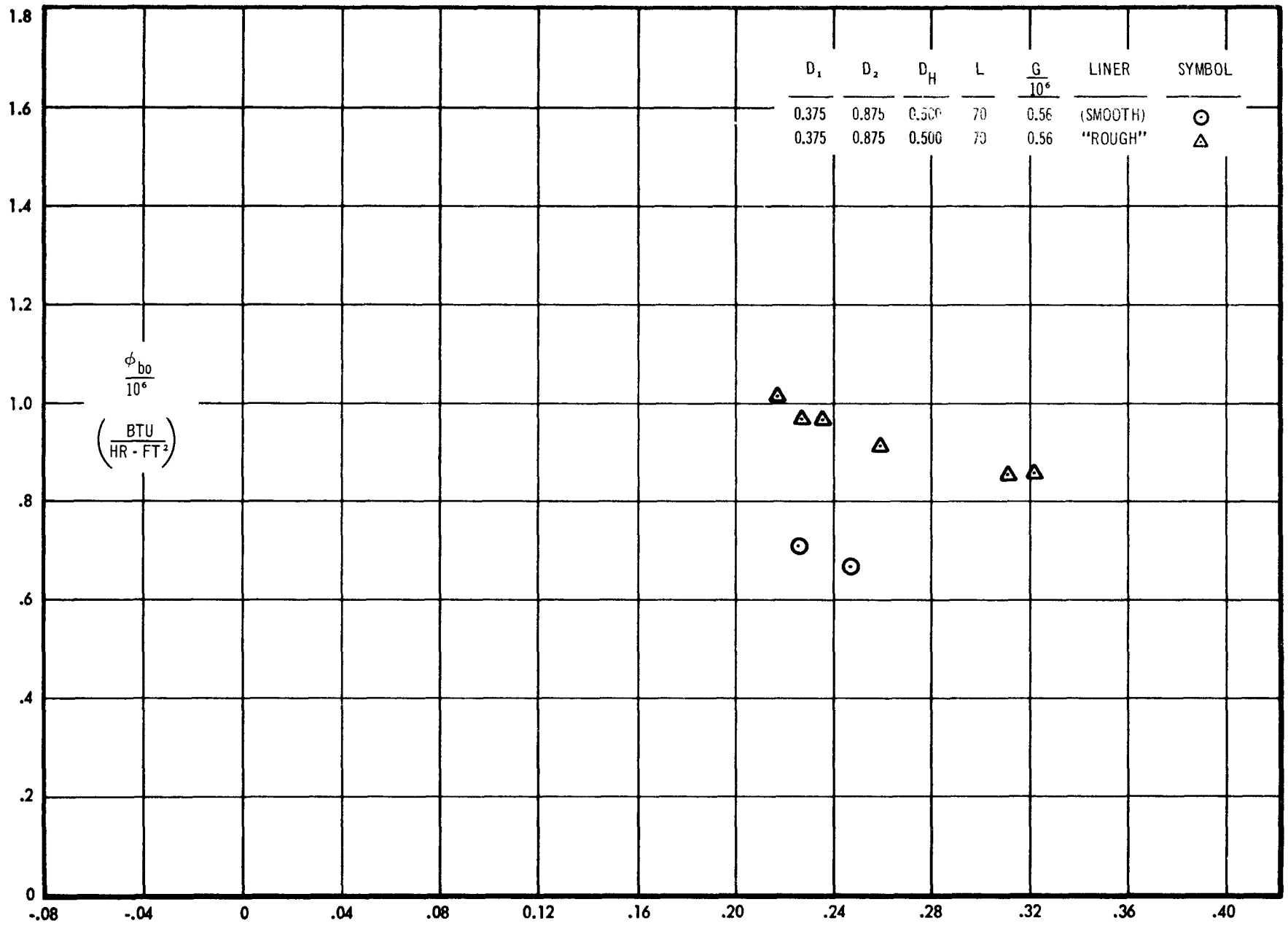

1075-36

FIGURE 33 EFFECT OF "ROUGH LINER" ON BURNOUT – 1000 PSIA

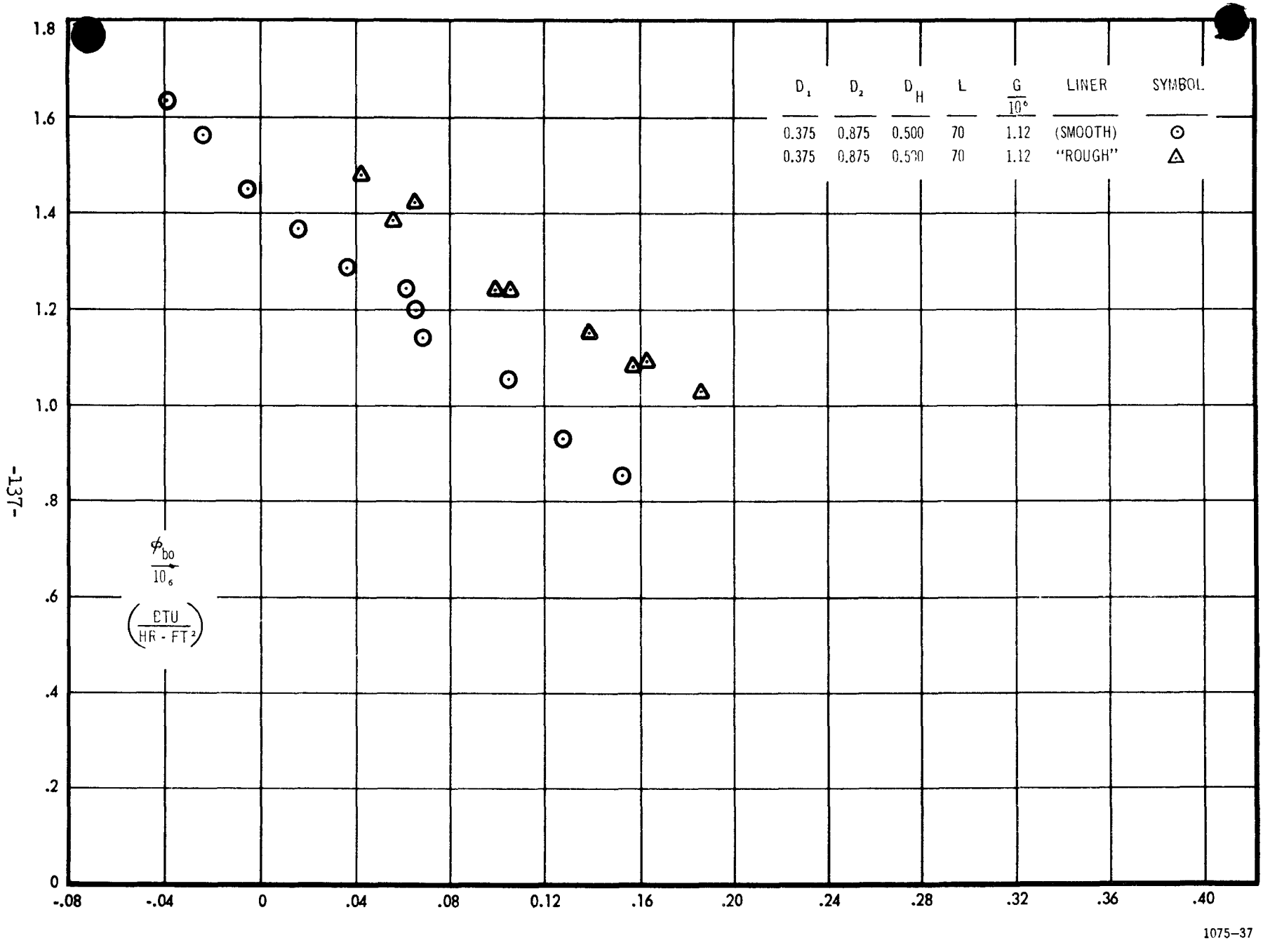

FIGURE 34 EFFECT OF ROUGH LINER ON BURNOUT – 1000 PSIA

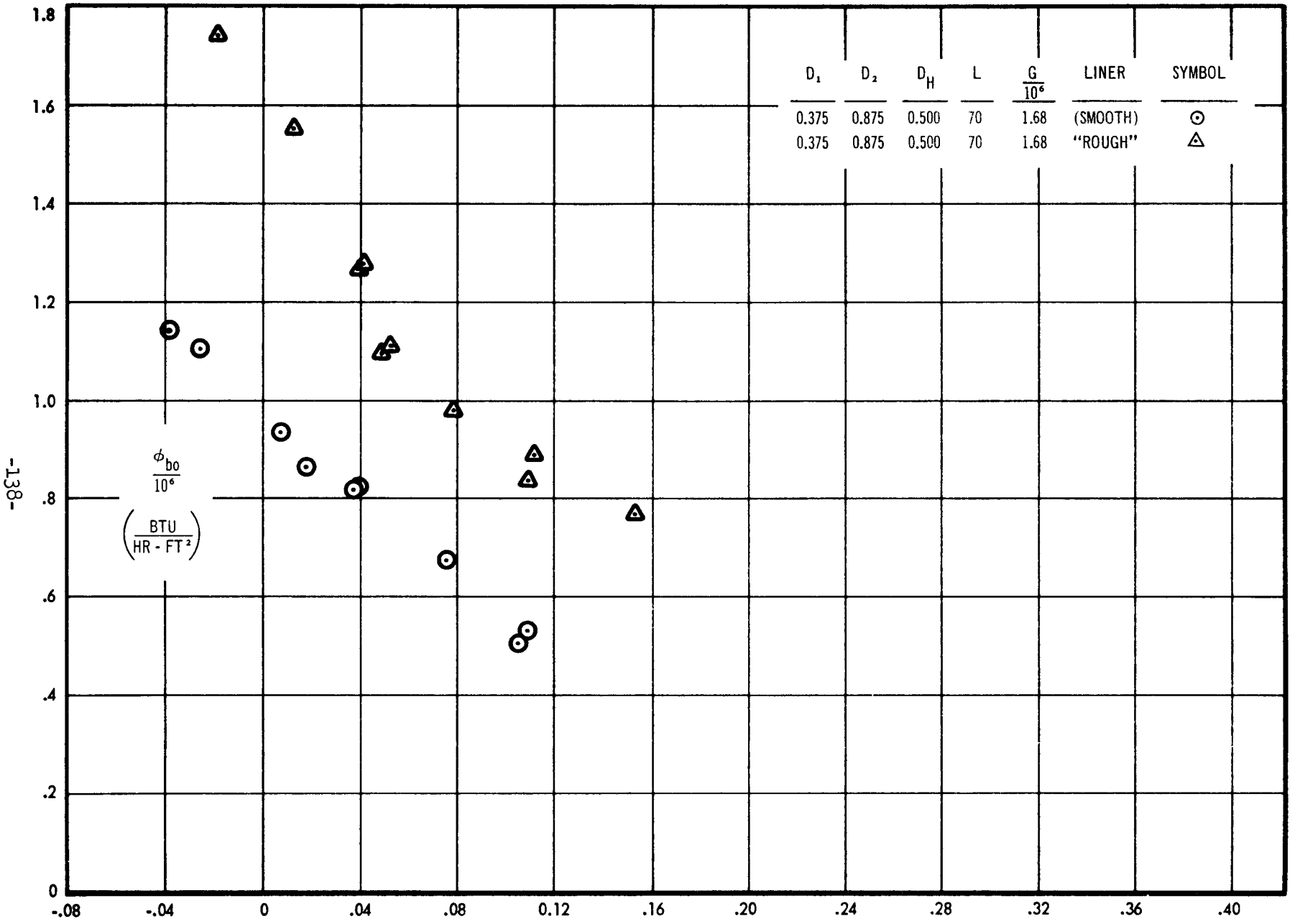

1075-38

FIGURE 35 EFFECT OF ROUGH LINER ON BURNOUT

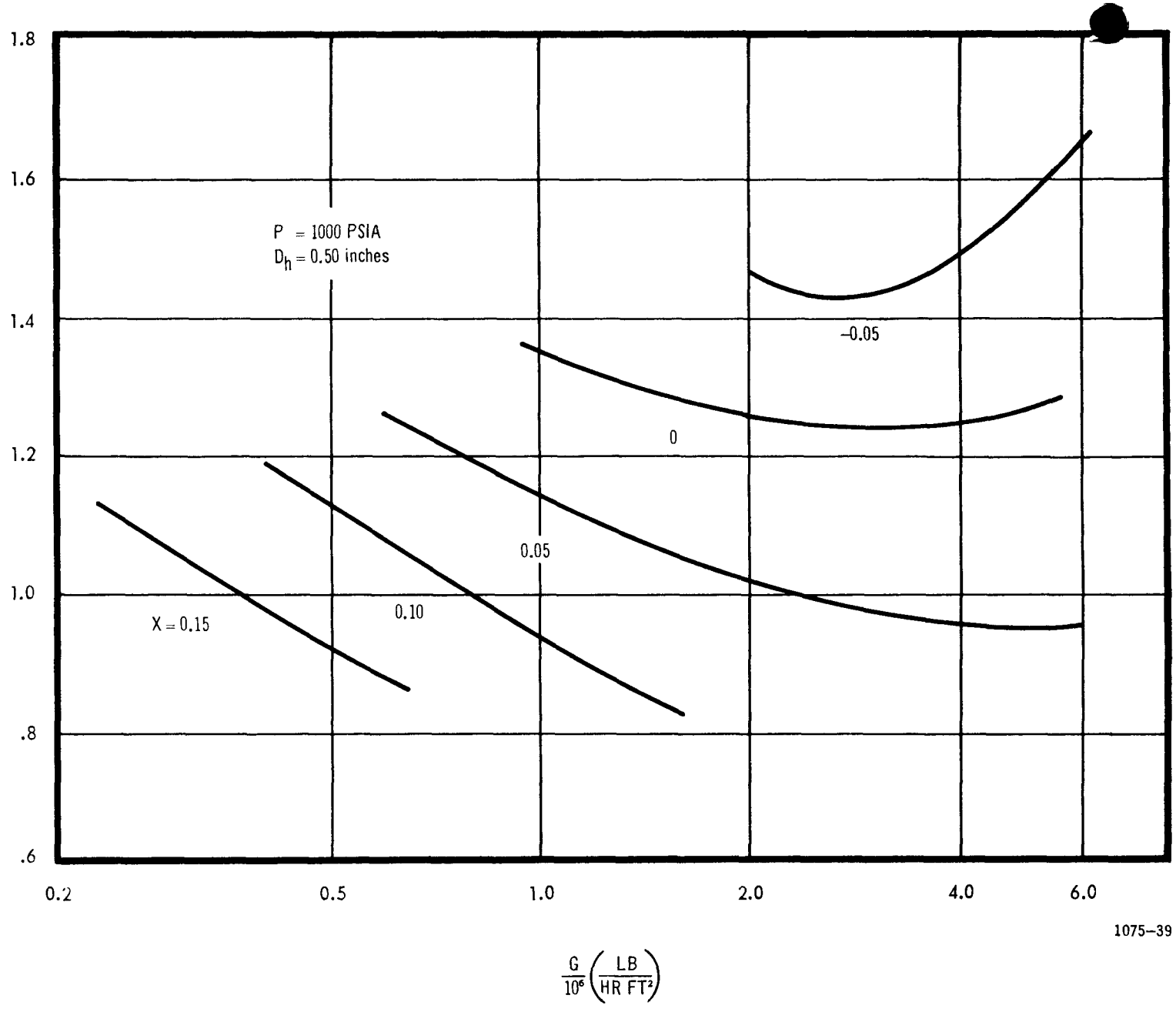

FIGURE 36 BURNOUT HEAT FLUX VS. FLOW; VARIOUS QUALITIES

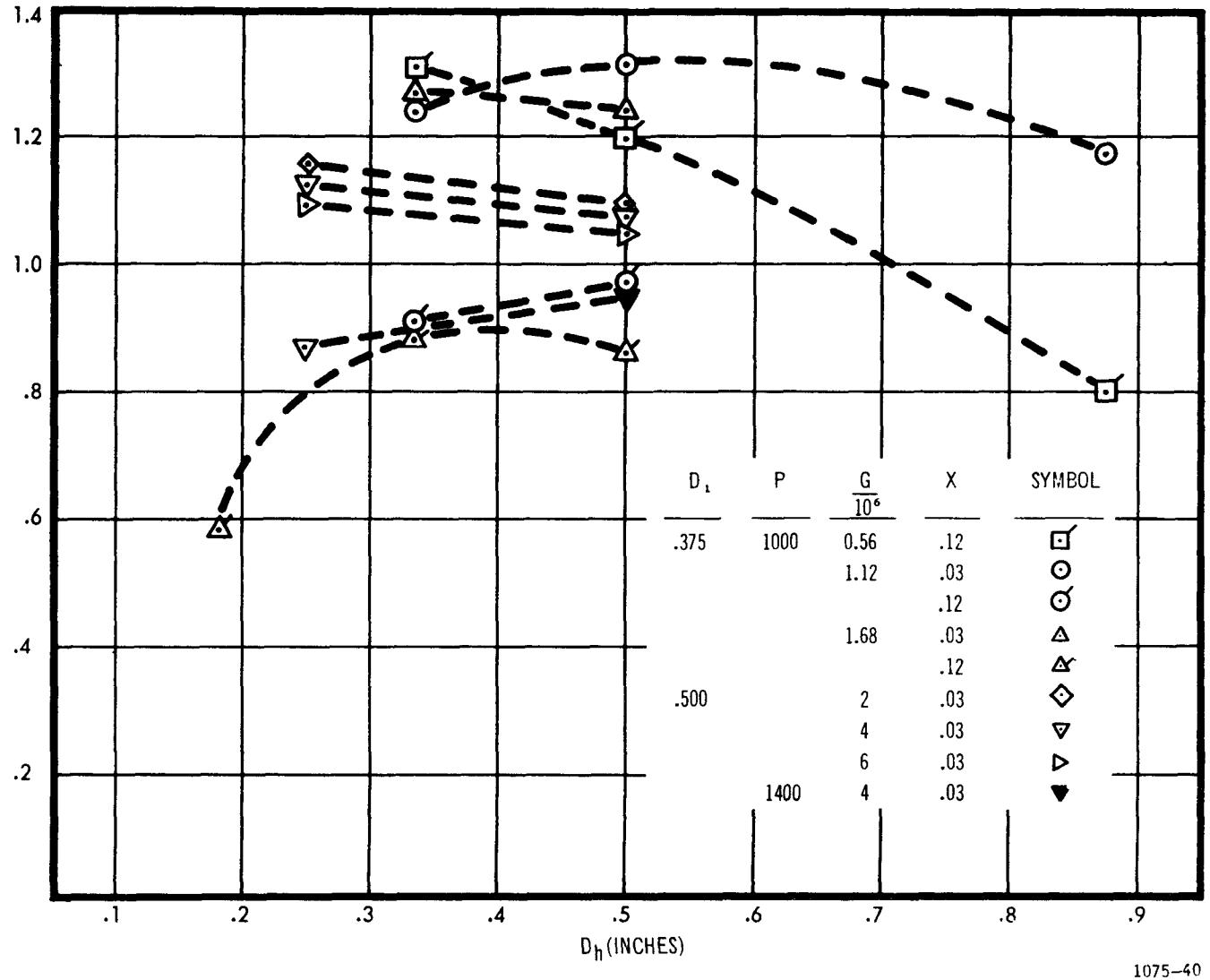

FIGURE 37 BURNOUT HEAT FLUX VERSUS HYDRAULIC DIAMETER; VARIOUS FLOW AND QUALITY

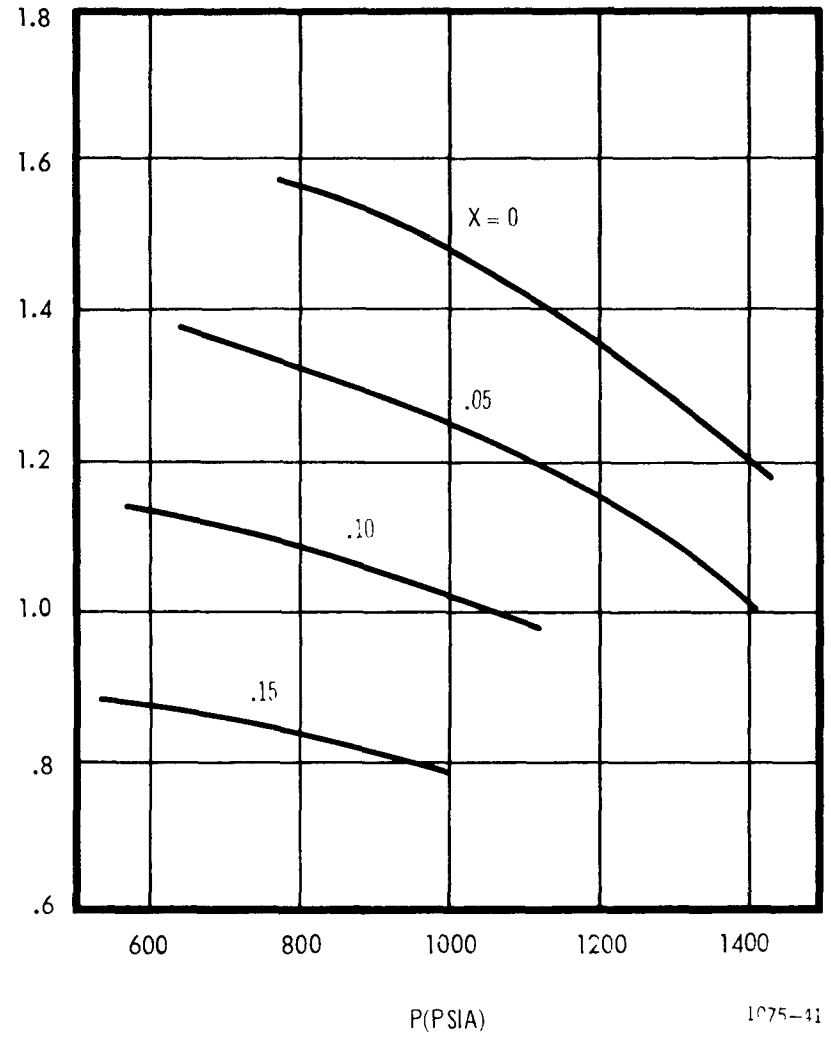

$\frac{\phi_{bo}}{10^6}$

$\left(\frac{BTU}{HR\ FT^2}\right)$

$D_h = 0.500$ inch

$\frac{G}{10^6} = 1.12\ \frac{LB}{HR\ FT^2}$

FIGURE 38 BURNOUT HEAT FLUX VS. PRESSURE, VARIOUS QUALITIES

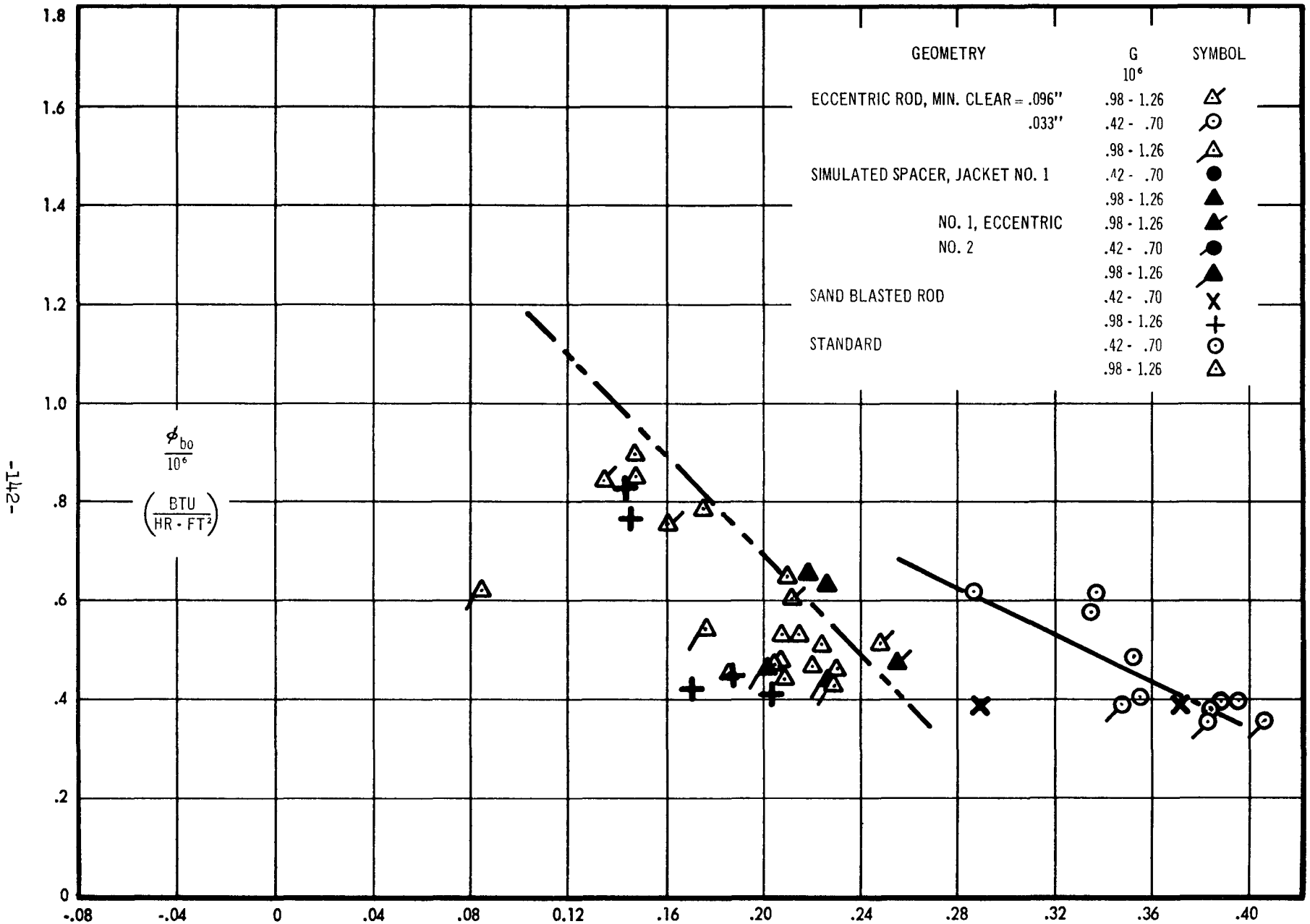

1075-42

FIGURE 39 COMPARISON OF SPECIAL GEOMETRY WITH CONSTANT FLOW RESULTS

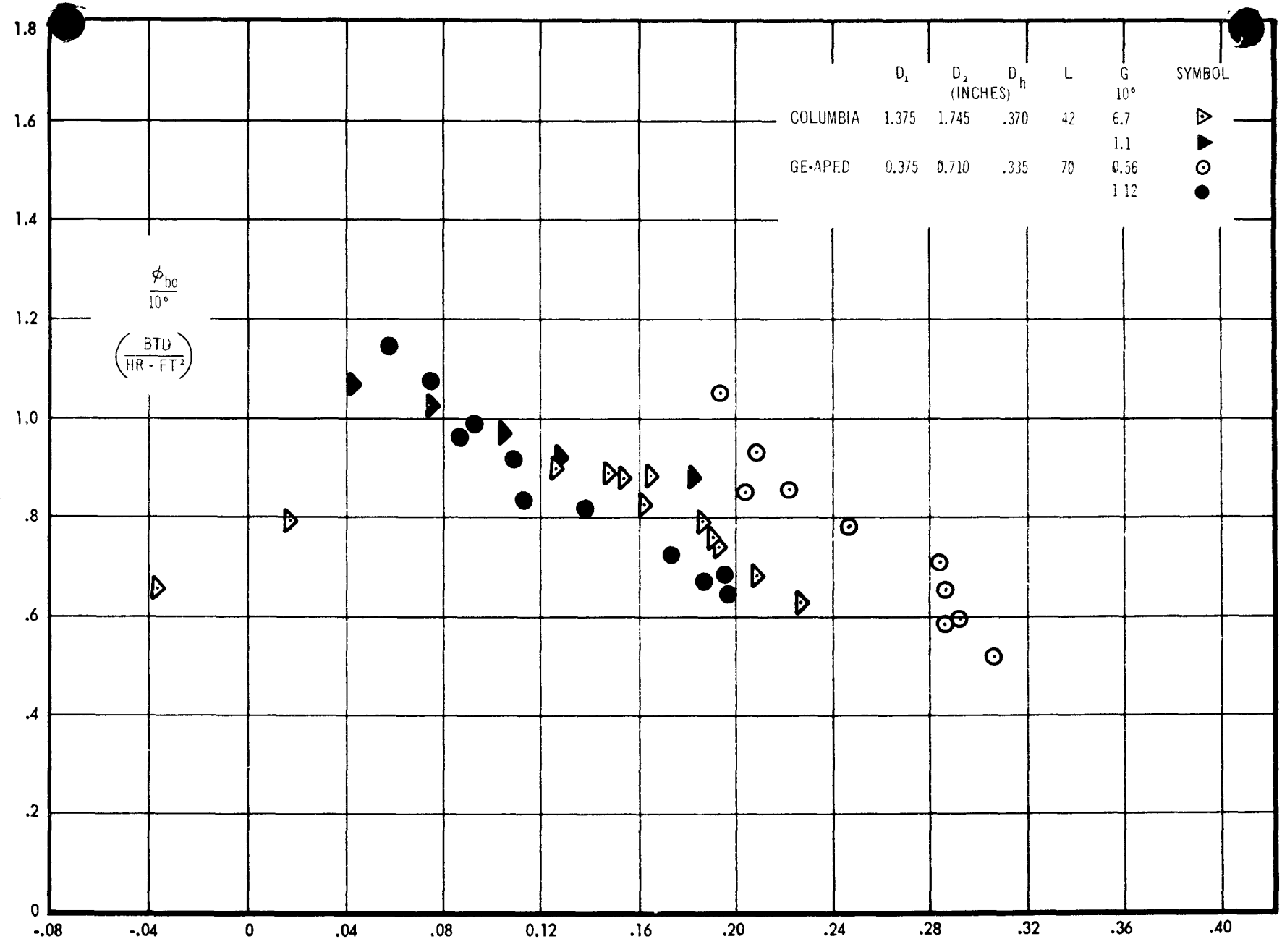

1075-43

FIGURE 40 COMPARISON OF GE-APED WITH COLUMBIA BURNOUT DATA, INTERNALLY HEATED ANNULUS, 1000 PSIA

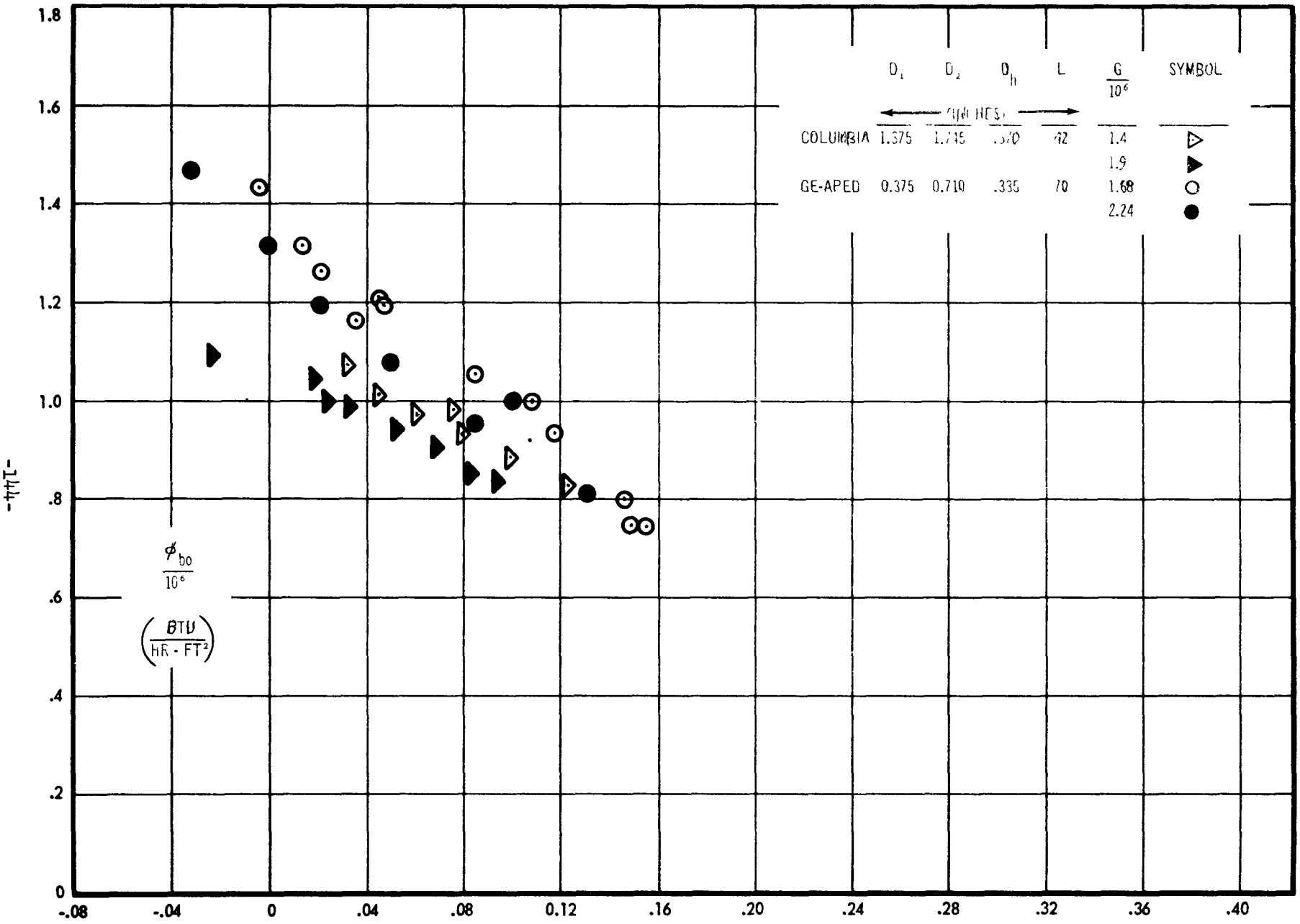

FIGURE 41 COMPARISON OF GE-APED WITH COLUMBIA BURNOUT DATA, INTERNALLY HEATED ANNULUS, 1000 PSIA

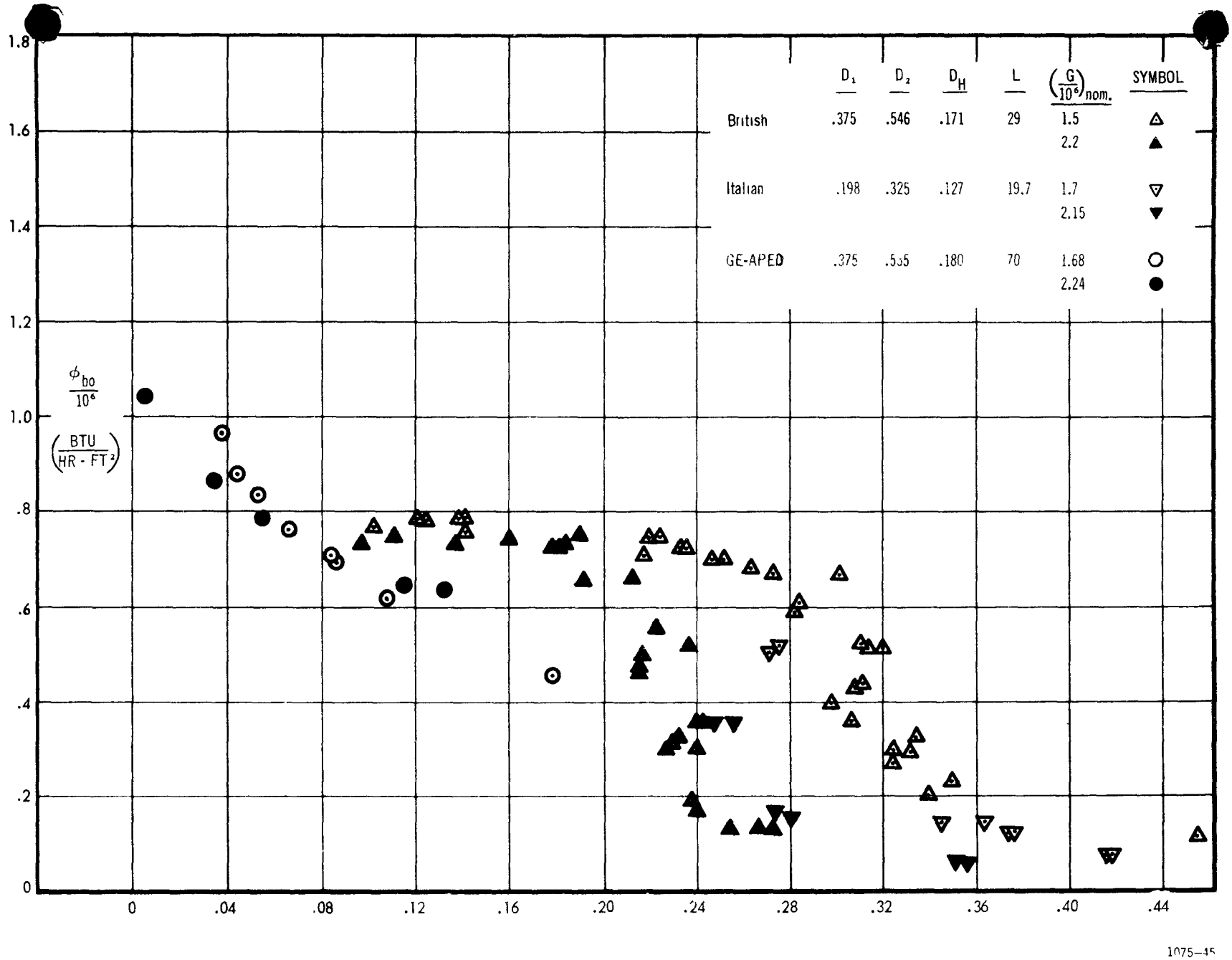

FIGURE 42 COMPARISON OF GE-APED WITH BRITISH (AERE) AND ITALIAN (CISE) BURNOUT DATA, INTERNALLY HEATED ANNULUS, 1000 PSIA (= 70.3 kg/cm²)

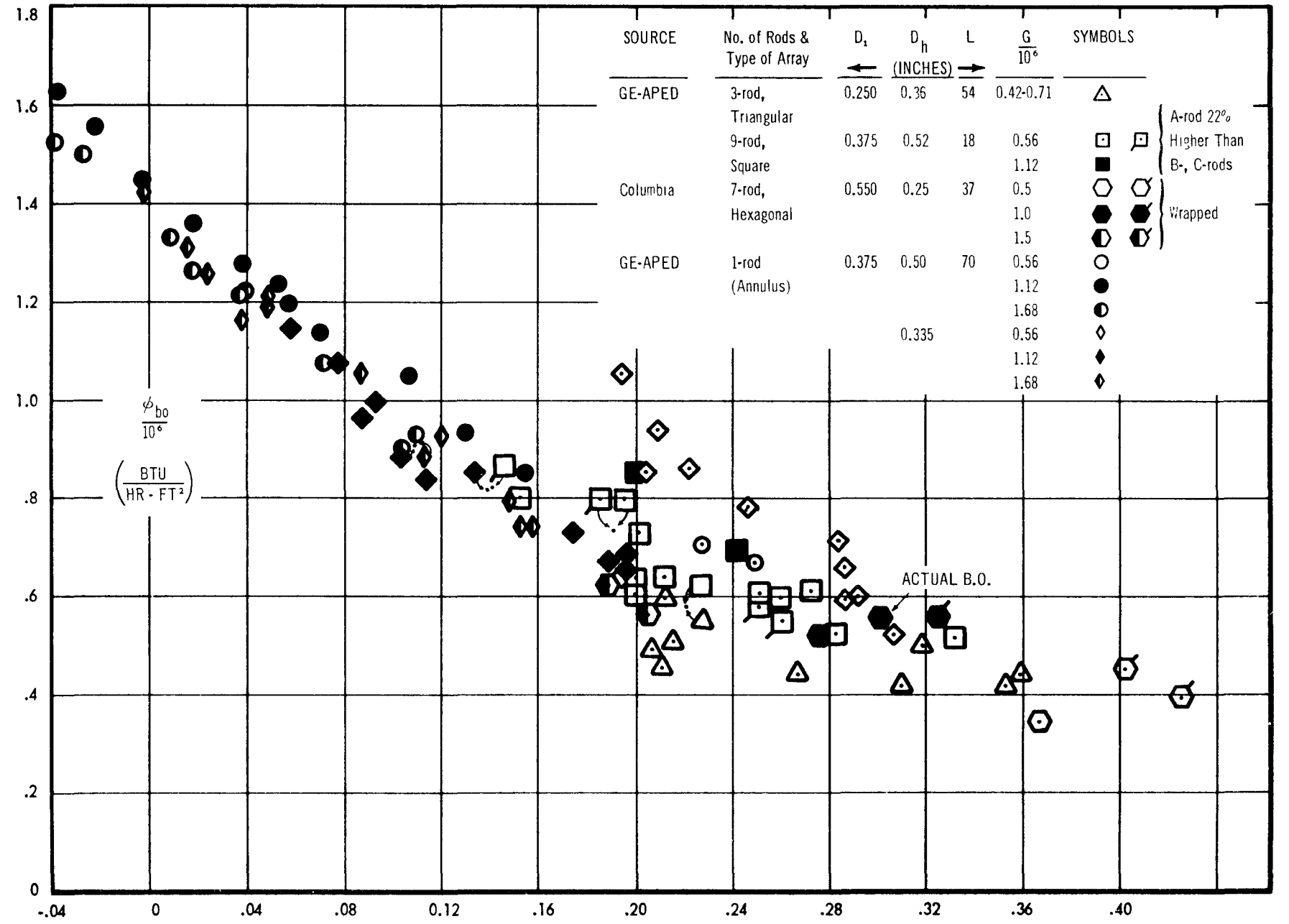

FIGURE 43 COMPARISON OF GE-APED SINGLE ROD DATA WITH APED AND COLUMBIA MULTIROD DATA, 1000 PSIA

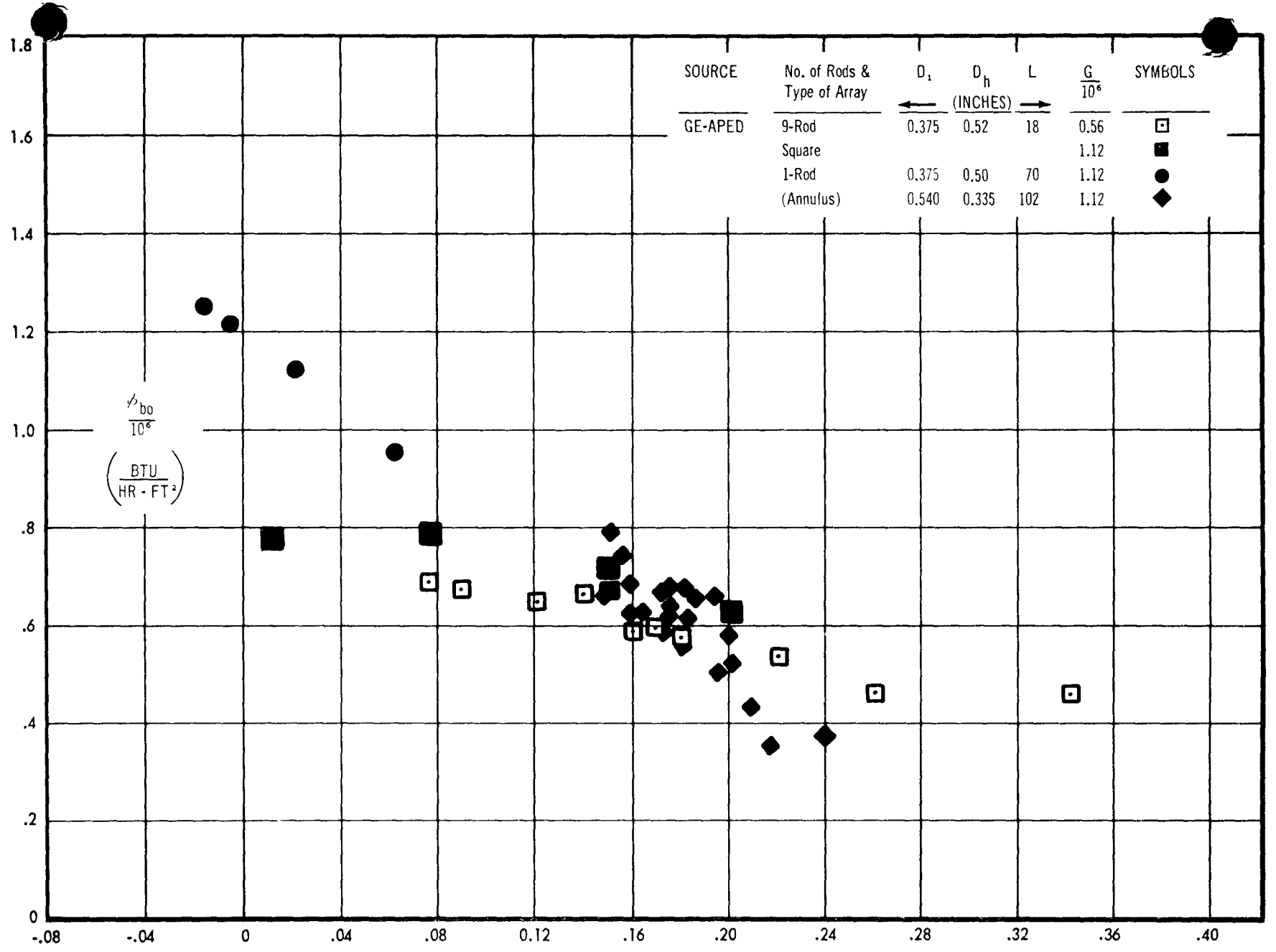

1075-47

FIGURE 44 COMPARISON OF GE-APED SINGLE ROD DATA WITH APED MULTIROD DATA 1400 PSIA

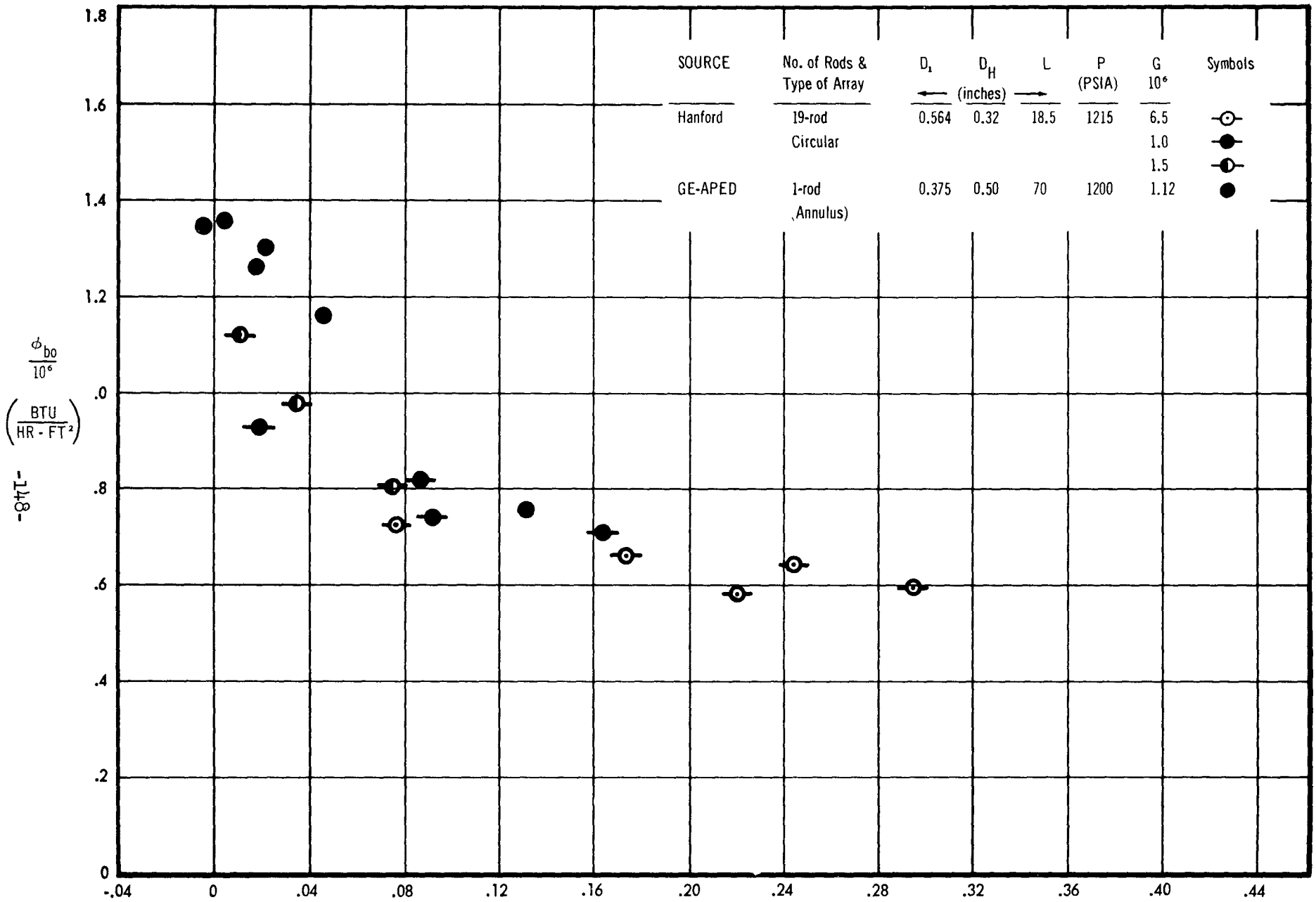

1075-48

FIGURE 45 COMPARISON OF GE-APED SINGLE RED DATA WITH HANFORD MULTIROD DATA

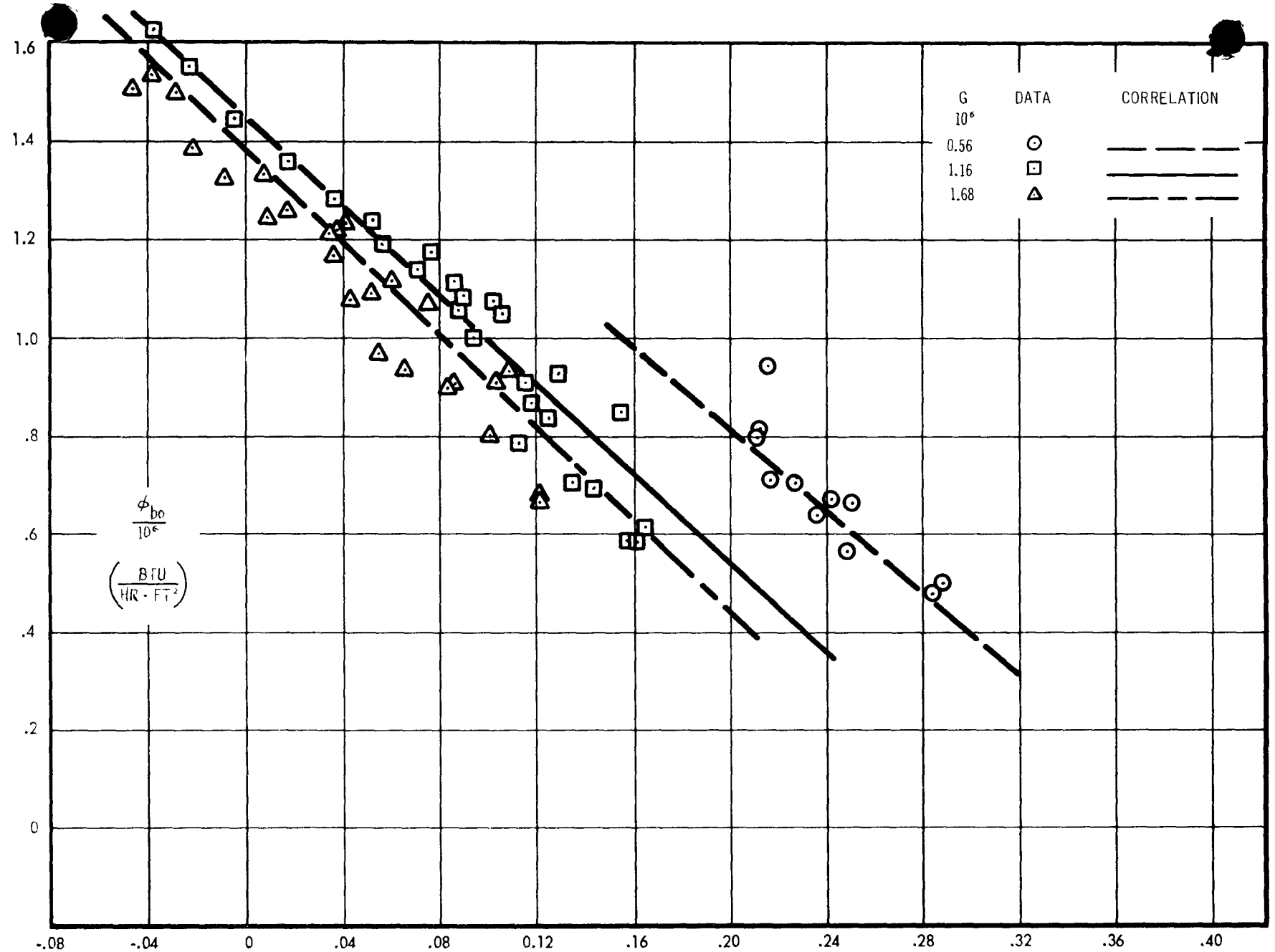

1075-49

FIGURE 46 BURNOUT HEAT FLUX VS. QUALITY – D_h - 6.50 INCH, P 100[illegible] PSIA

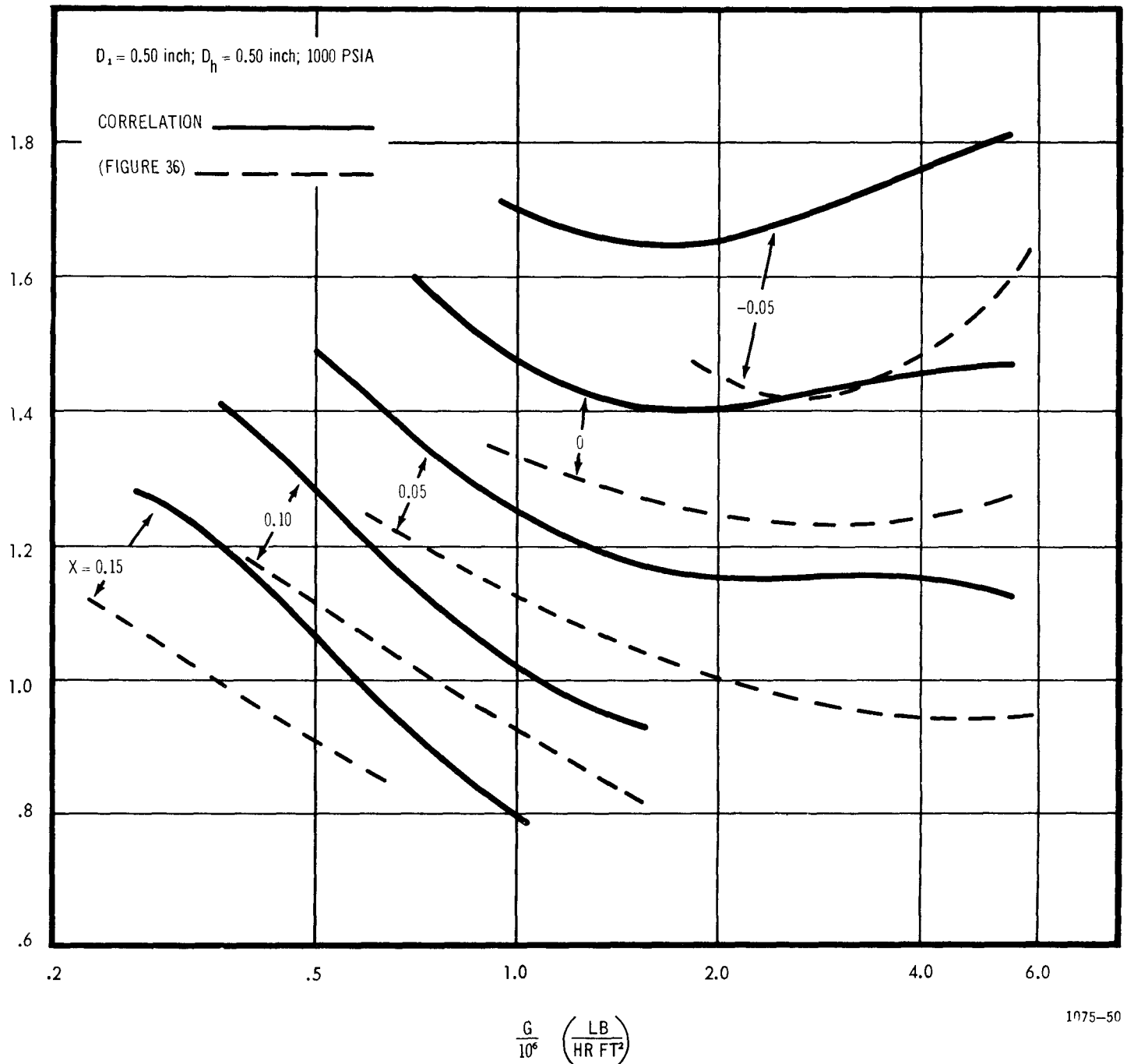

FIGURE 47 BURNOUT HEAT FLUX VS. FLOW

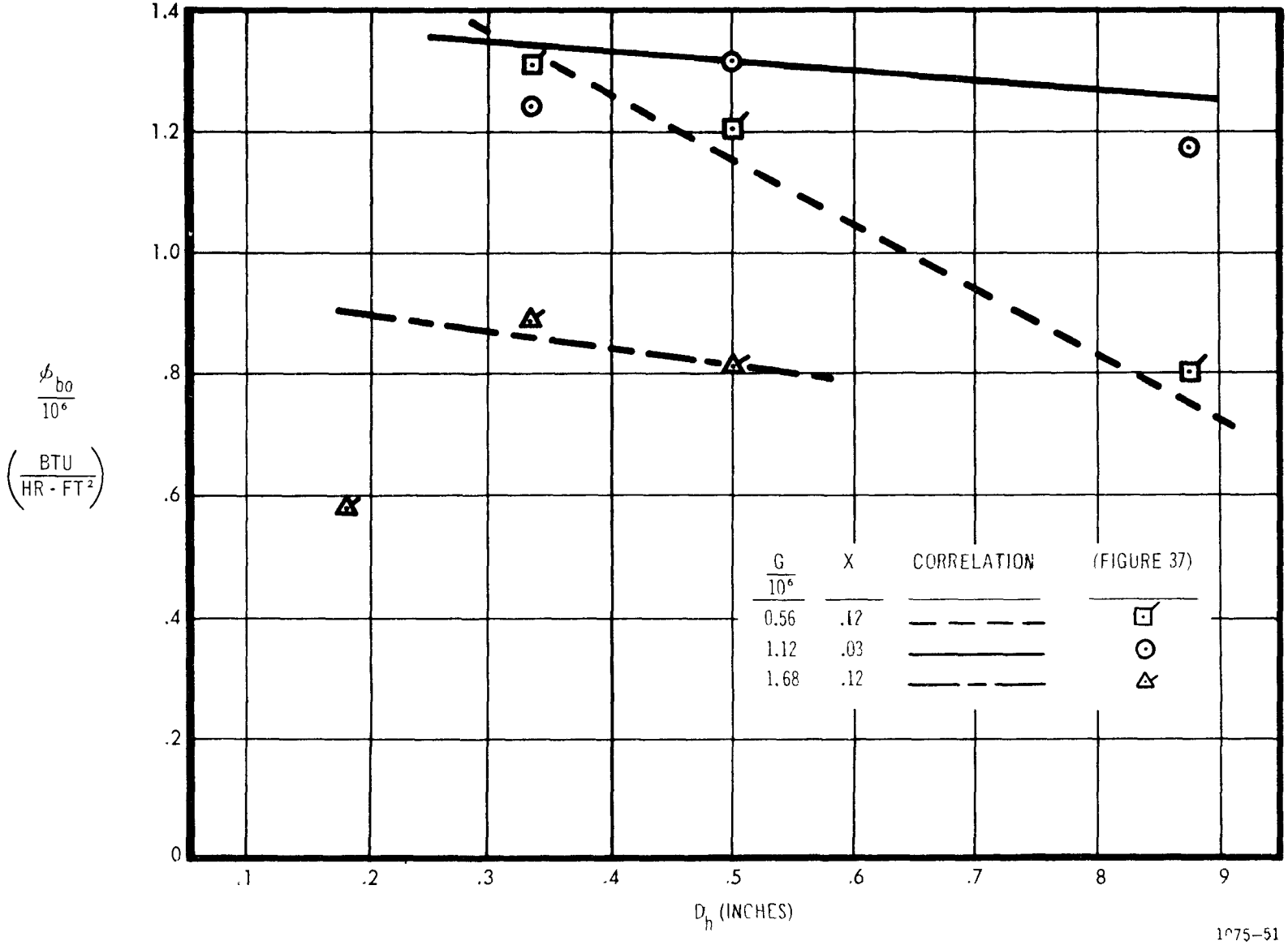

FIGURE 48 BURNOUT HEAT FLUX VS. HYDRAULIC DIAMETER – D_1 = 0.375 INCH; P = 1000 PSIA

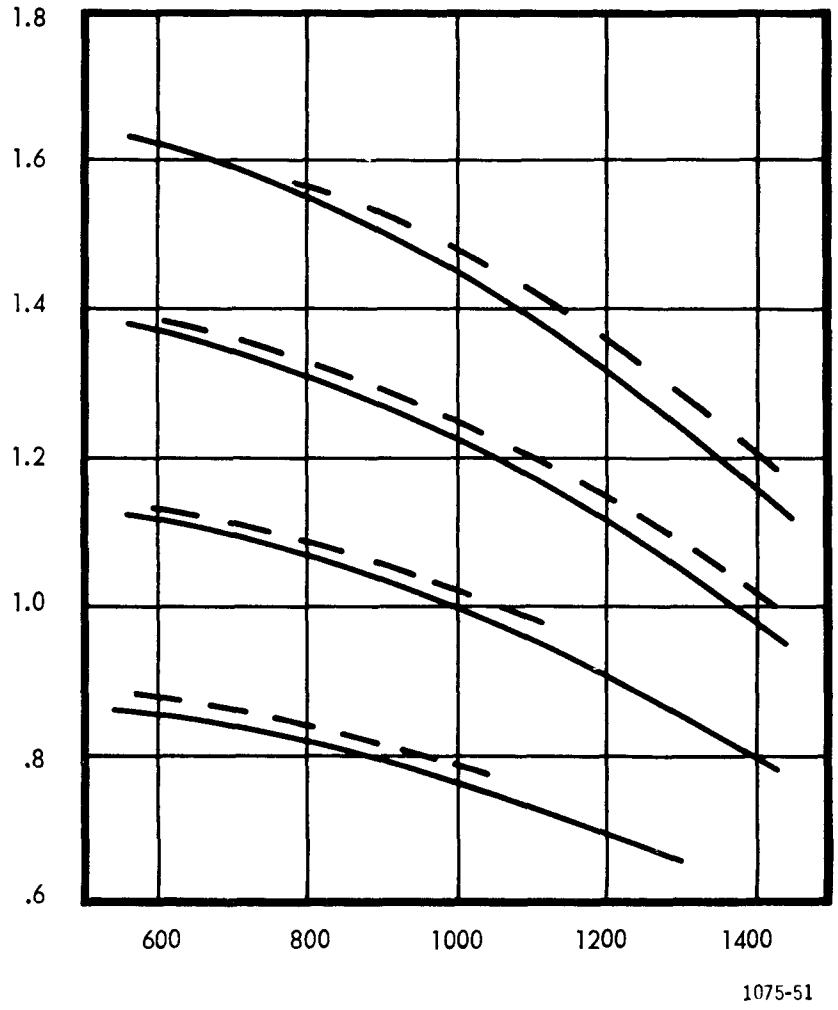

$\frac{\phi_{bo}}{10^6}$ $\left(\frac{BTU}{HR\ FT^2}\right)$

$D_1 = 0.375$ inch; $D_h = 0.500$ inch; $\frac{G}{10^6} = 1.12\ \frac{LB}{HR\ FT^2}$

CORRELATION ——————————

(FIGURE 40) — — — —

FIGURE 49 BURNOUT HEAT FLUX VS. PRESSURE

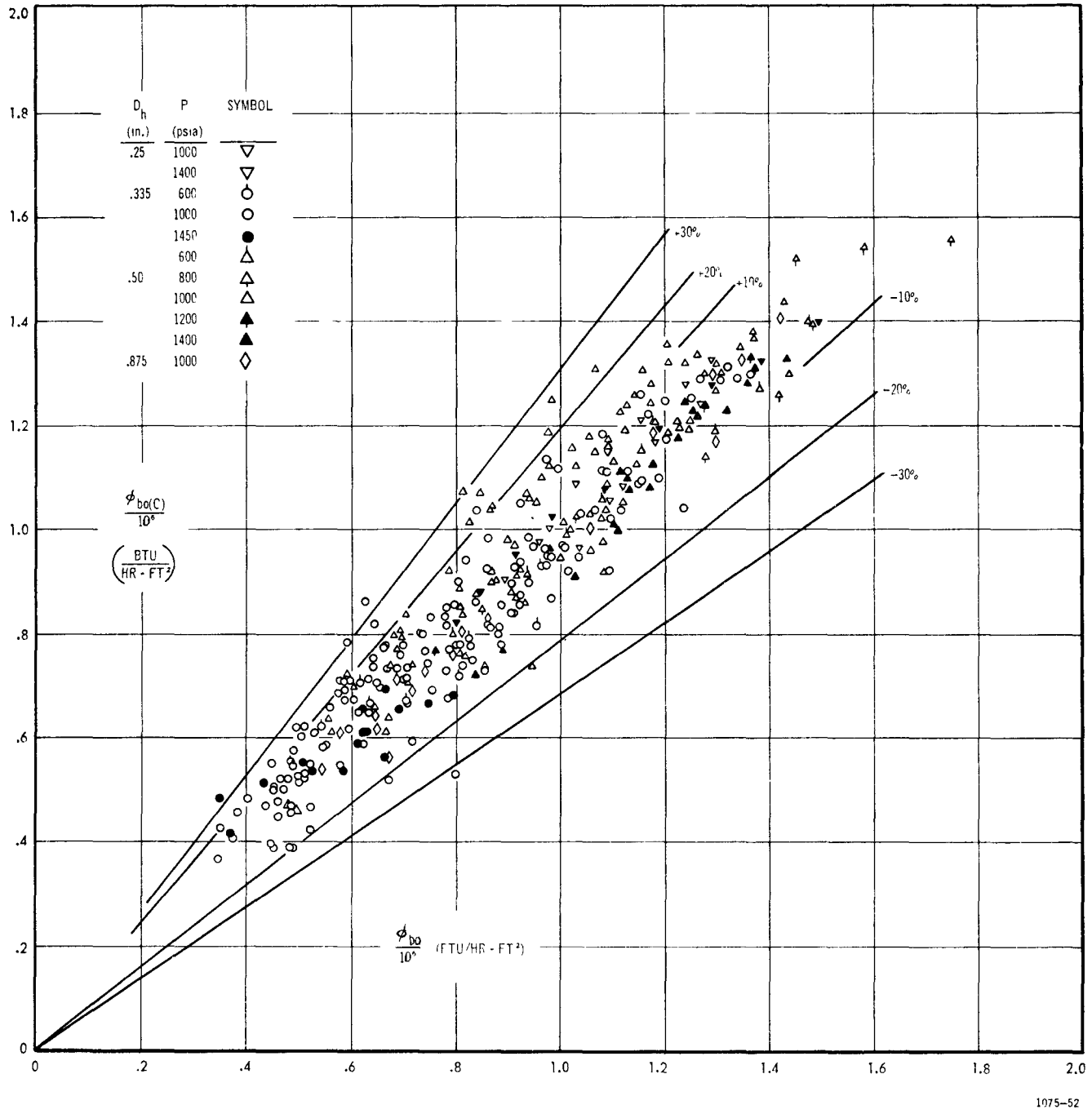

1075-52

FIGURE 50 CALCULATED VS. MEASURED BURNOUT HEAT FLUX, GE-APED SINGLE ROD DATA

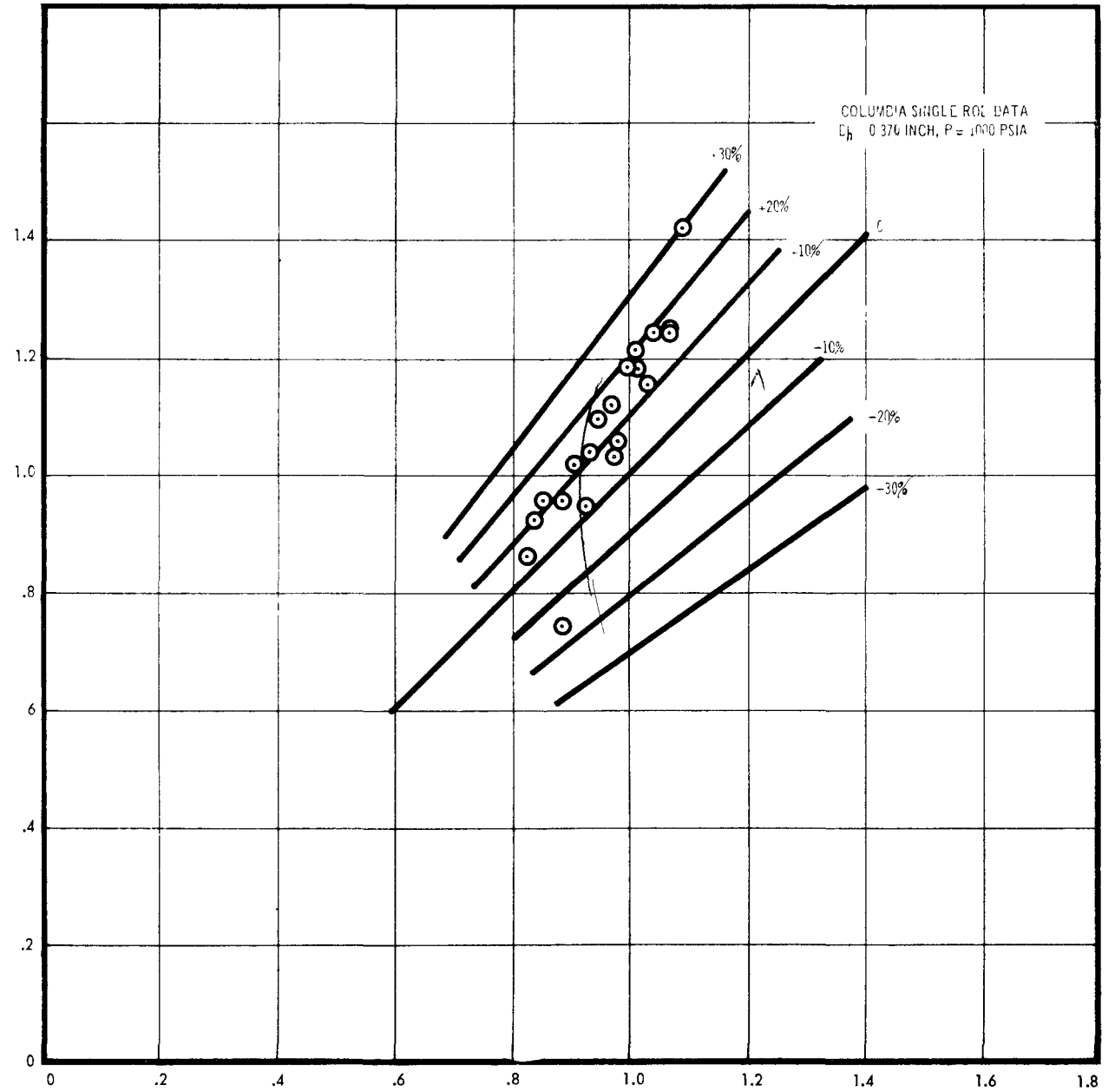

FIGURE 51 CALCULATED VS. MEASURED BURNOUT HEAT FLUX

1075–53